U.PORTO

FEUP FACULDADE DE ENGENHARIA
UNIVERSIDADE DO PORTO

Linear and Non-Linear Vibrations of Single-Layer Graphene Sheets

Tomás Rosas Coelho Chuaqui

Supervisor:
Prof. Dr. Pedro Leal Ribeiro

A Thesis submitted for the degree of

Master of Science in Mechanical Engineering

to Faculdade de Engenharia, Universidade do Porto

Porto, September 2016

Título: Vibrações Lineares e Não-Lineares de Folhas de Grafeno

Resumo

O estudo dos fenómenos vibratórios das folhas ou placas de grafeno (SLGSs) é fundamental para a correcta compreensão do comportamento dinâmico deste material relativamente recente. O grafeno tem sido tema de especial interesse científico nas últimas décadas, sobretudo devido às excelentes propriedades e à enorme diversidade de aplicações, como por exemplo dispositivos micro e nano-electrónicos, sensores, supercondensadores, células fotovoltaicas, mecanismos de filtragem de água e até mesmo a possibilidade de detecção e diagnóstico de doenças.

As vibrações destes dispositivos são caracterizadas pelas elevadas deflexões em relação às dimensões das folhas de grafeno, nomeadamente em relação à sua espessura, verificando-se a ocorrência de não-linearidades geométricas que provocam um aumento efetivo da rigidez da placa. Este é um fenómeno relativamente comum em sistemas altamente não-lineares e uma das consequências mais proeminentes é a variação das frequências naturais ao longo de um período de vibração, sendo que para deslocamentos significativos este efeito é mais pronunciado levando a frequências naturais mais elevadas. As formas naturais de vibração também variam durante um período de oscilação e o procedimento tipicamente usado para estudar fenómenos vibratórios lineares é insuficiente e manifestamente incapaz de descrever correctamente a dinâmica não-linear de um dado sistema.

Nesta dissertação foram estudadas as vibrações lineares e não-lineares de uma folha de grafeno em regime livre e sem amortecimento, tendo sido formulados dois modelos contínuos distintos considerando a teoria não-local de Eringen aplicada a uma placa fina (teoria de Kirchhoff) e incluindo não-linearidades geométricas de Von Kármán. No primeiro modelo, aplicou-se a versão p do método dos elementos finitos e estabeleceram-se as equações de movimento recorrendo ao método de Galerkin. Seguidamente empregou-se o método do balanceamento dos harmónicos (apenas com a consideração do harmónico fundamental) por forma a obter-se um sistema de equações não-lineares algébricas no domínio das frequências, sendo este resolvido numericamente através do método da continuação. O segundo modelo fundamenta-se na função de tensão de Airy considerando-se apenas uma função para o deslocamento transverso da placa (não se tratando de um modelo baseado em elementos finitos). De forma análoga ao primeiro modelo, os métodos de Galerkin e do balanceamento dos harmónicos (neste caso com três harmónicos) foram empregues de forma a discretizarem-se as variáveis espaciais e temporais das equações de movimento. Por fim, tentou-se conciliar os dois modelos referidos num modelo baseado simultaneamente na versão p do método dos elementos finitos e na função de tensão de Airy, sendo a formulação matemática correspondente devidamente apresentada.

Verificou-se cada modelo recorrendo a diversos resultados publicados na literatura. Obtiveram-se resultados válidos para os fenómenos vibratórios lineares e para a dinâmica não-linear local ($\mu = 0$) usando o primeiro modelo, no entanto, para o caso não-linear não-local as soluções obtidas não se encontram em conformidade com outros trabalhos publicados. O segundo modelo, por outro lado, foi validado e obtiveram-se resultados bastante satisfatórios.

Fez-se primeiramente uma análise linear, onde se estudou o efeito do tamanho da folha e dos efeitos não-locais nas frequências lineares e formas naturais. Comparou-se um modelo isotrópico e ortotrópico concluindo-se que o primeiro caso apresenta resultados

igualmente válidos. Na análise não-linear obtiveram-se curvas dorsais de diversas SLGSs, considerando o primeiro, segundo e quarto modos de vibração, usando diferentes valores de parâmetro não-local e estudou-se a influência do efeito de pequena escala em cada harmónico individualmente.

Palavras-Chave: Folhas de Grafeno; Nanoplacas; Modos de Vibração Lineares; Modos de Vibração Não-Lineares; Efeitos Não-Locais

Title: Linear and Non-Linear Vibrations of Single-Layer Graphene Sheets

Abstract

The study of the dynamics of single-layer graphene sheets (SLGSs) is fundamental for the correct understanding of the behaviour of this relatively new material. The promising properties and numerous applications in a vast range of fields such as micro and nano-electronics, sensors, supercapacitors, solar cells, water filtration devices and even disease diagnosis, have drawn the attention of several researchers in these last decades.

The oscillations of these devices when actuated under different conditions have large displacements when compared to the dimensions of the graphene sheet. The relatively high deflection to thickness ratio provokes geometric non-linearities which lead to an effective stiffening of the sheet. This phenomenon, also known as hardening-spring effect, is a common occurrence in highly non-linear systems and one of its prominent consequences is the variation of the natural frequencies during a period of vibration. In fact, for increasingly larger displacements, this effect is more pronounced and therefore the natural frequencies are higher. The mode shapes also change during a period of oscillation and the typical linear vibration procedure to determine the dynamics of a particular system fails to accurately describe these phenomena.

In this dissertation, the linear and non-linear undamped free vibration of SLGSs is studied. Two equivalent continuum models are formulated considering Eringen's non-local elasticity applied to Kirchhoff's thin plate theory with inclusion of Von Kármán's geometric non-linearity and the results obtained for both linear and non-linear oscillations are presented.

In the first model, the p-version finite element method is employed and the equations of motion are derived using the Galerkin method. The harmonic balance method is posteriorly applied to obtain the discretized system of non-linear algebraic equations in the frequency domain, considering only the first harmonic, which is subsequently solved by an arc-length continuation method. In the second model, a single function approach based on Airy stress potential is formulated and, similarly, the Galerkin and the harmonic balance method are used to discretize the spatial and time dependent functions from the equations of motion. In this model three harmonics are considered in the periodic solution of the transverse displacement of the SLGS. Finally, a combination of both models is attempted and the correspondent mathematical formulation is presented.

Each model was verified with different results published in the literature. The first model successfully predicted the linear behaviour of the sheets but the results obtained for the non-linear problem were not particularly good (when non-local effects were simultaneously considered). The second model, however, presented very accurate results, which were in very good agreement with the work of other authors.

A linear analysis was first performed, where the size and non-local effects on the SLGS's linear natural frequencies and mode shapes were studied. An isotropic and orthotropic model were compared and it was concluded that the first case is a perfectly valid simplification of a SLGS. In the non-linear analysis, the backbone curves of SLGSs were obtained with varying non-local parameter, considering the first, second and fourth modes of vibration, and the influence of the small-scale effect was verified on each individual harmonic considered in the periodic solution.

Keywords: Single-Layer Graphene Sheet (SLGS); Nanoplates; Linear modes of vibration; Non-linear modes of vibration; Non-local effects;

Acknowledgements

I would like to thank my supervisor Prof. Pedro Leal Ribeiro for his support, dedication, availability, and especially for his guidance, without which this dissertation would not have been possible.

I would like to thank my friend and colleague Marco Alves, for all his support, advice and for all the rewarding conversations we had during the time of this work and Dr. Hamed Akhavan for all his help and relevant suggestions.

I would like to thank all my friends, in particular, Luís Varandas, Miguel Carvalho and Ricardo Freitas, for all their support and for all the great moments we shared during the time of this degree.

Finally, I would like to thank my family for all their love and support, and for their constant encouragement.

Contents

List of Figures

List of Tables

List of Symbols

Roman and Greek symbols/Mathematical operators

a	length of the plate along x axis;
a_i	internal characteristic length;
a_1	constant in internal loop of continuation method;
a_2	constant in internal loop of continuation method;
a_3	constant in internal loop of continuation method;
A	cross-section of a beam;
A_1	quadratic function of the transverse displacement in Airy based model;
A_2	quadratic function of the transverse displacement in Airy based model;
b	length of the plate along y axis;
$dwaux$	amplitude of the first increment vector;
$\mathcal{D}_i$	transverse displacement second-order spatial partial derivative;
$error_1$	error in internal loop for convergence of continuation method;
$error_2$	error in internal loop for convergence of continuation method;
$error_3$	error in internal loop for convergence of continuation method;
e^0	empirical material constant;
E	isotropic Young's modulus;
E_1	orthotropic Young's modulus in direction 1;
E_2	orthotropic Young's modulus in direction 2;
f_i	generic applied force;
$f_{r,s}$	out-of-plane shape functions;
$\mathcal{F}_i$	membrane force;
$\mathcal{F}_i^L$	result from constitutive relation;
$g_{r,s}$	in-plane shape functions;
G	shear modulus;
G_{12}	orthotropic shear membrane modulus;
h	thickness of the plate;
$i\eta$	auxiliary variable;
$i\xi$	auxiliary variable;
I	second moment of area;
$j\eta$	auxiliary variable;
$j\xi$	auxiliary variable;
J	polar second moment of area;
k_r	bond stretching stiffness;
k_{xx}	curvature in the x direction;
k_{xy}	shear curvature;

k_{yy}	curvature in the y direction;
$k\eta$	auxiliary variable;
k_θ	angle bending stiffness;
$k\xi$	auxiliary variable;
k_ϕ	torsional stiffness;
$l\eta$	auxiliary variable;
$l\xi$	auxiliary variable;
L	length of a beam;
m	index of mode of vibration along y direction;
m_i	mass of ith particle;
M_{xx}	moment in x direction;
M_{xy}	in-plane shear moment;
M_{yy}	moment in y direction;
n	index of mode of vibration along x direction;
$\aleph$	non-linear terms in third equation of motion;
N_{xx}	in-plane normal force along x direction;
N_{xy}	in-plane shear force;
N_{yy}	in-plane normal force along y direction;
pi	number of in-plane shape functions;
po	number of out-of-plane shape functions;
pt	number of Airy stress functions;
$q^u_{rs}(t)$	generalized displacements u;
$q^v_{rs}(t)$	generalized displacements v;
$q^w_{rs}(t)$	generalized displacements w;
$q^\Phi_{rs}(t)$	generalized Airy stress functions;
Q_{ijkl}	elastic moduli components;
s	arc-length of continuation method;
t	time variable;
t_{ij}	stress tensor;
$t_{r,s}$	Airy stress potential shape functions;
t_1	initial time condition;
t_2	final time condition;
u	longitudinal displacement along x direction;
u^0	middle-plane longitudinal displacement along x direction;
$\dot{u}$	longitudinal velocity along x direction;
$\dot{u}^0$	middle-plane longitudinal velocity along x direction;
$\ddot{u}_i$	generic acceleration;
$\ddot{u}^0$	middle-plane longitudinal acceleration along x direction;
U	potential energy
U_A	stretching potential energy of a uniform beam;
U_{bonded}	potential energy of bonded atoms;
U_M	bending potential energy of a uniform beam;
$U_{non-bonded}$	potential energy of non-bonded atoms;
U_r	bond stretching energy;
U_T	torsional potential energy of a uniform beam;
U_θ	angle bending energy;
U_ϕ	torsional energy;

v	longitudinal displacement along y direction;
v^0	middle-plane longitudinal displacement along y direction;
$\dot{v}$	longitudinal velocity along y direction;
$\dot{v}^0$	middle-plane longitudinal velocity along y direction;
$\ddot{v}^0$	middle-plane longitudinal acceleration along y direction;
V	generic volume;
w	transverse displacement along z direction;
w_m	difference in amplitudes of consecutive transverse displacement vectors;
w^0	middle-plane transverse displacement along z direction;
$\dot{w}$	transverse velocity along z direction;
$\dot{w}^0$	middle-plane transverse velocity along z direction;
$\ddot{w}^0$	middle-plane transverse acceleration along z direction;
W	total transverse displacement at $x = y = 0$, $t = 0s$;
W_1	amplitude of the first harmonic at $x = y = 0$;
W_3	amplitude of the third harmonic at $x = y = 0$;
W_5	amplitude of the fifth harmonic at $x = y = 0$;

α	constant in the solution of a mode of vibration;
$\alpha\left(\lvert x' - x\rvert\right)$	non-local kernel function;
β	constant in the solution of a mode of vibration;
γ_{xy}	shear membrane strain;
γ_{xz}	transverse shear strain;
γ_{yz}	transverse shear strain;
γ^0_{xy}	shear membrane strain components (independent of z);
δk_{xx}	variation of the curvature in the x direction;
δk_{xy}	variation of the shear curvature;
δk_{yy}	variation of the curvature in the y direction;
δK	variation of kinetic energy;
$\delta \dot{u}$	variation of longitudinal velocity along x direction;
$\delta \dot{u}^0$	variation of middle-plane longitudinal velocity along x direction;
δU	variation of potential energy;
$\delta \dot{v}$	variation of longitudinal velocity along y direction;
$\delta \dot{v}^0$	variation of middle-plane longitudinal velocity along y direction;
δV	variation of work;
$\delta \dot{w}$	variation of transverse velocity along z direction;
$\delta \dot{w}^0$	variation of middle-plane transverse velocity along z direction;
$\delta \gamma_{xy}$	variation of shear membrane strain;
$\delta \gamma^0_{xy}$	variation of shear membrane strain components (independent of z);
$\delta \varepsilon_{xx}$	variation of normal strain along x direction;
$\delta \varepsilon^0_{xx}$	variation of normal strain components (independent of z) along x direction;
$\delta \varepsilon_{yy}$	variation of normal strain along y direction;
$\delta \varepsilon^0_{yy}$	variation of normal strain components (independent of z) along y direction;
$\delta \omega$	variation in frequency;
Δr	bond stretching displacement;
$\Delta \theta$	angle bending displacement;
$\Delta \phi$	torsional displacement;
$\Delta \omega_0^2$	increment in frequency;

ε_{kl}	strain tensor;
ε_{xx}	normal strain along x direction;
ε^0_{xx}	normal strain components (independent of z) along x direction;
ε_{xy}	half shear membrane strain;
ε_{yy}	normal strain along y direction;
ε^0_{yy}	normal strain components (independent of z) along y direction;
ε_{zz}	normal strain along z direction;
η	natural coordinate in y direction;
μ	non-local parameter;
ν	isotropic Poisson ratio;
ν_{12}	orthotropic Poisson ratio;
ν_{21}	orthotropic Poisson ratio;
ξ	natural coordinate in x direction;
ρ	density;
$\sigma_{ij}\,(x')$	local stress tensor at x';
σ_{xx}	normal stress along x direction;
σ_{yy}	normal stress along y direction;
τ_{xy}	shear membrane stress;
ϕ	Airy stress function (independent of h);
Φ	Airy stress function;
ω	frequency of vibration;
ω_i	frequency in ith increment;
Ω	area of the plate;

∇^2	laplacian operator;
$\mathcal{L}$	linear differential operator;
$\mathcal{L}_u$	rearranged first equation of motion;
$\mathcal{L}_v$	rearranged second equation of motion;
$\mathcal{L}_w$	rearranged third equation of motion;
$\mathcal{L}_\Phi$	rearranged compatibility equation;

Vectors and Matrices

$[A_{ij}]$	coefficient matrix;
$\left\{de^0\right\}$	vector of middle-plane displacements;
$[D_{ij}]$	coefficient matrix;
$\{F\}$	vector of residual forces;
$\{F_i\}$	interatomic force;
$[J]$	Jacobian matrix;
$[K_L]$	generic linear stiffness matrix;
$[K_{NL}]$	generic non-linear stiffness matrix;
$\left[K^1\right]$	linear stiffness matrix;
$\left[K^1_b\right]$	out-of-plane linear stiffness matrix;
$\left[K^1_p\right]$	in-plane linear stiffness matrix;
$\left[K^2\right]$	first-order non-linear stiffness matrix;
$\left[K^3\right]$	first-order non-linear stiffness matrix;

$\left[K^{3+5}\right]$ assemblage of $\left[K^3\right]$ and $\mu\left[K^5\right]$;
$\left[K^4\right]$ second-order non-linear stiffness matrix;
$\left[K^{4+6}\right]$ assemblage of $\left[K^4\right]$ and $\mu\left[K^6\right]$;
$\left[K^5\right]$ first-order non-linear non-local stiffness matrix;
$\left[K^6\right]$ second-order non-linear non-local stiffness matrix;
$\left[K^7_{ww}\right]$ first-order non-linear stiffness matrix;
$\left[K^8_{ww}\right]$ first-order non-linear stiffness matrix;
$[M]$ mass matrix;
$[M_b]$ out-of-plane mass matrix;
$[N]$ shape function matrix;
$\{q\}$ vector of generalized displacements;
$\left\{q^b\right\}$ out-of-plane generalized displacement vector;
$\{q^p\}$ in-plane generalized displacement vector;
$\left\{\ddot{q}^b\right\}$ out-of-plane acceleration vector;
$\left\{\ddot{q}^u\right\}$ generalized acceleration vector u;
$\left\{\ddot{q}^v\right\}$ generalized acceleration vector v;
$\left\{\ddot{q}^w\right\}$ generalized acceleration vector w;
$[Q_{ij}]$ elasticity matrix;
$\{r_i\}$ ith particle position vector;
$[S_{ij}]$ inverse of matrix $[A_{ij}]$;
$\{w_{ci}\}$ amplitude of vibration of ith harmonic;
$\{w\}_i$ transverse displacement vector in ith increment of continuation method;
$[X]$ linear compatibility equation matrix;
$[Y]$ first-order non-linear compatibility equation matrix;
$\{\delta w\}$ variation in transverse displacement vector;
$\{\delta w\}_1$ component of $\{\delta w\}$;
$\{\delta w\}_2$ component of $\{\delta w\}$;
$\Delta\{w\}_{i+1}$ first increment in transverse displacement vector;

Chapter 1

Introduction

1.1 General Introduction

Graphene is one of the most groundbreaking discoveries in materials science of the last decades and since the successful isolation of a single free standing graphene sheet by Novoselov and Geim in 2008, the extraordinary properties and possible applications of graphene have drawn the attention of the scientific community. Extensive research has been conducted in various fields, from micro and nano-electronics able to easily integrate numerous circuit processes and with considerably low power consumption, to solar cells, supercapacitors, flexible screens, water filtration devices and even disease detection and diagnosis [1–7].

Graphene and other fullerenes, such as carbon nanotubes, may revolutionize modern day electronics and perhaps eventually replace silicon semiconductor devices leading to faster, more powerful and smaller hardware [1].

The study of the dynamics of single-layer graphene sheets (SLGSs) is fundamental to the correct understanding of this relatively new material. In fact, for the successful implementation of the various promising applications described, it is key to accurately predict how SLGSs behave under different conditions. Since these nano-devices operate at very high frequencies, reaching the order of terahertz [1], and the amplitudes of motion are considerably small (in the order of the nanometer), the determination of their dynamic response in not particularly simple.

The amplitudes of motion of single-layer graphene sheets, despite being very small in absolute terms, are relatively large when compared to the dimensions of the sheet [8]. This large deflection to thickness ratio introduces geometric non-linearities which cannot be neglected [9, 10]. The typical linear vibration study, in which by solving an eigenvalue-type problem the natural frequencies and mode shapes can be determined, is not sufficient for the study of highly non-linear systems and a different methodology must be adopted.

Several approaches have been formulated in the past years to study the non-linear dynamic behaviour of SLGSs, such as molecular dynamics or atomistic approaches and equivalent continuum models integrating geometric non-linearity and small-scale effects [8, 11–14].

The study of the particular case of non-linear free vibration of SLGSs is crucial to the correct understanding of the dynamic response of the diversified, previously mentioned future applications of this material. Knowing the resonances, the natural frequencies and

the mode shapes of single-layer graphene sheets is therefore essential and further research in the area must be carried out, despite all the challenges that their investigation may present.

In this dissertation the linear and non-linear undamped free vibrations of single-layer graphene sheets are studied using two distinct continuum models. The first employs the p-version finite element method while the second is a single function model based on Airy stress potential. Lastly, a combination of both models was attempted and its mathematical formulation is presented.

1.2 Graphene: Research, Production and Applications

Graphene is a planar atomic layer of carbon atoms displayed in a benzene-ring structure (bonded in an hexagonal honeycomb structure), resulting from the ability of carbon to form three strong sp^2 covalent bonds. In practice, graphene is present in several carbonaceous structures as their building foundation, from recently discovered fullerenes, such as the Buckminster fullerene which corresponds to a hollow sphere of carbon hexagonal lattices and the more popular carbon nanotubes to ordinary graphite, comprised of stacked layers of graphene sheets held together by Van der Waal's forces [1, 15].

Graphene has received considerable attention since the innovative paper written by Novoselov et al. [16] and approximately a decade of research has promised various potential applications due to its excellent mechanical, thermal, electronic, magnetic and chemical properties. Graphene is the thinnest and strongest material ever measured (with an approximate Young modulus of 1 TPa, depending on the type of graphene), can sustain current densities six orders of magnitude higher than that of copper, shows record thermal conductivity of 5000 $\mathrm{Wm^{-1}K^{-1}}$ and stiffness [17], has an extremely large specific surface area of 2630 $\mathrm{m^2g^{-1}}$ [18] and combines conflicting qualities such as brittleness and ductility [8, 19–22]. The possible applications range from the field of nano and microelectronics, such as micro-electromechanical systems (MEMS) and nano-electromechanical systems (NEMS), nano-sensors capable of gene mutation and disease detection, gas detection and DNA sequencing [2, 3] to longer lasting batteries [23], corrosion prevention [24], display panels by successfully replacing previous scarce indium-thin oxide (ITO) and delivering more reliable solutions for flexible and bendable displays [4], dye-sensitized highly efficient and low production cost solar cells [5] and foldable circuit boards [25].

After the successful isolation of graphene (which was thought to be unstable in ambient conditions) from bulk pyrolytic graphite by mechanical exfoliation with Scotch tape and various groundbreaking experiments, which granted Novoselov and Geim the 2010's Nobel prize in physics, the main focus turned to large-scale synthesis of graphene. Evidently, the adhesive tape method, where flakes of graphite are removed with tape and subsequently deposited upon a silica slide, being progressively exfoliated until one atom thick layer of graphite (or graphene) is obtained, is not suitable for mass production and to this day a viable, inexpensive solution is yet to be found. Several methods, however, have been experimented. A variation of the "Hummers" method devised in 1958 to produce graphitic oxide [26] has been studied. The process implies the reduction of the oxide until graphene is left or, otherwise, partially-reduced graphene oxide is obtained. Several other production methods exist but are less used and are described in detail in [27]. These include ion implantation [28], chemical vapour deposition [29], liquid-phase exfoliation [30, 31] and

epitaxial growth upon a silicon carbide substrate [32].

According to [1] one of the most promising applications of graphene is high speed electronic devices such as field effect transistors. In fact, the exceedingly high charge carrier mobility of graphene, which has been shown, under optimal conditions, to be approximately 200000 $cm^{-2}V^{-1}s$ [33], permits extremely high frequencies of operation of these transistors at the order of terahertz. However, unlike typical semi-conductors which have band gaps allowing the two possible states "on" and "off", graphene sheets exhibit zero band gaps, hence the difficulty in the application of the material to everyday electronics. Designing derivatives with band gap has been attempted but is still a work in progress. Another obstacle is the fabrication of defect free transistors as irregularities generally appear on the graphene sheet during the manufacturing process of the devices. Other possible application is the development of graphene data storage hardware, enabling a significant reduction in the size of the current technology since graphene oxide-based devices have been shown to have data capacities of 0.2 $Tbitscm^{-3}$, which is approximately tens times the storage of current hardware. Smart windows and flexible touch screens are also possible and interesting projects. The former consists of a sandwich structure comprised of a layer of liquid crystals between composite electrodes of flexible polymer and graphene. In presence of an electrical field, the window becomes opaque, and in its absence, transparent.

Due to the large internal surface area of graphene, supercapacitors are perhaps one of the most noteworthy applications, since the fundamental requirement for the fabrication of the latter is a high internal surface area material able to store charge. These devices are used in energy storage and can deliver significantly higher currents than a regular capacitor, which could be potentially used to accelerate electric cars, trains, aeroplanes and heavy machinery, serving as an ecological alternative to regular internal combustion engines. As mentioned before, photovoltaic cells are also a possible application, in this case dye-sensitized solar cells, which are as efficient as a typical platinum based electrode solar cell at a fraction of the cost, due to the scarcity of platinum and consequently its high cost.

A distinct and possibly revolutionary area for graphene application is the field of electroanalysis. The adsorptive properties of graphene have been repeatedly reported and one notable example is the usage of graphene as a support for DNA oligonucleotides typical of Alzheimer's disease. By binding with the DNA strands associated with Alzheimer's disease, the electrode surface is blocked, thus changing the impedance which is subsequently measured allowing the diagnosis of the disease. This procedure could be applied to various diseases and despite the questionable feasibility in the near future, it remains a remarkable possibility. Note that [1] contains a detailed description of each of the applications mentioned above.

Lastly, desalination using single layer graphene sheets with nanoporous [6] and water purification by ultra-thin graphene nanofiltration [7] are both groundbreaking applications. Given the high permeability of this material, which is several orders of magnitude higher than that of conventional reverse osmosis membranes, desalination has been proved to be effective using freestanding graphene sheets with nano-scale porosities. The main difficulty is to accurately produce pores with the right size in order to filter salt molecules. In addition, ultra-thin, low cost and high performance nanofiltration membranes using

chemically converted graphene have been intensively studied and show great potential in water purification, allowing high rejection of organic dyes and moderate retention of ion salts. These graphene devices conciliate several advantages typical of an inorganic ceramic nanofiltration membrane, such as thermal stability, certain solvent resistance, high strength and durability with polymer-like characteristics such as flexibility.

1.3 Graphene Sheet Modelling

Due to the difficulty in graphene's manufacture and the added complexity of dealing with nano-sized structures, experimental work with graphene sheets has been relatively limited. In fact, the first experimental evidence of a single layer graphene was conducted in [34] and besides Novoselov and Geim's work not many researchers have obtained empirical results for graphene's properties. On the other hand, computational modelling has been frequently implemented as it offers an inexpensive and practical alternative. These models can be generally categorized as atomistic/molecular or continuum models. The former refer to the group of simulations where each individual particle that comprises the system of interest is considered (note that particle may refer to either individual molecules, atoms or even their nuclei). Within this category, several different approaches have been conducted in the past to study the behaviour and the properties of graphene sheets, such as *ab initio* and classical molecular dynamics simulations.

Atomistic models are commonly used in physics and molecular mechanics as these allow to accurately predict the dynamic behaviour of nano-structures with generally greater certainty than simpler continuum models. However, the computational effort demanded in the first case is typically a lot higher than in the latter, particularly for simulations of large structures where the discretization to the atomic level is excessive. Therefore, continuum and hybrid models (formulated with both approaches) have been implemented as an alternative to the more elaborate and rather computationally costly atomistic counterpart. In the former, a graphene sheet is generally assumed to have the typical behaviour of a continuum plate, whilst in atomistic modelling the space-frame structure of graphene is considered.

In 2007 Eringen's non-local elasticity theory was applied to a thin plate, considering Kirchhoff hypotheses [35]. In 2010 J.N.Reddy proposed a non-local non-linear model for both classical and shear deformation theories for beams and plates [36], R.Ansari et al. devised an isotropic non-local model for the study of free vibrations of single layer graphene sheets [11], a non-linear SLGS was modelled using a hybrid atomistic-structural element in [12] and in 2011 E.Jomehzadeh and A.Saidi studied the large vibration of multilayered graphene sheets resorting to an orthotropic non-linear, non-local continuum model [8]. Due to the increasing interest in possible graphene/piezoelectric sandwich films as nano-sensors and actuators, a non-linear non-local continuum model was applied to study the vibration characteristics of such films under electric loading [15]. In 2016 a non-local continuum model using kp-Ritz element-free method was developed in order to study large deformations of SLGSs [13], where modified Newton-Raphson and arc-length continuation method were employed to solve the non-linear equations. Lastly, a multiscale model considering material and geometric non-linearity was implemented for the first time to study the dynamic response of single layer graphene sheets under harmonic excitation in [14]. It was concluded that geometric non-linearity has a dominant effect on hardening

of the sheet when compared to material non-linearity.

In this work a continuum model considering geometric non-linearity and non-local elasticity will be formulated but it seems manifestly necessary to briefly introduce the molecular dynamics approach.

1.3.1 Molecular Dynamics

According to [19, 37–39], molecular dynamics simulations (or MD for abbreviation) have been widely used since around 1970 to study the bonding and interactions of macromolecules such as proteins and nucleic acids. Since molecular dynamics are independent from the mechanism or processes to be investigated, in the sense that no assumptions are previously made about the system of interest, these simulations can be applied to various fields of investigation. One major area of application is chemistry and biochemistry, allowing researchers to study the dynamics of biomolecules, protein folding and the effects of pharmaceutical chemicals. Other applications range from statistical mechanics and physics to thermodynamics, fluid dynamics and materials science.

Two main families of MD simulations can be distinguished depending on the mathematical formalism used to describe the system. One approach entirely neglects the quantum nature of chemical bonds and classical mechanics are solely taken into account, while in first-principles or *ab initio* MD, the electron density function for the valence electrons responsible for inter-atomic bonding is considered according to the laws of quantum mechanics. For large systems the first MD simulations (without consideration of quantum effects) are typically used due to their relatively higher simplicity.

The general procedure adopted in any MD simulation starts with the definition of the initial conditions of the particles. Therefore, for a system comprised of n particles, for every ith particle their respective initial position $\{r_i(t_0)\}$ and velocity $\{v_i(t_0)\}$ must be defined. The determination of these initial conditions is not deterministic and a probability distribution must be considered. In MD Maxwell-Boltzmann distributions are often considered and for a given temperature the velocity of a given particle is chosen for its probability of occurrence. The second step is the determination of an adequate potential function $U(\{r_i\})$, which represents the potential energy of n interacting atoms as a function of their respective positions. The forces among all the atoms of the system can be derived from this interaction potential, and can be given as its gradient with respect to each individual atomic displacement:

$$\{F_i\} = -\nabla_{r_i} U(\{r_i\}) = -\left(\frac{\partial U}{\partial x_i}, \frac{\partial U}{\partial y_i}, \frac{\partial U}{\partial z_i}\right) \tag{1.1}$$

The potential energy U can be divided according to whether the atoms are bonded or not. Bonded atoms show potential energy in the form of stretching, angle bending and torsion of their covalent bonds while non-bonded atoms interact mainly due to Van der Waals and electrostatic forces. The total potential energy U can therefore be written as a sum of the bonded and non-bonded terms.

$$U = U_{bonded} + U_{non-bonded} \tag{1.2}$$

It should be noted that electrons are not restricted to a fixed boundary and that the concept of atom is not necessarily accurate considering the quantum mechanics perspective. In fact, electrons may be shared by various nuclei and this unbounded behaviour results in decentralized electronic clouds which therefore determine chemical bonding. The consideration of both nuclei and the disperse electronic cloud represents a difficult task since the solution of Schrödinger equation is not available for practically interesting systems. However, the electronic and nuclear problems can be separated by the consideration of Born-Oppenheimer approximation as the difference in mass of nuclei and its electrons is significant. The concept of potential energy surface can be introduced and the dynamics of the nuclei can be studied without taking each electron individually. In fact, the transitional characteristics of the electronic cloud are neglected and an averaged electronic field is considered since the electron cloud equilibrates almost instantaneously for each position of the nuclei. Consequently, instead of solving the quantum mechanics problem, the electronic cloud effect on the nuclei can be represented by the already mentioned potential function (the determination of which might be difficult and is generally adjusted according to empirical results) and the evolution of the system in time can be followed by solving the equations of motion for each particle considering Newtonian mechanics:

$$\{F_i\} = m_i \frac{\partial^2 \{r_i(t)\}}{\partial t^2} \tag{1.3}$$

Single layered graphene sheets can therefore be modelled as space-frame structures and the equations of motion are established in a similar fashion to that of a macroscopic system. The overall mass and stiffness matrices are derived from the equivalent matrices of various beams and concentrated masses. These are used to simulate carbon atoms and the covalent bonds that connect them. Note that the radii of carbon atom nuclei is considered negligible ($r_c = 2.7 \times 10^{-5}$ A) and that the masses of the electrons are not significant. Thus, the carbon atom has an estimated diameter of 0.34 nm and has the concentrated mass of its nuclei ($m_c = 1.9943 \times 10^{-23}$ g). These are positioned at the ends of the beams, which reproduce the joints of the covalent bonds. For the potential energy of the system, electrostatic and Van der Waals forces are neglected and only the total steric or bonded potential energy is calculated (the energy related with the position and space occupied by each atom in the molecule, which decreases, for instance, if there are overlapping electron clouds due to a reduction in the distance between bonded atoms), which can be written as:

$$U_{bonded} = \sum U_r + \sum U_\theta + \sum U_\phi \tag{1.4}$$

where U_r is the bond stretching energy, U_θ is the angle bending energy and U_ϕ is the torsional potential energy (sum of out-of-plane and dihedral angle torsional energies). Note that these are independent and can be defined respectively as:

$$U_r = \frac{1}{2} k_r \left(\Delta r\right)^2 \tag{1.5a}$$

$$U_\theta = \frac{1}{2} k_\theta \left(\Delta \theta\right)^2 \tag{1.5b}$$

$$U_\phi = \frac{1}{2} k_\phi \left(\Delta \phi\right)^2 \tag{1.5c}$$

k_r, k_θ and k_ϕ are the bond stretching, angle bending and torsional stiffnesses and (Δr), $(\Delta \theta)$ and $(\Delta \phi)$ are the corresponding deviations from the equilibrium position and are displayed in Figure 1.1.

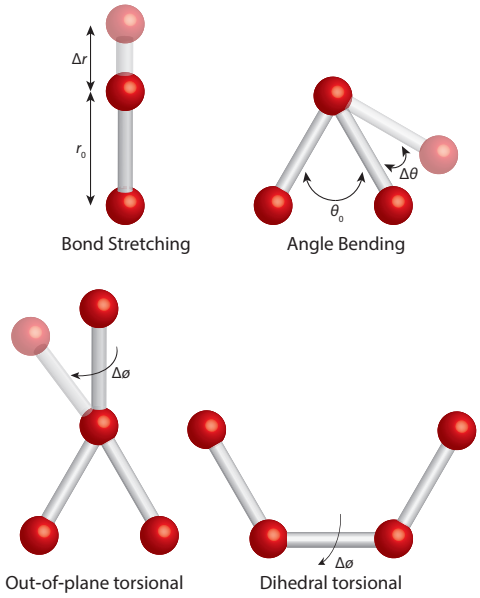

Figure 1.1: Potential energies in molecular mechanics

Writing the equivalent energies for a typical beam according to structural mechanics one has:

$$U_A = \frac{1}{2} \int_0^L \frac{N^2}{EA} \mathrm{d}l = \frac{1}{2} \frac{N^2 L}{EA} = \frac{1}{2} \frac{EA}{L} \left(\Delta L\right)^2 \tag{1.6a}$$

$$U_M = \frac{1}{2} \int_0^L \frac{M^2}{EI} \mathrm{d}l = \frac{2EI}{L} \alpha^2 = \frac{1}{2} \frac{EI}{L} \left(2\alpha\right)^2 \tag{1.6b}$$

$$U_T = \frac{1}{2} \int_0^L \frac{T^2}{GJ} \mathrm{d}l = \frac{1}{2} \frac{T^2 L}{GJ} = \frac{1}{2} \frac{GJ}{L} \left(\Delta \beta\right)^2 \tag{1.6c}$$

where U_A, U_M and U_T denote the stretching energy of a uniform beam under axial load, the bending potential energy due to a bending load and the torsional energy due to torsional load respectively; E, A and L are the Young modulus, the cross-section and the

length of the beam, I and α designate the second moment of area and rotational angle of the beam ends; β, G and J are the bending angle, the shear modulus and the polar second moment of area respectively. Considering the equivalence between the potential energies of the covalent bonds depicted in (1.5) and the potential energies of a beam (1.6) one can establish the following relations for the properties of a beam in terms of covalent stiffnesses or force field constants:

$$\frac{EA}{L} = k_r \tag{1.7a}$$

$$\frac{EI}{L} = k_\theta \tag{1.7b}$$

$$\frac{GJ}{L} = k_\phi \tag{1.7c}$$

The corresponding values for each force field constant are displayed below in Table 1.1, according to [19].

Table 1.1: Force field constants of the covalent bonds

k_r	6.52×10^{-7} Nnm^{-1}
k_θ	8.76×10^{-10} Nnmrad^{-2}
k_ϕ	2.78×10^{-10} Nnmrad^{-2}

Specific parameters of the beam with circular cross-section can be obtained from equations (1.7), such as the diameter, the Young modulus and the shear modulus:

$$d = 4\sqrt{\frac{k_\theta}{k_r}} \tag{1.8a}$$

$$E = \frac{k_r^2 L}{4\pi k_\theta} \tag{1.8b}$$

$$G = \frac{k_r^2 k_\phi L}{8\pi k_\theta^2} \tag{1.8c}$$

The solutions of the system of equations of motion are the positions $\{r_i(t)\}$ and velocities $\{v_i(t)\}$ of the particles. These are obtained by the discretization and subsequent numerical integration of the differential equations, generally using the Verlet algorithm and/or its variants, such as leapfrog and velocity Verlet algorithm [37, 38]. The Verlet algorithm for the determination of particles' positions can be written as follows:

$$\{r_i(t+\Delta t)\} \approx 2\{r_i(t)\} - \{r_i(t-\Delta t)\} + \frac{\{F_i(t)\}}{m_i}\Delta t^2 \tag{1.9}$$

Since the vibrational frequencies in a molecular system can reach periods of around 10 fs (femtoseconds) and modern computers only allow the calculation of 10^6 to 10^8 timesteps, the simulations using MD depict short processes of 1-100 ns of duration. As a consequence,

for an adequate description of the system of interest, the timestep is intentionally as large as possible. This, however, might jeopardize accuracy if high order derivatives are used in the integration algorithm. The Verlet algorithm is therefore an excellent option because of its low order in time. In addition, it only requires one expensive calculation per step (force evaluation) and is rather easy to program. After updating the positions and velocities in the new time increment, the forces acting upon the nuclei have to be recalculated by applying the gradient of the potential function.

Molecular dynamics present some limitations besides being computationally costly. In fact, as mentioned before, in classical MD simulations quantum effects are not considered and Schrödinger equation is replaced by Newton's second law of motion. The validity of such replacement is evidently dependent on the scale of the system. Quantum effects become significant when inter-particle distance is rather small, which might be problematic if light elements are being studied. In this case, quantum corrections are generally superimposed to the classical MD model. Another disadvantage which was already briefly referred is the time-scale limitation, seeing that the maximum timestep of the numerical integration is defined by the fastest motion in the system (in the order of femtoseconds). As a consequence and given the processing capabilities of modern computers, the total duration of a simulation is unfortunately rather short. In addition, the scale of the system of interest might be problematic as well. Indeed, the number of atoms that can be included in a MD simulation typically varies between 10^4 to 10^8 and, therefore, large systems or structures cannot be studied by a molecular dynamics simulation, typically requiring a continuum approach [37, 38].

On the other hand, since the mechanical characteristics of single layer graphene sheets are predicted to be chirality dependent, it is necessary to accurately determine the elastic properties for each possible configuration [19, 40, 41] (chiral vector for zig-zag and armchair configurations is displayed in Figure 1.2). The number of layers of a graphene sheet also influences its mechanical properties and is another aspect to be taken into account. These models prove to be very useful as they allow the determination of the elastic properties of different types of graphene sheets, either single or multiple layered and with different chirality, without resorting to practical experiments, which can be later implemented in an equivalent continuum model. The validity of the results obtained via molecular dynamics simulations is also generally very good since the only input in the model is a potential function and no other assumptions are made about the system or processes to be investigated, providing a detailed description of the molecules/atoms behaviour.

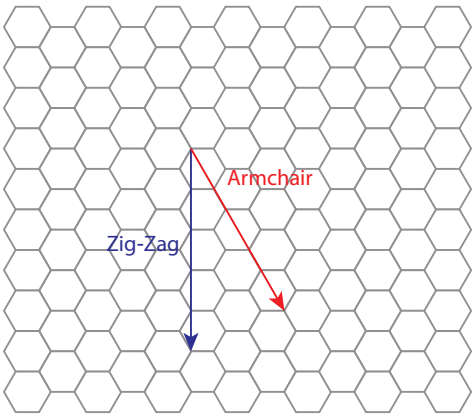

Figure 1.2: Chiral vector for zig-zag and armchair SLGS

1.3.2 Equivalent Continuum Model

In this study an equivalent continuum model will be developed considering the classical plate theory, based on Kirchhoff hypotheses. Classical plate theory is widely recognized for its accurate depiction of thin plate's behaviour, since for this case neglecting transverse shear strains and transverse normal strain is not problematic. The plate is assumed to be infinitely rigid in the transverse direction therefore underestimating deflection, which may lead to erroneous results for thick plates. However, for a one carbon atom thick sheet the increment in computational effort associated with Mindlin-Reissner plate theories, where shear strains through the thickness are considered, is not worthy.

Oscillations of a graphene sheet have generally large amplitudes, which, depending on the boundary conditions imposed, are generally at the order of magnitude of the sheet's thickness [8]. Typically, large deflections cannot be accurately described by linear models, where the stiffness of the structure is constant within the whole period of vibration. A viable option is to consider geometrical nonlinearity, which arises from the increase in in-plane membrane stresses. In fact, according to [9, 10], large deflections provoke higher membrane stresses effectively stiffening or hardening the plate. This results in higher values for the natural frequencies, which are therefore intrinsically dependent on the amplitude of vibration of the sheet. The consequence of this phenomena, typically designated by hardening spring effect, is increased natural frequencies which vary in a given period of vibration and reduced transverse displacements. Mode shapes are also changed by the amplitude of vibration. Unlike linear analysis where the displacement at a given point is proportional to the displacement of that point in the mode shape with a similar frequency to that of the excitation, in geometrically non-linear vibration the concept of mode shape is questionable since in a single period it changes according to the amplitude of oscillation. Indeed, in non-linear dynamics the mode shape shifts from the linear one to a shape that constantly changes during a period of vibration [10]. The change in natural frequencies typical of non-linear dynamics may also give birth to an important phenomenon known as internal resonance, which occurs when multiple natural frequencies become commensurable and mode interaction appears, leading to multi-mode vibration where energy exchanges between modes [42]. Other consequences of the consideration of geometric non-linearity will be discussed later in greater minuteness.

For the study of nanostructures, in this particular case a single layer graphene sheet,

original continuum modelling is inadequate since the small-scale effect resultant from individual atomic interaction is neglected. In fact, when the structure is small in size to molecular or even atomic scale, Hooke's elasticity is not sufficient as it lacks the ability to accurately describe the stress tensor at an arbitrary reference point of the system [43]. Generally, non-local elasticity theory is implemented to address this issue by the assumption that the stress tensor at the reference is dependent on the strains of the whole structure and not only of that single point. Non-local elasticity was developed by Eringen [44] and first employed in a continuum model by Peddieson [45], where a non-local version of Bernoulli/Euler beam was formulated. Eringen's non-local elasticity theory will be used in this study and will be described in detail in chapter 2.

1.4 Objectives

In the present work, the linear and non-linear modes of vibration of a single layer graphene sheet were investigated. Two equivalent continuum models were formulated to study the linear and non-linear vibrations of SLGSs, where the first employs the p-version finite element method and the second is a single function model based on Airy's stress potential. A combination of both models was also attempted but unfortunately, mainly due to time limitations, it was left to further research. The continuum models developed in this work are based on Kirchhoff's thin plate theory and include Von Kármán geometric non-linearity. The small-scale effects are also included in both models by the consideration of Eringen's non-local elasticity and the time domain equations of motion are obtained in the weak formulation after the application of the Galerkin method. For the study of linear vibration, the eigenvalue-type problem is solved using *Maple 2015* software and the linear natural frequencies and mode shapes are obtained. For the non-linear problem, the harmonic balance method is employed and the frequency domain equations of motion are derived, which are posteriorly solved by an arc-length continuation method implemented in *Fortran*. The variation of the natural frequencies with the amplitude of vibration of a single layer graphene sheet is subsequently studied.

1.5 Thesis Outline

In chapter 2 the mathematical formulation of the first model (based on the p-version finite element method) is presented. The determination of the equations of motion is demonstrated in detail, from the initial consideration of Kirchhoff's thin plate theory to the application of the Galerkin method and the harmonic balance method. The arc-length continuation method employed to solve the non-linear system of equations is also thoroughly described.

In chapter 3 the model devised in the previous chapter is verified by comparing the results obtained with those in the present literature. For the linear vibration problem, size and non-local effects on the linear natural frequencies and mode shapes are investigated and a comparison between an isotropic and orthotropic model is performed. For the non-linear case, the backbone curves are obtained with different parameters and are then compared with the results given by different authors.

In chapter 4 the model based on Airy's stress function is formulated and posteriorly validated. The backbone curves are obtained with a different number of harmonics and the

influence of the small-scale effect is studied on each individual harmonic. Lastly, different modes of vibration of an orthotropic single layer graphene sheet are investigated.

In chapter 5 the conclusions of this thesis and possible future work in the subject are presented.

Chapter 2

Mathematical Formulation

2.1 Introduction

In this chapter the mathematical formulation of the p-version finite element model will be presented. The chapter is divided according to the order in which the model was developed and in the first section the Kirchhoff plate theory is introduced. The general displacement field and the associated strains are calculated and the equations of motion are subsequently determined, after the definition of the energies involved in the system and the application of Hamilton's Principle. In the following section, Eringen's non-local theory is summarized and introduced in the already established equations of motion. The p-version finite element method is then briefly described and the Galerkin method is applied in order to convert the differential equations into a weak formulation system. After the discretization in the spatial variables, the harmonic balance method is used to discretize the time continuous equations into algebraic frequency domain ones, allowing finally the application of an arc-length continuation method to numerically solve the non-linear equations.

2.2 Kirchhoff Plate Theory

According to [36, 46] and considering the rectangular Cartesian coordinates (x, y, z), an initially undeformed thin plate with its middle plane, denoted Ω, coincident with the xy-plane, can have its displacement field written as:

$$u(x, y, z, t) = u^0(x, y, t) - z\frac{\partial w^0}{\partial x} \tag{2.1a}$$

$$v(x, y, z, t) = v^0(x, y, t) - z\frac{\partial w^0}{\partial y} \tag{2.1b}$$

$$w(x, y, z, t) = w^0(x, y, t) \tag{2.1c}$$

where u^0, v^0, w^0 refer to the displacements in the middle plane in the x, y, z coordinate directions respectively and can be visualized in Figure 2.1.

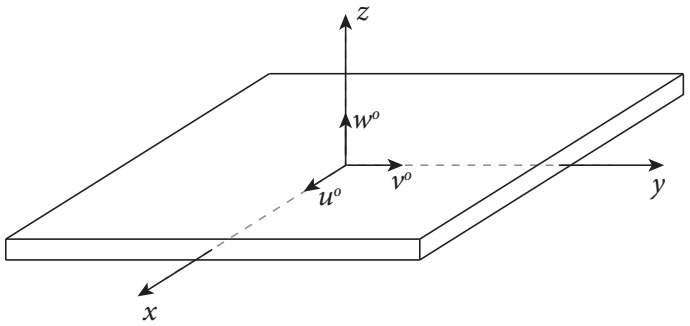

Figure 2.1: Axis and middle-plane displacements of the plate

For an accurate modelling of a thin nano-plate it is necessary to consider the geometric non-linear terms of the strains associated with the displacement field, since the plate is assumed to have a high amplitude motion to thickness ratio. These are generally referred as Von Kármán strains, which are non-linear with respect to the transverse displacement [36, 46]:

$$\varepsilon_{xx} = \varepsilon^0_{xx} + zk_{xx} = \frac{\partial u^0}{\partial x} + \frac{1}{2}\left(\frac{\partial w^0}{\partial x}\right)^2 - z\frac{\partial^2 w^0}{\partial x^2} \tag{2.2a}$$

$$\gamma_{xy} = 2\varepsilon_{xy} = \gamma^0_{xy} + zk_{xy} = \frac{\partial u^0}{\partial y} + \frac{\partial v^0}{\partial x} + \frac{\partial w^0}{\partial x}\frac{\partial w^0}{\partial y} - 2z\frac{\partial^2 w^0}{\partial x \partial y} \tag{2.2b}$$

$$\varepsilon_{yy} = \varepsilon^0_{yy} + zk_{yy} = \frac{\partial v^0}{\partial y} + \frac{1}{2}\left(\frac{\partial w^0}{\partial y}\right)^2 - z\frac{\partial^2 w^0}{\partial y^2} \tag{2.2c}$$

$$\gamma_{xz} = 0 \tag{2.2d}$$

$$\gamma_{yz} = 0 \tag{2.2e}$$

$$\varepsilon_{zz} = 0 \tag{2.2f}$$

The effects of transverse shear deformation are evidently neglected in the Kirchhoff plate theory.

According to Hamilton's Principle, the variation of mechanical energy in time is null:

$$\int_{t_1}^{t_2} \{\delta U + \delta V - \delta K\}\, \mathrm{d}t \;\; = \;\; 0 \tag{2.3}$$

where δU, δV, δK designate the variation in potential energy, the variation in work and the variation in kinetic energy respectively.

The variation in potential energy can be written as follows:

$$\begin{aligned} \delta U &= \int_\Omega \int_{-\frac{h}{2}}^{\frac{h}{2}} (\sigma_{xx}\delta\varepsilon_{xx} + \sigma_{yy}\delta\varepsilon_{yy} + \tau_{xy}\delta\gamma_{xy})\mathrm{d}z\mathrm{d}\Omega \\ &= \int_\Omega \int_{-\frac{h}{2}}^{\frac{h}{2}} (\sigma_{xx}(\delta\varepsilon^0_{xx} + z\delta k_{xx}) + \sigma_{yy}(\delta\varepsilon^0_{yy} + z\delta k_{yy}) + \tau_{xy}(\delta\gamma^0_{xy} + z\delta k_{xy}))\mathrm{d}z\mathrm{d}\Omega \end{aligned} \tag{2.4}$$

Considering the stress resultant in-plane forces N_{xx},N_{yy},N_{xy} and moments M_{xx},M_{yy},M_{xy} and their relation with the stress field, one can write:

$$\left\{ \begin{array}{c} N_{xx} \\ N_{yy} \\ N_{xy} \end{array} \right\} = \int_{-\frac{h}{2}}^{\frac{h}{2}} \left\{ \begin{array}{c} \sigma_{xx} \\ \sigma_{yy} \\ \tau_{xy} \end{array} \right\} \mathrm{d}z \tag{2.5a}$$

$$\left\{ \begin{array}{c} M_{xx} \\ M_{yy} \\ M_{xy} \end{array} \right\} = \int_{-\frac{h}{2}}^{\frac{h}{2}} \left\{ \begin{array}{c} \sigma_{xx} \\ \sigma_{yy} \\ \tau_{xy} \end{array} \right\} z\mathrm{d}z \tag{2.5b}$$

After substituting (2.5) in (2.4) and subsequently integrating along the thickness of the plate, the variation in potential energy can be written as a function of membrane forces and moments and of variations in strain components:

$$\delta U = \int_{\Omega} (N_{xx}\delta\varepsilon^0_{xx} + M_{xx}\delta k_{xx} + N_{yy}\delta\varepsilon^0_{yy} + M_{yy}\delta k_{yy} + N_{xy}\delta\gamma^0_{xy} + M_{xy}\delta k_{xy})\mathrm{d}\Omega \tag{2.6}$$

These variation in strains are given below:

$$\delta\varepsilon^0_{xx} = \frac{\partial}{\partial x}\delta u^0 + \frac{\partial w^0}{\partial x}\frac{\partial}{\partial x}\delta w^0 \tag{2.7a}$$

$$\delta k_{xx} = -\frac{\partial^2}{\partial x^2}\delta w^0 \tag{2.7b}$$

$$\delta\varepsilon^0_{yy} = \frac{\partial}{\partial y}\delta v^0 + \frac{\partial w^0}{\partial y}\frac{\partial}{\partial y}\delta w^0 \tag{2.7c}$$

$$\delta k_{yy} = -\frac{\partial^2}{\partial y^2}\delta w^0 \tag{2.7d}$$

$$\delta\gamma^0_{xy} = \frac{\partial}{\partial y}\delta u^0 + \frac{\partial}{\partial x}\delta v^0 + \frac{\partial}{\partial x}\delta w^0\frac{\partial w^0}{\partial y} + \frac{\partial w^0}{\partial x}\frac{\partial}{\partial y}\delta w^0 \tag{2.7e}$$

$$\delta k_{xy} = -2\frac{\partial^2}{\partial x\partial y}\delta w^0 \tag{2.7f}$$

Similarly, the variation in kinetic energy can be expressed as:

$$\begin{aligned} \delta K = &\int_{\Omega}\int_{-\frac{h}{2}}^{\frac{h}{2}} \rho\left(\dot{u}\delta\dot{u} + \dot{v}\delta\dot{v} + \dot{w}\delta\dot{w}\right)\mathrm{d}z\mathrm{d}\Omega = \\ &\int_{\Omega}\int_{-\frac{h}{2}}^{\frac{h}{2}} \rho\left[\left(\dot{u}^0 - z\frac{\partial\dot{w}^0}{\partial x}\right)\left(\delta\dot{u}^0 - z\frac{\partial}{\partial x}\delta\dot{w}^0\right) + \left(\dot{v}^0 - z\frac{\partial}{\partial y}\delta\dot{w}^0\right)\left(\delta\dot{v}^0 - z\frac{\partial}{\partial y}\delta\dot{w}^0\right) + \dot{w}^0\delta\dot{w}^0\right] \\ &\mathrm{d}z\mathrm{d}\Omega = \int_{\Omega}\left[\rho h\left(\dot{u}^0\delta\dot{u}^0 + \dot{v}^0\delta\dot{v}^0 + \dot{w}^0\delta\dot{w}^0\right) + \frac{\rho h^3}{12}\left(\frac{\partial\dot{w}^0}{\partial x}\frac{\partial}{\partial x}\delta\dot{w}^0 + \frac{\partial\dot{w}^0}{\partial y}\frac{\partial}{\partial y}\delta\dot{w}^0\right)\right]\mathrm{d}\Omega \end{aligned} \tag{2.8}$$

where $\dot{u}^0$,$\dot{v}^0$,$\dot{w}^0$ denote the velocity components in the middle plane in the x, y, z directions and $\delta\dot{u}^0$,$\delta\dot{v}^0$,$\delta\dot{w}^0$ their variation respectively.

Introducing (2.7a)-(2.7f) into (2.6) and substituting δU and δK in equation (2.3), considering no forces applied (which results in $\delta V = 0$) since only free vibration will be studied, and proceeding by integrating so as to remove all derivatives of variational terms:

$$
\begin{aligned}
0 &= \int_{t_1}^{t_2} (\delta U - \delta K)\,\mathrm{d}t \\
&= \int_{t_1}^{t_2} \left\{ \int_\Omega \left[N_{xx} \left(\frac{\partial}{\partial x}\delta u^0 + \frac{\partial w^0}{\partial x}\frac{\partial}{\partial x}\delta w^0 \right) + M_{xx} \left(-\frac{\partial^2}{\partial x^2}\delta w^0 \right) + N_{yy} \left(\frac{\partial}{\partial y}\delta v_0 + \frac{\partial w^0}{\partial y}\frac{\partial}{\partial y}\delta w^0 \right) \right.\right. \\
&+ M_{yy} \left(-\frac{\partial^2}{\partial y^2}\delta w^0 \right) + N_{xy} \left(\frac{\partial}{\partial y}\delta u^0 + \frac{\partial}{\partial x}\delta v^0 + \frac{\partial}{\partial x}\delta w^0 \frac{\partial w^0}{\partial y} + \frac{\partial w^0}{\partial x}\frac{\partial}{\partial y}\delta w^0 \right) \\
&\left. + M_{xy} \left(-2\frac{\partial^2}{\partial x \partial y}\delta w^0 \right) \right] \mathrm{d}\Omega - \int_\Omega \left[\rho h \left(\dot{u}^0 \delta \dot{u}^0 + \dot{v}^0 \delta \dot{v}^0 + \dot{w}^0 \delta \dot{w}^0 \right) + \frac{\rho h^3}{12} \left(\frac{\partial \dot{w}^0}{\partial x}\frac{\partial}{\partial x}\delta \dot{w}^0 \right.\right. \\
&\left.\left. + \frac{\partial \dot{w}^0}{\partial y}\frac{\partial}{\partial y}\delta \dot{w}^0 \right) \right] \mathrm{d}\Omega \Bigg\} \mathrm{d}t = \int_{t_1}^{t_2} \int_\Omega \left\{ - \left[\frac{\partial N_{xx}}{\partial x} + \frac{\partial N_{xy}}{\partial y} - \rho h \ddot{u}^0 \right] \delta u^0 - \left[\frac{\partial N_{yy}}{\partial y} + \frac{\partial N_{xy}}{\partial x} - \rho h \ddot{v}^0 \right] \right. \\
&\delta v^0 - \left[\aleph + \frac{\partial^2 M_{xx}}{\partial x^2} + \frac{\partial^2 M_{yy}}{\partial y^2} + 2\frac{\partial^2 M_{xy}}{\partial y \partial x} - \rho h \ddot{w}^0 + \frac{\rho h^3}{12} \left(\frac{\partial^2 \ddot{w}^0}{\partial x^2} + \frac{\partial^2 \ddot{w}^0}{\partial y^2} \right) \right] \delta w^0 \Bigg\} \mathrm{d}\Omega \mathrm{d}t
\end{aligned}
\tag{2.9}
$$

where $\aleph$ represents the resulting non-linear terms from the inclusion of geometrical non-linearity:

$$
\aleph = \frac{\partial}{\partial x} \left(N_{xx}\frac{\partial w^0}{\partial x} + N_{xy}\frac{\partial w^0}{\partial y} \right) + \frac{\partial}{\partial y} \left(N_{xy}\frac{\partial w^0}{\partial x} + N_{yy}\frac{\partial w^0}{\partial y} \right) \tag{2.10}
$$

The equations of motion of the plate are finally obtained by collecting the terms affected by δu^0,δv^0,δw^0 and setting each to zero:

$$
\frac{\partial N_{xx}}{\partial x} + \frac{\partial N_{xy}}{\partial y} = \rho h \ddot{u}^0 \tag{2.11}
$$

$$
\frac{\partial N_{xy}}{\partial x} + \frac{\partial N_{yy}}{\partial y} = \rho h \ddot{v}^0 \tag{2.12}
$$

$$
\frac{\partial^2 M_{xx}}{\partial x^2} + 2\frac{\partial^2 M_{xy}}{\partial y \partial x} + \frac{\partial^2 M_{yy}}{\partial y^2} + \aleph = \rho h \ddot{w}^0 - \underbrace{\frac{\rho h^3}{12} \left(\frac{\partial^2 \ddot{w}^0}{\partial x^2} + \frac{\partial^2 \ddot{w}^0}{\partial y^2} \right)}_{\text{rotary inertia}} \tag{2.13}
$$

The rotary inertia will be neglected as these terms are relevant at higher frequencies of vibration and generally have very little influence on the dynamics of thin plates. The in-plane inertia components will also be neglected since these are considerably small [47]:

$$\frac{\partial N_{xx}}{\partial x} + \frac{\partial N_{xy}}{\partial y} = 0 \tag{2.14}$$

$$\frac{\partial N_{xy}}{\partial x} + \frac{\partial N_{yy}}{\partial y} = 0 \tag{2.15}$$

$$\frac{\partial^2 M_{xx}}{\partial x^2} + 2\frac{\partial^2 M_{xy}}{\partial y \partial x} + \frac{\partial^2 M_{yy}}{\partial y^2} + \aleph = \rho h \ddot{w}^0 \tag{2.16}$$

With this assumption it is now possible to simplify (2.10) considering the first two equations of motion (2.14) and (2.15):

$$\begin{aligned} \aleph = & \frac{\partial N_{xx}}{\partial x}\frac{\partial w^0}{\partial x} + N_{xx}\frac{\partial^2 w^0}{\partial x^2} + \frac{\partial N_{xy}}{\partial x}\frac{\partial w^0}{\partial y} + N_{xy}\frac{\partial^2 w^0}{\partial x \partial y} \\ & + \frac{\partial N_{xy}}{\partial y}\frac{\partial w^0}{\partial x} + N_{xy}\frac{\partial^2 w^0}{\partial y \partial x} + \frac{\partial N_{yy}}{\partial y}\frac{\partial w^0}{\partial y} + N_{yy}\frac{\partial^2 w^0}{\partial y^2} \\ \approx & N_{xx}\frac{\partial^2 w^0}{\partial x^2} + 2N_{xy}\frac{\partial^2 w^0}{\partial y \partial x} + N_{yy}\frac{\partial^2 w^0}{\partial y^2} \end{aligned} \tag{2.17}$$

2.3 Non-Local Elasticity

Eringen's theory of non-local continuum mechanics includes scale effects and long-range atomic interactions allowing the modelling of nanosized structures. It can be included in a continuum model of an atomic lattice structure so as to avoid discrete atomistic or molecular simulations that imply a significantly larger computational effort. Considering [35, 44], for a generic non-local linear elastic solid, the equations of motion are:

$$t_{ij,j} + f_i = \rho \ddot{u}_i \tag{2.18}$$

with ρ,f_i,u_i designating the mass density, applied forces and the displacement vector respectively. The stress tensor t_{ij} in non-local elasticity is defined by:

$$t_{ij}(x) = \int_V \alpha\left(|x' - x|\right) \sigma_{ij}(x') \mathrm{d}v(x') \tag{2.19}$$

where x is a reference point in the body, $\alpha\left(|x' - x|\right)$ is the non-local kernel function (the properties of which have been thoroughly discussed in [4]) and $\sigma_{ij}(x')$ is the local stress tensor of classical elasticity theory at any point x'. Based on this theory, the stress at an arbitrary point in not only a function of the components of strain at that point but also a function of strain at all other points of the structure. It is obviously a size-dependent theory and for large dimensions it reduces to the traditional local theory of elasticity (when the internal characteristic length is much smaller than the external or macroscopic length of the structure).

Solving the integral relation between stress and displacements presented in (2.19) is rather difficult so, alternatively, Eringen proposed a simpler equivalent differential constitutive relation which has been widely adopted [44]. First, when the non-local kernel function of x, $\alpha(|x|)$, takes on a Green's function of a linear differential operator $\mathcal{L}$:

$$\mathcal{L}\alpha\left(|x'-x|\right) = \delta\left(|x'-x|\right) \tag{2.20}$$

Simplifying the constitutive relation above:

$$\mathcal{L}t_{ij} = \sigma_{ij} \tag{2.21}$$

Analogously, the integro-partial differential equation (2.18) can be reduced to a much simpler partial differential equation:

$$\sigma_{ij,j} + \mathcal{L}(f_i - \ddot{u}_i) = 0 \tag{2.22}$$

Finally, by matching the dispersion curves with lattice models, Eringen proposed the following definition for the linear differential operator:

$$\mathcal{L} = 1 - (e_0 a_i)^2 \nabla^2 \tag{2.23}$$

and applying (2.23) to (2.21):

$$\left[1 - (e_0 a_i)^2 \nabla^2\right] t_{ij} = Q_{ijkl}\varepsilon_{kl} \tag{2.24}$$

where a_i is an internal characteristic length (lattice parameter, granular size or molecular diameter), e_0 is an empirical material constant, Q_{ijkl} are the elastic modulus components, ε_{kl} is the strain tensor and ∇^2 denotes de Laplacian operator $\nabla^2 = \frac{\partial^2}{\partial x^2} + \frac{\partial^2}{\partial y^2}$. Hereafter, for a matter of simplicity, a non-local parameter $\mu = (e_0 a_i)^2$ is employed.

Extending the non-local elastic theory to a thin plate structure, the constitutive relations between the in-plane forces N_{xx}, N_{yy}, N_{yy}, the moments M_{xx}, M_{yy}, M_{yy} and the displacements considering (2.24), (2.5a), (2.5b) and (2.2a)-(2.2f) can be written as follows:

$$\left\{\begin{array}{c} N_{xx} \\ N_{yy} \\ N_{xy} \end{array}\right\} - \mu\nabla^2 \left\{\begin{array}{c} N_{xx} \\ N_{yy} \\ N_{xy} \end{array}\right\} = \left[\begin{array}{ccc} A_{11} & A_{12} & 0 \\ A_{12} & A_{22} & 0 \\ 0 & 0 & A_{33} \end{array}\right] \left\{\begin{array}{c} \frac{\partial u^0}{\partial x} + \frac{1}{2}\left(\frac{\partial w^0}{\partial x}\right)^2 \\ \frac{\partial v^0}{\partial y} + \frac{1}{2}\left(\frac{\partial w^0}{\partial y}\right)^2 \\ \frac{\partial u^0}{\partial y} + \frac{\partial v^0}{\partial x} + \frac{\partial w^0}{\partial x}\frac{\partial w^0}{\partial y} \end{array}\right\} \tag{2.25}$$

$$\left\{\begin{array}{c} M_{xx} \\ M_{yy} \\ M_{xy} \end{array}\right\} - \mu\nabla^2 \left\{\begin{array}{c} M_{xx} \\ M_{yy} \\ M_{xy} \end{array}\right\} = -\left[\begin{array}{ccc} D_{11} & D_{12} & 0 \\ D_{12} & D_{22} & 0 \\ 0 & 0 & D_{33} \end{array}\right] \left\{\begin{array}{c} \frac{\partial^2 w^0}{\partial x^2} \\ \frac{\partial^2 w^0}{\partial y^2} \\ 2\frac{\partial^2 w^0}{\partial x \partial y} \end{array}\right\} \tag{2.26}$$

where the coefficients of matrix $[A_{ij}]$ and $[D_{ij}]$ can be determined by integrating the respective elasticity matrix coefficients along the thickness of the plate:

$$(A_{ij}, D_{ij}) = \int_{-\frac{h}{2}}^{\frac{h}{2}} Q_{ij} \left(1, z^2\right) \mathrm{d}z = (h, \frac{h^3}{12}) Q_{ij} \tag{2.27}$$

For the generic case of an orthotropic material, the elasticity matrix $[Q_{ij}]$ can be defined as:

$$[Q_{ij}] = \begin{bmatrix} \frac{E_1}{1-\nu_{12}\nu_{21}} & \frac{\nu_{12}E_2}{1-\nu_{12}\nu_{21}} & 0 \\ \frac{\nu_{12}E_2}{1-\nu_{12}\nu_{21}} & \frac{E_2}{1-\nu_{12}\nu_{21}} & 0 \\ 0 & 0 & G_{12} \end{bmatrix} \tag{2.28}$$

where the Poisson ratio ν_{21} can be determined in the following way:

$$\nu_{21} = \frac{\nu_{12}E_2}{E_1} \tag{2.29}$$

and for the particular case of an isotropic material, the matrix $[Q_{ij}]$ is given by:

$$[Q_{ij}] = \begin{bmatrix} \frac{E}{1-\nu^2} & \frac{\nu E}{1-\nu^2} & 0 \\ \frac{\nu E}{1-\nu^2} & \frac{E}{1-\nu^2} & 0 \\ 0 & 0 & \frac{E}{2(1+\nu)} \end{bmatrix} \tag{2.30}$$

Applying the linear differential operator $\mathcal{L}$ to the equations of motion (2.14), (2.15), (2.16) and considering the constitutive relations expressed in (2.25) and (2.26):

$$\frac{\partial}{\partial x}\left\{A_{11}\left(\frac{\partial u^0}{\partial x} + \frac{1}{2}\left(\frac{\partial w^0}{\partial x}\right)^2\right) + A_{12}\left(\frac{\partial v^0}{\partial y} + \frac{1}{2}\left(\frac{\partial w^0}{\partial y}\right)^2\right)\right\} + \frac{\partial}{\partial y}\left\{A_{33}\left(\frac{\partial u^0}{\partial y} + \frac{\partial v^0}{\partial x} + \frac{\partial w^0}{\partial x}\frac{\partial w^0}{\partial y}\right)\right\} = 0 \tag{2.31}$$

$$\frac{\partial}{\partial y}\left\{A_{12}\left(\frac{\partial u^0}{\partial x} + \frac{1}{2}\left(\frac{\partial w^0}{\partial x}\right)^2\right) + A_{22}\left(\frac{\partial v^0}{\partial y} + \frac{1}{2}\left(\frac{\partial w^0}{\partial y}\right)^2\right)\right\} + \frac{\partial}{\partial x}\left\{A_{33}\left(\frac{\partial u^0}{\partial y} + \frac{\partial v^0}{\partial x} + \frac{\partial w^0}{\partial x}\frac{\partial w^0}{\partial y}\right)\right\} = 0 \tag{2.32}$$

$$-D_{11}\frac{\partial^4 w^0}{\partial x^4} - 2\left(D_{12} + 2D_{33}\right)\frac{\partial^4 w^0}{\partial x^2 \partial y^2} - D_{22}\frac{\partial^4 w^0}{\partial y^4} + \mathcal{L}\left(\aleph\right) = (1 - \mu\nabla^2)\rho h\ddot{w}^0 \tag{2.33}$$

Simplifying the term $\mathcal{L}(\aleph)$ is necessary to posteriorly formulate a viable discrete model. Two different approaches were considered as ways of simplifying this problem. The first attempt was proposed by Reddy in [36] but was discarded here due to its oversimplification.

Regardless, considering (2.17), the approximation proposed in [36] is as follows:

$$\begin{aligned}\mathcal{L}(\aleph) &= \mathcal{L}\left(N_{xx}\frac{\partial^2 w^0}{\partial x^2} + 2N_{xy}\frac{\partial^2 w^0}{\partial y \partial x} + N_{yy}\frac{\partial^2 w^0}{\partial y^2}\right) \\ &\approx \mathcal{L}\left(N_{xx}\right)\frac{\partial^2 w^0}{\partial x^2} + \mathcal{L}\left(2N_{xy}\right)\frac{\partial^2 w^0}{\partial y \partial x} + \mathcal{L}\left(N_{yy}\right)\frac{\partial^2 w^0}{\partial y^2}\end{aligned} \tag{2.34}$$

Taking the constitutive relations for the forces N_{xx}, N_{yy}, N_{xy} established in (2.25) into account, (2.34) becomes:

$$\begin{aligned}\mathcal{L}(\aleph) \approx &\left[A_{11}\left(\frac{\partial u^0}{\partial x} + \frac{1}{2}\left(\frac{\partial w^0}{\partial x}\right)^2\right) + A_{12}\left(\frac{\partial v^0}{\partial y} + \frac{1}{2}\left(\frac{\partial w^0}{\partial y}\right)^2\right)\right]\frac{\partial^2 w^0}{\partial x^2} \\ &+ 2A_{33}\left(\frac{\partial u^0}{\partial y} + \frac{\partial v^0}{\partial x} + \frac{\partial w^0}{\partial x}\frac{\partial w^0}{\partial y}\right)\frac{\partial^2 w^0}{\partial x \partial y} \\ &+ \left[A_{12}\left(\frac{\partial u^0}{\partial x} + \frac{1}{2}\left(\frac{\partial w^0}{\partial x}\right)^2\right) + A_{22}\left(\frac{\partial v^0}{\partial y} + \frac{1}{2}\left(\frac{\partial w^0}{\partial y}\right)^2\right)\right]\frac{\partial^2 w^0}{\partial y^2}\end{aligned} \tag{2.35}$$

It should be noted that in this simplification the effect of the non-local parameter on the non-linear terms vanishes, hence the oversimplification. The alternative approximation, which was considered in this work, is similar to the one used in [48]. Defining $\mathcal{L}(\aleph)$ generically:

$$\mathcal{L}(\aleph) = \mathcal{L}\left(\sum_{i=1}^{3}\mathcal{F}_i\mathcal{D}_i\right) \tag{2.36}$$

where $\mathcal{F}_i$ denotes a membrane force N_{xx}, $2N_{xy}$ or N_{yy} and $\mathcal{D}_i$ designates a second order spatial partial derivative of the transverse displacement $\frac{\partial^2 w^0}{\partial x^2}$, $\frac{\partial^2 w^0}{\partial y \partial x}$ or $\frac{\partial^2 w^0}{\partial y^2}$. Considering the constitutive relations, which are applicable to the force component $\mathcal{F}_i$, equation (2.25) can be written in generic terms as follows:

$$\mathcal{L}(\mathcal{F}_i) = \left(1 - \mu\nabla^2\right)\mathcal{F}_i = \mathcal{F}_i^L \tag{2.37}$$

where $\mathcal{F}_i^L$ is the product between the coefficients matrix $[A_{ij}]$ and the strain components vector. Therefore:

$$\mathcal{F}_i = \mathcal{F}_i^L + \mu\nabla^2\mathcal{F}_i \tag{2.38}$$

Rewriting (2.36) with (2.38):

$$\begin{aligned}\mathcal{L}(\aleph) &= \sum_{i=1}^{3}\left(1-\mu\nabla^2\right)\left(\mathcal{F}_i\mathcal{D}_i\right) = \sum_{i=1}^{3}\left(1-\mu\nabla^2\right)\left[\left(\mathcal{F}_i^L+\mu\nabla^2\mathcal{F}_i\right)\mathcal{D}_i\right] \\ &= \sum_{i=1}^{3}\left(1-\mu\nabla^2\right)\left(\mathcal{F}_i^L\mathcal{D}_i\right) + \underbrace{\left(1-\mu\nabla^2\right)\left[\left(\mu\nabla^2\mathcal{F}_i\right)\mathcal{D}_i\right]}_{\text{neglected}} \\ &\approx \sum_{i=1}^{3}\left(1-\mu\nabla^2\right)\left(\mathcal{F}_i^L\mathcal{D}_i\right)\end{aligned} \tag{2.39}$$

The terms resulting from this simplification will be presented further ahead.

2.4 The p-Version Finite Element Method

The most commonly used h-version finite element method relies on the increase of the number of elements used in the study of a given structure to ensure accuracy of the approximate model. In other words, a refined mesh or grid of elements (without changing the displacement field approximation in each element), which implies a reduction of each element's size, results in a better approximation, therefore providing more reliable results. Alternatively, it is possible to improve the accuracy by improving the approximation of the displacement field within the element using more and/or higher order polynomial shape functions with the element grid unchanged. The latter is known as the p-version finite element method. According to [10, 49], this variation gives more accurate results with fewer degrees of freedom than the h-version and allows the modelling of simple structures using only one element, thus greatly reducing the computational effort. In other words, the convergence ratio is significantly greater for the first case than the latter. However, for more complex structures, one element may not be sufficient to accurately represent them and multiple elements might have to be used.

Considering [10, 50–52], the sets of shape functions used are derived from Rodrigue's form of Legendre's orthogonal polynomials. For in-plane displacements, the set of shape functions used is given by:

$$g_r(\xi) = \sum_{n=0}^{\lfloor r/2\rfloor}\frac{(-1)^n(2r-2n-5)!!}{2^n n!(r-2n-1)!}\xi^{r-2n-1}, r>2 \tag{2.40}$$

and for the out-of-plane set of shape functions:

$$f_r(\xi) = \sum_{n=0}^{\lfloor r/2\rfloor}\frac{(-1)^n(2r-2n-7)!!}{2^n n!(r-2n-1)!}\xi^{r-2n-1}, r>4 \tag{2.41}$$

where $r!! = r(r-2)...(2 \text{ or } 1), 0!! = (-1)!! = 1$ and $\lfloor r/2\rfloor$ designates the integer part of $r/2$. The in-plane shape functions $g_r(\xi)$ have zero value at $\xi=-1$ and $\xi=1$ while the

out-of-plane shape functions $f_r(\xi)$ have both zero value and slope at those points, which are applicable to the case of a fully clamped plate. For a pinned plate or simply supported plate in all edges, the slope of the out-of-plane shape functions is not zero at the points mentioned since rotation is allowed and therefore it is possible to use the in-plane set typically used in a fully clamped case as out-of-plane functions.

Depending on the case to be studied, the appropriate set of shape functions can be selected by using solely odd or even indexes. The former correspond to symmetric shape functions with respect to the centre point $\xi = 0$ whilst the latter are anti-symmetric about the same point. Note that ξ and η refer to the natural or dimensionless coordinates and relate to the global x, y coordinates as follows (considering only one element to model the whole plate):

$$x = \frac{a}{2}\xi \tag{2.42a}$$

$$y = \frac{b}{2}\eta \tag{2.42b}$$

The middle plane displacements can be defined as the product of a shape function matrix and the vector of generalized nodal displacements:

$$\begin{aligned}\left\{de^0\right\} &= \left\{\begin{array}{c} u^0 \\ v^0 \\ w^0 \end{array}\right\} = [N]\{q\} \\ &= \left[\begin{array}{ccc} g_1g_1; g_1g_2; ...; g_{pi}g_{pi} & 0 & 0 \\ 0 & g_1g_1; g_1g_2; ...; g_{pi}g_{pi} & 0 \\ 0 & 0 & f_1f_1; f_1f_2; ...f_{po}f_{po} \end{array}\right]\{q\}\end{aligned} \tag{2.43}$$

with $\{q\}^T$ defined by:

$$\{q\}^T = \left\{\begin{array}{cccc} q^u_{11}; q^u_{12}; ...; q^u_{pipi} & q^v_{11}; q^v_{12}; ...; q^v_{pipi} & q^w_{11}; q^w_{12}; ...; q^w_{popo} \end{array}\right\} \tag{2.44}$$

where g_{ij}, f_{ij} stand for $g_i(x)g_j(y)$, $f_i(x)f_j(y)$ and pi, po denote the number of in-plane and out-of-plane shape functions used respectively.

Rewriting the matrix product expressed in (2.43) in a compact form:

$$\left\{de^0\right\} = \left\{\begin{array}{l} \sum_{r=1}^{pi}\sum_{s=1}^{pi} g_r(\xi)\, g_s(\eta)\, q^u_{rs}(t) \\ \sum_{r=1}^{pi}\sum_{s=1}^{pi} g_r(\xi)\, g_s(\eta)\, q^v_{rs}(t) \\ \sum_{r=1}^{po}\sum_{s=1}^{po} f_r(\xi)\, f_s(\eta)\, q^w_{rs}(t) \end{array}\right. \tag{2.45}$$

2.5 Galerkin Method

Converting the equations of motion of (2.31), (2.32) and (2.33) to a weak formulation by the application of the Galerkin method allows the discretization of a continuous partial differential equation problem into an algebraic one.

For the transformation of the global coordinates x, y into natural coordinates ξ, η it is necessary to establish the following relations derived from (2.42a) and (2.42b):

$$\mathrm{d}x = \frac{a}{2}\mathrm{d}\xi \tag{2.46a}$$

$$\mathrm{d}y = \frac{b}{2}\mathrm{d}\eta \tag{2.46b}$$

$$\frac{\mathrm{d}}{\mathrm{d}x} = \frac{2}{a}\frac{\mathrm{d}}{\mathrm{d}\xi} \tag{2.46c}$$

$$\frac{\mathrm{d}}{\mathrm{d}y} = \frac{2}{b}\frac{\mathrm{d}}{\mathrm{d}\eta} \tag{2.46d}$$

Applying the Galerkin method to the equations of motion expressed in a natural coordinate system, considering (2.46a) and (2.46b):

$$\frac{a}{2}\frac{b}{2}\int_{-1}^{1}\int_{-1}^{1} g_r(\xi)\, g_s(\eta)\, \mathcal{L}_u(\xi,\eta,t)\, \mathrm{d}\xi\mathrm{d}\eta \tag{2.47a}$$

$$\frac{a}{2}\frac{b}{2}\int_{-1}^{1}\int_{-1}^{1} g_r(\xi)\, g_s(\eta)\, \mathcal{L}_v(\xi,\eta,t)\, \mathrm{d}\xi\mathrm{d}\eta \tag{2.47b}$$

$$\frac{a}{2}\frac{b}{2}\int_{-1}^{1}\int_{-1}^{1} f_r(\xi)\, f_s(\eta)\, \mathcal{L}_w(\xi,\eta,t)\, \mathrm{d}\xi\mathrm{d}\eta \tag{2.47c}$$

where $\mathcal{L}_u$, $\mathcal{L}_v$, $\mathcal{L}_w$ are equations (2.31), (2.32) and (2.33) respectively, rearranged with all operands in one subexpression.

In order to consider all possible products between shape functions, eight auxiliary variables were used, in which n denotes the number of shape functions (*pi* for in-plane and *po* for out-of plane). This procedure was similar to the one used in [53].

As it was previously mentioned, the notation $\lfloor\rfloor$ designates the integer part of a given number.

$$\begin{array}{cccc} i\xi = \lfloor\frac{i-1}{n}\rfloor + 1 & j\xi = \lfloor\frac{j-1}{n}\rfloor + 1 & k\xi = \lfloor\frac{k-1}{n}\rfloor + 1 & l\xi = \lfloor\frac{l-1}{n}\rfloor + 1 \\ i\eta = i - \lfloor\frac{i-1}{n}\rfloor \times n & j\eta = j - \lfloor\frac{j-1}{n}\rfloor \times n & k\eta = k - \lfloor\frac{k-1}{n}\rfloor \times n & l\eta = l - \lfloor\frac{l-1}{n}\rfloor \times n \end{array} \tag{2.48}$$

For a matter of simplification, both the Galerkin method and the transformation of coordinates within $\mathcal{L}_u$, $\mathcal{L}_v$ and $\mathcal{L}_w$ were applied to each constitutive term individually, as it will be demonstrated ahead. Also, the shape functions considered such as $g_{i\xi}(\xi)$, $g_{i\eta}(\eta)$,..., will be written in the more compact form $g_{i\xi}$, $g_{i\eta}$,..., respectively, omitting the argument to avoid redundancy. For the first equation of motion, considering (2.47a):

$$\begin{aligned}\mathcal{L}_u(x,y,t) = \frac{\partial}{\partial x}\left\{A_{11}\left(\underbrace{\frac{\partial u^0}{\partial x}}_{\mathrm{t}(1)} + \underbrace{\frac{1}{2}\left(\frac{\partial w^0}{\partial x}\right)^2}_{\mathrm{t}(2)}\right) + A_{12}\left(\underbrace{\frac{\partial v^0}{\partial y}}_{\mathrm{t}(3)} + \underbrace{\frac{1}{2}\left(\frac{\partial w^0}{\partial y}\right)^2)}_{\mathrm{t}(4)}\right)\right\} \\ + \frac{\partial}{\partial y}\left\{A_{33}\left(\underbrace{\frac{\partial u^0}{\partial y}}_{\mathrm{t}(5)} + \underbrace{\frac{\partial v^0}{\partial x}}_{\mathrm{t}(6)} + \underbrace{\frac{\partial w^0}{\partial x}\frac{\partial w^0}{\partial y}}_{\mathrm{t}(7)}\right)\right\}\end{aligned} \tag{2.49}$$

$$\begin{aligned}t(1) &= A_{11}\frac{b}{a}\int_{-1}^{1}\int_{-1}^{1} g_{i\xi}g_{i\eta}\frac{\partial^2}{\partial\xi^2}\left(g_{j\xi}g_{j\eta}\right)\mathrm{d}\xi\mathrm{d}\eta q^u(j) \\ &= -A_{11}\frac{b}{a}\int_{-1}^{1}\frac{\partial g_{i\xi}}{\partial\xi}\frac{\partial g_{j\xi}}{\partial\xi}\mathrm{d}\xi\int_{-1}^{1} g_{i\eta}g_{j\eta}\mathrm{d}\eta q^u(j)\end{aligned} \tag{2.50}$$

$$\begin{aligned}t(2) &= \frac{b}{a^2}A_{11}\int_{-1}^{1}\int_{-1}^{1} g_{i\xi}g_{i\eta}\frac{\partial}{\partial\xi}\left(\frac{\partial\left(f_{j\xi}f_{j\eta}\right)}{\partial\xi}\frac{\partial\left(f_{k\xi}f_{k\eta}\right)}{\partial\xi}\right)\mathrm{d}\xi\mathrm{d}\eta q^w(k)q^w(j) \\ &= -\frac{b}{a^2}A_{11}\int_{-1}^{1}\frac{\partial g_{i\xi}}{\partial\xi}\frac{\partial f_{j\xi}}{\partial\xi}\frac{\partial f_{k\xi}}{\partial\xi}\mathrm{d}\xi\int_{-1}^{1} g_{i\eta}f_{j\eta}f_{k\eta}\mathrm{d}\eta q^w(k)q^w(j)\end{aligned} \tag{2.51}$$

$$\begin{aligned}t(3) &= A_{12}\int_{-1}^{1}\int_{-1}^{1} g_{i\xi}g_{i\eta}\frac{\partial}{\partial\xi}\left(\frac{\partial\left(g_{j\xi}g_{j\eta}\right)}{\partial\eta}\right)\mathrm{d}\xi\mathrm{d}\eta q^v(j) \\ &= -A_{12}\int_{-1}^{1}\frac{\partial g_{i\xi}}{\partial\xi}g_{j\xi}\mathrm{d}\xi\int_{-1}^{1} g_{i\eta}\frac{\partial g_{j\eta}}{\partial\eta}\mathrm{d}\eta q^v(j)\end{aligned} \tag{2.52}$$

$$\begin{aligned}t(4) &= \frac{A_{12}}{b}\int_{-1}^{1}\int_{-1}^{1} g_{i\xi}g_{i\eta}\frac{\partial}{\partial\xi}\left(\frac{\partial\left(f_{j\xi}f_{j\eta}\right)}{\partial\eta}\frac{\partial\left(f_{k\xi}f_{k\eta}\right)}{\partial\eta}\right)\mathrm{d}\xi\mathrm{d}\eta q^w(k)q^w(j) \\ &= -\frac{A_{12}}{b}\int_{-1}^{1}\frac{\partial g_{i\xi}}{\partial\xi}f_{j\xi}f_{k\xi}\mathrm{d}\xi\int_{-1}^{1} g_{i\eta}\frac{\partial f_{j\eta}}{\partial\eta}\frac{\partial f_{k\eta}}{\partial\eta}\mathrm{d}\eta q^w(k)q^w(j)\end{aligned} \tag{2.53}$$

$$\begin{aligned}t(5) &= A_{33}\frac{a}{b}\int_{-1}^{1}\int_{-1}^{1} g_{i\xi}g_{i\eta}\frac{\partial^2}{\partial\eta^2}\left(g_{j\xi}g_{j\eta}\right)\mathrm{d}\xi\mathrm{d}\eta q^u(j) \\ &= -A_{33}\frac{a}{b}\int_{-1}^{1} g_{i\xi}g_{j\xi}\mathrm{d}\xi\int_{-1}^{1}\frac{\partial g_{i\eta}}{\partial\eta}\frac{\partial g_{j\eta}}{\partial\eta}\mathrm{d}\eta q^u(j)\end{aligned} \tag{2.54}$$

$$\begin{aligned}t(6) &= A_{33}\int_{-1}^{1}\int_{-1}^{1} g_{i\xi}g_{i\eta}\frac{\partial}{\partial\eta}\left(\frac{\partial\left(g_{j\xi}g_{j\eta}\right)}{\partial\xi}\right)\mathrm{d}\xi\mathrm{d}\eta q^v(j) \\ &= -A_{33}\int_{-1}^{1} g_{i\xi}\frac{\partial g_{j\xi}}{\partial\xi}\mathrm{d}\xi\int_{-1}^{1}\frac{\partial g_{i\eta}}{\partial\eta}g_{j\eta}\mathrm{d}\eta q^v(j)\end{aligned} \tag{2.55}$$

$$\begin{aligned}t(7) &= A_{33}\frac{2}{b}\int_{-1}^{1}\int_{-1}^{1} g_{i\xi}g_{i\eta}\frac{\partial}{\partial\eta}\left(\frac{\partial\left(f_{j\xi}f_{j\eta}\right)}{\partial\xi}\frac{\partial\left(f_{k\xi}f_{k\eta}\right)}{\partial\eta}\right)\mathrm{d}\xi\mathrm{d}\eta q^w(k)q^w(j) \\ &= -A_{33}\frac{2}{b}\int_{-1}^{1} g_{i\xi}\frac{\partial f_{j\xi}}{\partial\xi}f_{k\xi}\mathrm{d}\xi\int_{-1}^{1}\frac{\partial g_{i\eta}}{\partial\eta}f_{j\eta}\frac{\partial f_{k\eta}}{\partial\eta}\mathrm{d}\eta q^w(k)q^w(j)\end{aligned} \tag{2.56}$$

Proceeding similarly for the second equation of motion and considering (2.47b):

$$\begin{aligned}\mathcal{L}_v(x,y,t) = &\frac{\partial}{\partial y}\left\{A_{12}\left(\underbrace{\frac{\partial u^0}{\partial x}}_{\mathrm{t}(8)} + \underbrace{\frac{1}{2}\left(\frac{\partial w^0}{\partial x}\right)^2}_{\mathrm{t}(9)}\right) + A_{22}\left(\underbrace{\frac{\partial v^0}{\partial y}}_{\mathrm{t}(10)} + \underbrace{\frac{1}{2}\left(\frac{\partial w^0}{\partial y}\right)^2}_{\mathrm{t}(11)}\right)\right\} \\ &+ \frac{\partial}{\partial x}\left\{A_{33}\left(\underbrace{\frac{\partial u^0}{\partial y}}_{\mathrm{t}(12)} + \underbrace{\frac{\partial v^0}{\partial x}}_{\mathrm{t}(13)} + \underbrace{\frac{\partial w^0}{\partial x}\frac{\partial w^0}{\partial y}}_{\mathrm{t}(14)}\right)\right\}\end{aligned} \tag{2.57}$$

$$\begin{aligned}t(8) &= A_{12}\int_{-1}^{1}\int_{-1}^{1} g_{i\xi}g_{i\eta}\frac{\partial}{\partial\eta}\left(\frac{\partial\left(g_{j\xi}g_{j\eta}\right)}{\partial\xi}\right)\mathrm{d}\xi\mathrm{d}\eta q^u(j) \\ &= -A_{12}\int_{-1}^{1} g_{i\xi}\frac{\partial g_{j\xi}}{\partial\xi}\mathrm{d}\xi\int_{-1}^{1}\frac{\partial g_{i\eta}}{\partial\eta}g_{j\eta}\mathrm{d}\eta q^u(j)\end{aligned} \tag{2.58}$$

$$\begin{aligned}t(9) &= \frac{A_{12}}{a}\int_{-1}^{1}\int_{-1}^{1} g_{i\xi}g_{i\eta}\frac{\partial}{\partial\eta}\left(\frac{\partial\left(f_{j\xi}f_{j\eta}\right)}{\partial\xi}\frac{\partial\left(f_{k\xi}f_{k\eta}\right)}{\partial\xi}\right)\mathrm{d}\xi\mathrm{d}\eta q^w(k)q^w(j) \\ &= -\frac{A_{12}}{a}\int_{-1}^{1} g_{i\xi}\frac{\partial f_{j\xi}}{\partial\xi}\frac{\partial f_{k\xi}}{\partial\xi}\mathrm{d}\xi\int_{-1}^{1}\frac{\partial g_{i\eta}}{\partial\eta}f_{j\eta}f_{k\eta}\mathrm{d}\eta q^w(k)q^w(j)\end{aligned} \tag{2.59}$$

$$\begin{aligned}t(10) &= A_{22}\frac{a}{b}\int_{-1}^{1}\int_{-1}^{1} g_{i\xi}g_{i\eta}\frac{\partial^2\left(g_{j\xi}g_{j\eta}\right)}{\partial\eta^2}\mathrm{d}\xi\mathrm{d}\eta q^v(j) \\ &= -A_{22}\frac{a}{b}\int_{-1}^{1} g_{i\xi}g_{j\xi}\mathrm{d}\xi\int_{-1}^{1}\frac{\partial g_{i\eta}}{\partial\eta}\frac{\partial g_{j\eta}}{\partial\eta}\mathrm{d}\eta q^v(j)\end{aligned} \tag{2.60}$$

$$\begin{aligned}t(11) &= A_{22}\frac{a}{b^2}\int_{-1}^{1}\int_{-1}^{1} g_{i\xi}g_{i\eta}\frac{\partial}{\partial\eta}\left(\frac{\partial\left(f_{j\xi}f_{j\eta}\right)}{\partial\eta}\frac{\partial\left(f_{k\xi}f_{k\eta}\right)}{\partial\eta}\right)\mathrm{d}\xi\mathrm{d}\eta q^w(k)q^w(j) \\ &= -A_{22}\frac{a}{b^2}\int_{-1}^{1} g_{i\xi}f_{j\xi}f_{k\xi}\mathrm{d}\xi\int_{-1}^{1}\frac{\partial g_{i\eta}}{\partial\eta}\frac{\partial f_{j\eta}}{\partial\eta}\frac{\partial f_{k\eta}}{\partial\eta}\mathrm{d}\eta q^w(k)q^w(j)\end{aligned} \tag{2.61}$$

$$\begin{aligned}t(12) &= A_{33}\int_{-1}^{1}\int_{-1}^{1} g_{i\xi}g_{i\eta}\frac{\partial}{\partial\xi}\left(\frac{\partial\left(g_{j\xi}g_{j\eta}\right)}{\partial\eta}\right)\mathrm{d}\xi\mathrm{d}\eta q^u(j) \\ &= -A_{33}\int_{-1}^{1}\frac{\partial g_{i\xi}}{\partial\xi}g_{j\xi}\mathrm{d}\xi\int_{-1}^{1} g_{i\eta}\frac{\partial g_{j\eta}}{\partial\eta}\mathrm{d}\eta q^u(j)\end{aligned} \tag{2.62}$$

$$\begin{aligned}t(13) &= A_{33}\frac{b}{a}\int_{-1}^{1}\int_{-1}^{1} g_{i\xi}g_{i\eta}\frac{\partial^2}{\partial\xi^2}\left(g_{j\xi}g_{j\eta}\right)\mathrm{d}\xi\mathrm{d}\eta q^v(j) \\ &= -A_{33}\frac{b}{a}\int_{-1}^{1}\frac{\partial g_{i\xi}}{\partial\xi}\frac{\partial g_{j\xi}}{\partial\xi}\mathrm{d}\xi\int_{-1}^{1} g_{i\eta}g_{j\eta}\mathrm{d}\eta q^v(j)\end{aligned} \tag{2.63}$$

$$\begin{aligned}t(14) &= A_{33}\frac{2}{a}\int_{-1}^{1}\int_{-1}^{1} g_{i\xi}g_{i\eta}\frac{\partial}{\partial\xi}\left(\frac{\partial\left(f_{j\xi}f_{j\eta}\right)}{\partial\xi}\frac{\partial\left(f_{k\xi}f_{k\eta}\right)}{\partial\eta}\right)\mathrm{d}\xi\mathrm{d}\eta q^w(k)q^w(j) \\ &= -A_{33}\frac{2}{a}\int_{-1}^{1}\frac{\partial g_{i\xi}}{\partial\xi}\frac{\partial f_{j\xi}}{\partial\xi}f_{k\xi}\mathrm{d}\xi\int_{-1}^{1} g_{i\eta}f_{j\eta}\frac{\partial f_{k\eta}}{\partial\eta}\mathrm{d}\eta q^w(k)q^w(j)\end{aligned} \tag{2.64}$$

For the third equation and considering (2.47c):

$$\mathcal{L}_w(x,y,t) = \underbrace{-D_{11}\frac{\partial^4 w^0}{\partial x^4}}_{\mathrm{t}(15)} \underbrace{-2\left(D_{12}+2D_{33}\right)\frac{\partial^4 w^0}{\partial x^2 \partial y^2}}_{\mathrm{t}(16)} \underbrace{-D_{22}\frac{\partial^4 w^0}{\partial y^4}}_{\mathrm{t}(17)} + \underbrace{\mathcal{L}(\aleph)}_{\mathrm{t}(18)} - (\underbrace{1}_{\mathrm{t}(19)} - \underbrace{\mu\nabla^2}_{\mathrm{t}(20)})\rho h\ddot{w}^0 \tag{2.65}$$

$$\begin{aligned} t(15) &= -D_{11}\frac{4b}{a^3}\int_{-1}^{1}\int_{-1}^{1} f_{i\xi}f_{i\eta}\frac{\partial^4}{\partial\xi^4}\left(f_{j\xi}f_{j\eta}\right)\mathrm{d}\xi\mathrm{d}\eta q^w(j) \\ &= -D_{11}\frac{4b}{a^3}\int_{-1}^{1}\frac{\partial^2 f_{i\xi}}{\partial\xi^2}\frac{\partial^2 f_{j\xi}}{\partial\xi^2}\mathrm{d}\xi\int_{-1}^{1} f_{i\eta}f_{j\eta}\mathrm{d}\eta q^w(j) \end{aligned} \tag{2.66}$$

$$\begin{aligned} t(16) &= -2\left(D_{12}+2D_{33}\right)\frac{4}{ab}\int_{-1}^{1}\int_{-1}^{1} f_{i\xi}f_{i\eta}\frac{\partial^4}{\partial\xi^2\partial\eta^2}\left(f_{j\xi}f_{j\eta}\right)\mathrm{d}\xi\mathrm{d}\eta q^w(j) \\ &= -\frac{8}{ab}\left(D_{12}+2D_{33}\right)\int_{-1}^{1}\frac{\partial f_{i\xi}}{\partial\xi}\frac{\partial f_{j\xi}}{\partial\xi}\mathrm{d}\xi\int_{-1}^{1}\frac{\partial f_{i\eta}}{\partial\eta}\frac{\partial f_{j\eta}}{\partial\eta}\mathrm{d}\eta q^w(j) \end{aligned} \tag{2.67}$$

$$\begin{aligned} t(17) &= -D_{22}\frac{4a}{b^3}\int_{-1}^{1}\int_{-1}^{1} f_{i\xi}f_{i\eta}\frac{\partial^4}{\partial\eta^4}\left(f_{j\xi}f_{j\eta}\right)\mathrm{d}\xi\mathrm{d}\eta q^w(j) \\ &= -D_{22}\frac{4a}{b^3}\int_{-1}^{1} f_{i\xi}f_{j\xi}\mathrm{d}\xi\int_{-1}^{1}\frac{\partial^2 f_{i\eta}}{\partial\eta^2}\frac{\partial^2 f_{j\eta}}{\partial\eta^2}\mathrm{d}\eta q^w(j) \end{aligned} \tag{2.68}$$

$$t(19) = -\frac{\rho hab}{4}\int_{-1}^{1} f_{i\xi}f_{j\xi}\mathrm{d}\xi\int_{-1}^{1} f_{i\eta}f_{j\eta}\mathrm{d}\eta\ddot{q}^w(j) \tag{2.69}$$

$$t(20) = -\rho h\mu\left[\frac{b}{a}\int_{-1}^{1}\frac{\partial f_{i\xi}}{\partial\xi}\frac{\partial f_{j\xi}}{\partial\xi}\mathrm{d}\xi\int_{-1}^{1} f_{i\eta}f_{j\eta}\mathrm{d}\eta + \frac{a}{b}\int_{-1}^{1} f_{i\xi}f_{j\xi}\mathrm{d}\xi\int_{-1}^{1}\frac{\partial f_{i\eta}}{\partial\eta}\frac{\partial f_{j\eta}}{\partial\eta}\mathrm{d}\eta\right]\ddot{q}^w(j) \tag{2.70}$$

Expanding the term t(18) in (2.65) according to the approximation (2.39):

$$\mathcal{L}(\aleph) \approx \sum_{i=1}^{3}\left[\underbrace{\mathcal{F}_i^L\mathcal{D}_i}_{\mathrm{t}(18.1)} - \underbrace{\mu\nabla^2\left(\mathcal{F}_i^L\mathcal{D}_i\right)}_{\mathrm{t}(18.2)}\right] \tag{2.71}$$

For the subterm t(18.1) the simplification implemented in (2.17) will not be used. Instead, it is preferable to use the equation (2.10) to facilitate the integration by parts and avoid higher order derivatives. Note that consequently the index of the sum operator and the terms of $\mathcal{F}_i^L$ and $\mathcal{D}_i$ are not the same as those given in (2.36). However, the principle in practice is exactly the same. Thus, the subterm t(18.1) can be written as:

$$\frac{\partial}{\partial x}\left\{\left[A_{11}\left(\underbrace{\frac{\partial u^0}{\partial x}}_{\mathrm{t}(18.1.1)}+\underbrace{\frac{1}{2}\left(\frac{\partial w^0}{\partial x}\right)^2}_{\mathrm{t}(18.1.2)}\right)+A_{12}\left(\underbrace{\frac{\partial v^0}{\partial y}}_{\mathrm{t}(18.1.3)}+\underbrace{\frac{1}{2}\left(\frac{\partial w^0}{\partial y}\right)^2}_{\mathrm{t}(18.1.4)}\right)\right]\frac{\partial w^0}{\partial x}\right.$$
$$+\left[A_{33}\left(\underbrace{\frac{\partial u^0}{\partial y}}_{\mathrm{t}(18.1.5)}+\underbrace{\frac{\partial v^0}{\partial x}}_{\mathrm{t}(18.1.6)}+\underbrace{\frac{\partial w^0}{\partial x}\frac{\partial w^0}{\partial y}}_{\mathrm{t}(18.1.7)}\right)\right]\frac{\partial w^0}{\partial y}\Bigg\}+\frac{\partial}{\partial y}\left\{\left[A_{33}\left(\underbrace{\frac{\partial u^0}{\partial y}}_{\mathrm{t}(18.1.8)}+\underbrace{\frac{\partial v^0}{\partial x}}_{\mathrm{t}(18.1.9)}+\underbrace{\frac{\partial w^0}{\partial x}\frac{\partial w^0}{\partial y}}_{\mathrm{t}(18.1.10)}\right)\right]\frac{\partial w^0}{\partial x}\right.$$
$$\left.+\left[A_{12}\left(\underbrace{\frac{\partial u^0}{\partial x}}_{\mathrm{t}(18.1.11)}+\underbrace{\frac{1}{2}\left(\frac{\partial w^0}{\partial x}\right)^2}_{\mathrm{t}(18.1.12)}\right)+A_{22}\left(\underbrace{\frac{\partial v^0}{\partial y}}_{\mathrm{t}(18.1.13)}+\underbrace{\frac{1}{2}\left(\frac{\partial w^0}{\partial y}\right)^2}_{\mathrm{t}(18.1.14)}\right)\right]\frac{\partial w^0}{\partial y}\right\} \tag{2.72}$$

$$\begin{aligned}t(18.1.1)&=A_{11}\frac{2b}{a^2}\int_{-1}^{1}\int_{-1}^{1}f_{i\xi}f_{i\eta}\frac{\partial}{\partial\xi}\left(\frac{\partial\left(g_{j\xi}g_{j\eta}\right)}{\partial\xi}\frac{\partial\left(f_{k\xi}f_{k\eta}\right)}{\partial\xi}\right)\mathrm{d}\xi\mathrm{d}\eta q^u(j)q^w(k)\\&=-A_{11}\frac{2b}{a^2}\int_{-1}^{1}\frac{\partial f_{i\xi}}{\partial\xi}\frac{\partial g_{j\xi}}{\partial\xi}\frac{\partial f_{k\xi}}{\partial\xi}\mathrm{d}\xi\int_{-1}^{1}f_{i\eta}g_{j\eta}f_{k\eta}\mathrm{d}\eta q^u(j)q^w(k)\end{aligned} \tag{2.73}$$

$$\begin{aligned}t(18.1.2)&=A_{11}\frac{2b}{a^3}\int_{-1}^{1}\int_{-1}^{1}f_{i\xi}f_{i\eta}\frac{\partial}{\partial\xi}\left(\frac{\partial\left(f_{j\xi}f_{j\eta}\right)}{\partial\xi}\frac{\partial\left(f_{k\xi}f_{k\eta}\right)}{\partial\xi}\frac{\partial\left(f_{l\xi}f_{l\eta}\right)}{\partial\xi}\right)\mathrm{d}\xi\mathrm{d}\eta q^w(l)q^w(k)q^w(j)\\&=-A_{11}\frac{2b}{a^3}\int_{-1}^{1}\frac{\partial f_{i\xi}}{\partial\xi}\frac{\partial f_{j\xi}}{\partial\xi}\frac{\partial f_{k\xi}}{\partial\xi}\frac{\partial f_{l\xi}}{\partial\xi}\mathrm{d}\xi\int_{-1}^{1}f_{i\eta}f_{j\eta}f_{k\eta}f_{l\eta}\mathrm{d}\eta q^w(l)q^w(k)q^w(j)\end{aligned} \tag{2.74}$$

$$\begin{aligned}t(18.1.3)&=A_{12}\frac{2}{a}\int_{-1}^{1}\int_{-1}^{1}f_{i\xi}f_{i\eta}\frac{\partial}{\partial\xi}\left(\frac{\partial\left(g_{j\xi}g_{j\eta}\right)}{\partial\eta}\frac{\partial\left(f_{k\xi}f_{k\eta}\right)}{\partial\xi}\right)\mathrm{d}\xi\mathrm{d}\eta q^v(j)q^w(k)\\&=-A_{12}\frac{2}{a}\int_{-1}^{1}\frac{\partial f_{i\xi}}{\partial\xi}g_{j\xi}\frac{\partial f_{k\xi}}{\partial\xi}\mathrm{d}\xi\int_{-1}^{1}f_{i\eta}\frac{\partial g_{j\eta}}{\partial\eta}f_{k\eta}\mathrm{d}\eta q^v(j)q^w(k)\end{aligned} \tag{2.75}$$

$$\begin{aligned}t(18.1.4)&=A_{12}\frac{2}{ab}\int_{-1}^{1}\int_{-1}^{1}f_{i\xi}f_{i\eta}\frac{\partial}{\partial\xi}\left(\frac{\partial\left(f_{j\xi}f_{j\eta}\right)}{\partial\eta}\frac{\partial\left(f_{k\xi}f_{k\eta}\right)}{\partial\eta}\frac{\partial\left(f_{l\xi}f_{l\eta}\right)}{\partial\xi}\right)\mathrm{d}\xi\mathrm{d}\eta q^w(l)q^w(k)q^w(j)\\&=-A_{12}\frac{2}{ab}\int_{-1}^{1}\frac{\partial f_{i\xi}}{\partial\xi}f_{j\xi}f_{k\xi}\frac{\partial f_{l\xi}}{\partial\xi}\mathrm{d}\xi\int_{-1}^{1}f_{i\eta}\frac{\partial f_{j\eta}}{\partial\eta}\frac{\partial f_{k\eta}}{\partial\eta}f_{l\eta}\mathrm{d}\eta q^w(l)q^w(k)q^w(j)\end{aligned} \tag{2.76}$$

$$\begin{aligned}t(18.1.5)&=A_{33}\frac{2}{b}\int_{-1}^{1}\int_{-1}^{1}f_{i\xi}f_{i\eta}\frac{\partial}{\partial\xi}\left(\frac{\partial\left(g_{j\xi}g_{j\eta}\right)}{\partial\eta}\frac{\partial\left(f_{k\xi}f_{k\eta}\right)}{\partial\eta}\right)\mathrm{d}\xi\mathrm{d}\eta q^u(j)q^w(k)\\&=-A_{33}\frac{2}{b}\int_{-1}^{1}\frac{\partial f_{i\xi}}{\partial\xi}g_{j\xi}f_{k\xi}\mathrm{d}\xi\int_{-1}^{1}f_{i\eta}\frac{\partial g_{j\eta}}{\partial\eta}\frac{\partial f_{k\eta}}{\partial\eta}\mathrm{d}\eta q^u(j)q^w(k)\end{aligned} \tag{2.77}$$

$$\begin{aligned}t(18.1.6)&=A_{33}\frac{2}{a}\int_{-1}^{1}\int_{-1}^{1}f_{i\xi}f_{i\eta}\frac{\partial}{\partial\xi}\left(\frac{\partial\left(g_{j\xi}g_{j\eta}\right)}{\partial\xi}\frac{\partial\left(f_{k\xi}f_{k\eta}\right)}{\partial\eta}\right)\mathrm{d}\xi\mathrm{d}\eta q^v(j)q^w(k)\\&=-A_{33}\frac{2}{a}\int_{-1}^{1}\frac{\partial f_{i\xi}}{\partial\xi}\frac{\partial g_{j\xi}}{\partial\xi}f_{k\xi}\mathrm{d}\xi\int_{-1}^{1}f_{i\eta}g_{j\eta}\frac{\partial f_{k\eta}}{\partial\eta}\mathrm{d}\eta q^v(j)q^w(k)\end{aligned} \tag{2.78}$$

$$t(18.1.7) = A_{33}\frac{4}{ab}\int_{-1}^{1}\int_{-1}^{1} f_{i\xi}f_{i\eta}\frac{\partial}{\partial\xi}\left(\frac{\partial\left(f_{j\xi}f_{j\eta}\right)}{\partial\xi}\frac{\partial\left(f_{k\xi}f_{k\eta}\right)}{\partial\eta}\frac{\partial\left(f_{l\xi}f_{l\eta}\right)}{\partial\eta}\right)\mathrm{d}\xi\mathrm{d}\eta q^{w}(l)q^{w}(k)q^{w}(j)$$
$$= -A_{33}\frac{4}{ab}\int_{-1}^{1}\frac{\partial f_{i\xi}}{\partial\xi}\frac{\partial f_{j\xi}}{\partial\xi}f_{k\xi}f_{l\xi}\mathrm{d}\xi\int_{-1}^{1} f_{i\eta}f_{j\eta}\frac{\partial f_{k\eta}}{\partial\eta}\frac{\partial f_{l\eta}}{\partial\eta}\mathrm{d}\eta q^{w}(l)q^{w}(k)q^{w}(j) \tag{2.79}$$

$$t(18.1.8) = A_{33}\frac{2}{b}\int_{-1}^{1}\int_{-1}^{1} f_{i\xi}f_{i\eta}\frac{\partial}{\partial\eta}\left(\frac{\partial\left(g_{j\xi}g_{j\eta}\right)}{\partial\eta}\frac{\partial\left(f_{k\xi}f_{k\eta}\right)}{\partial\xi}\right)\mathrm{d}\xi\mathrm{d}\eta q^{u}(j)q^{w}(k)$$
$$= -A_{33}\frac{2}{b}\int_{-1}^{1} f_{i\xi}g_{j\xi}\frac{\partial f_{k\xi}}{\partial\xi}\mathrm{d}\xi\int_{-1}^{1}\frac{\partial f_{i\eta}}{\partial\eta}\frac{\partial g_{j\eta}}{\partial\eta}f_{k\eta}\mathrm{d}\eta q^{u}(j)q^{w}(k) \tag{2.80}$$

$$t(18.1.9) = A_{33}\frac{2}{a}\int_{-1}^{1}\int_{-1}^{1} f_{i\xi}f_{i\eta}\frac{\partial}{\partial\eta}\left(\frac{\partial\left(g_{j\xi}g_{j\eta}\right)}{\partial\xi}\frac{\partial\left(f_{k\xi}f_{k\eta}\right)}{\partial\xi}\right)\mathrm{d}\xi\mathrm{d}\eta q^{v}(j)q^{w}(k)$$
$$= -A_{33}\frac{2}{a}\int_{-1}^{1} f_{i\xi}\frac{\partial g_{j\xi}}{\partial\xi}\frac{\partial f_{k\xi}}{\partial\xi}\mathrm{d}\xi\int_{-1}^{1}\frac{\partial f_{i\eta}}{\partial\eta}g_{j\eta}f_{k\eta}\mathrm{d}\eta q^{v}(j)q^{w}(k) \tag{2.81}$$

$$t(18.1.10) = A_{33}\frac{4}{ab}\int_{-1}^{1}\int_{-1}^{1} f_{i\xi}f_{i\eta}\frac{\partial}{\partial\eta}\left(\frac{\partial\left(f_{j\xi}f_{j\eta}\right)}{\partial\xi}\frac{\partial\left(f_{k\xi}f_{k\eta}\right)}{\partial\eta}\frac{\partial\left(f_{l\xi}f_{l\eta}\right)}{\partial\xi}\right)\mathrm{d}\xi\mathrm{d}\eta q^{w}(l)q^{w}(k)q^{w}(j)$$
$$= -A_{33}\frac{4}{ab}\int_{-1}^{1} f_{i\xi}\frac{\partial f_{j\xi}}{\partial\xi}f_{k\xi}\frac{\partial f_{l\xi}}{\partial\xi}\mathrm{d}\xi\int_{-1}^{1}\frac{\partial f_{i\eta}}{\partial\eta}f_{j\eta}\frac{\partial f_{k\eta}}{\partial\eta}f_{l\eta}\mathrm{d}\eta q^{w}(l)q^{w}(k)q^{w}(j) \tag{2.82}$$

$$t(18.1.11) = A_{12}\frac{2}{b}\int_{-1}^{1}\int_{-1}^{1} f_{i\xi}f_{i\eta}\frac{\partial}{\partial\eta}\left(\frac{\partial\left(g_{j\xi}g_{j\eta}\right)}{\partial\xi}\frac{\partial\left(f_{k\xi}f_{k\eta}\right)}{\partial\eta}\right)\mathrm{d}\xi\mathrm{d}\eta q^{u}(j)q^{w}(k)$$
$$= -A_{12}\frac{2}{b}\int_{-1}^{1} f_{i\xi}\frac{\partial g_{j\xi}}{\partial\xi}f_{k\xi}\mathrm{d}\xi\int_{-1}^{1}\frac{\partial f_{i\eta}}{\partial\eta}g_{j\eta}\frac{\partial f_{k\eta}}{\partial\eta}\mathrm{d}\eta q^{u}(j)q^{w}(k) \tag{2.83}$$

$$t(18.1.12) = A_{12}\frac{2}{ab}\int_{-1}^{1}\int_{-1}^{1} f_{i\xi}f_{i\eta}\frac{\partial}{\partial\eta}\left(\frac{\partial\left(f_{j\xi}f_{j\eta}\right)}{\partial\xi}\frac{\partial\left(f_{k\xi}f_{k\eta}\right)}{\partial\xi}\frac{\partial\left(f_{l\xi}f_{l\eta}\right)}{\partial\eta}\right)\mathrm{d}\xi\mathrm{d}\eta q^{w}(l)q^{w}(k)q^{w}(j)$$
$$= -A_{12}\frac{2}{ab}\int_{-1}^{1} f_{i\xi}\frac{\partial f_{j\xi}}{\partial\xi}\frac{\partial f_{k\xi}}{\partial\xi}f_{l\xi}\mathrm{d}\xi\int_{-1}^{1}\frac{\partial f_{i\eta}}{\partial\eta}f_{j\eta}f_{k\eta}\frac{\partial f_{l\eta}}{\partial\eta}\mathrm{d}\eta q^{w}(l)q^{w}(k)q^{w}(j) \tag{2.84}$$

$$t(18.1.13) = A_{22}\frac{2a}{b^2}\int_{-1}^{1}\int_{-1}^{1} f_{i\xi}f_{i\eta}\frac{\partial}{\partial\eta}\left(\frac{\partial\left(g_{j\xi}g_{j\eta}\right)}{\partial\eta}\frac{\partial\left(f_{k\xi}f_{k\eta}\right)}{\partial\eta}\right)\mathrm{d}\xi\mathrm{d}\eta q^{v}(j)q^{w}(k)$$
$$= -A_{22}\frac{2a}{b^2}\int_{-1}^{1} f_{i\xi}g_{j\xi}f_{k\xi}\mathrm{d}\xi\int_{-1}^{1}\frac{\partial f_{i\eta}}{\partial\eta}\frac{\partial g_{j\eta}}{\partial\eta}\frac{\partial f_{k\eta}}{\partial\eta}\mathrm{d}\eta q^{v}(j)q^{w}(k) \tag{2.85}$$

$$t(18.1.14) = A_{22}\frac{2a}{b^3}\int_{-1}^{1}\int_{-1}^{1} f_{i\xi}f_{i\eta}\frac{\partial}{\partial\eta}\left(\frac{\partial\left(f_{j\xi}f_{j\eta}\right)}{\partial\eta}\frac{\partial\left(f_{k\xi}f_{k\eta}\right)}{\partial\eta}\frac{\partial\left(f_{l\xi}f_{l\eta}\right)}{\partial\eta}\right)\mathrm{d}\xi\mathrm{d}\eta q^{w}(l)q^{w}(k)q^{w}(j)$$
$$= -A_{22}\frac{2a}{b^3}\int_{-1}^{1} f_{i\xi}f_{j\xi}f_{k\xi}f_{l\xi}\mathrm{d}\xi\int_{-1}^{1}\frac{\partial f_{i\eta}}{\partial\eta}\frac{\partial f_{j\eta}}{\partial\eta}\frac{\partial f_{k\eta}}{\partial\eta}\frac{\partial f_{l\eta}}{\partial\eta}\mathrm{d}\eta q^{w}(l)q^{w}(k)q^{w}(j) \tag{2.86}$$

Using the simplification mentioned before in (2.17), prior to the substitution of the in-plane forces by the constitutive relation, one may rewrite subterm t(18.2) as follows:

$$
\begin{aligned}
&-\mu\nabla^2\left(N_{xx}\frac{\partial^2 w^0}{\partial x^2}+2N_{xy}\frac{\partial^2 w^0}{\partial y\partial x}+N_{yy}\frac{\partial^2 w^0}{\partial y^2}\right)\\
=&-\mu\left[\frac{\partial}{\partial x}\left(\underbrace{\frac{\partial N_{xx}}{\partial x}\frac{\partial^2 w^0}{\partial x^2}}_{\text{t(18.2.1)}}+\underbrace{N_{xx}\frac{\partial^3 w^0}{\partial x^3}}_{\text{t(18.2.2)}}+\underbrace{2\frac{\partial N_{xy}}{\partial x}\frac{\partial^2 w^0}{\partial y\partial x}}_{\text{t(18.2.3)}}+\underbrace{2N_{xy}\frac{\partial^3 w^0}{\partial x\partial y\partial x}}_{\text{t(18.2.4)}}+\underbrace{\frac{\partial N_{yy}}{\partial x}\frac{\partial^2 w^0}{\partial y^2}}_{\text{t(18.2.5)}}+\underbrace{N_{yy}\frac{\partial^3 w^0}{\partial x\partial y^2}}_{\text{t(18.2.6)}}\right)\right.\\
&\left.+\frac{\partial}{\partial y}\left(\underbrace{\frac{\partial N_{xx}}{\partial y}\frac{\partial^2 w^0}{\partial x^2}}_{\text{t(18.2.7)}}+\underbrace{N_{xx}\frac{\partial^3 w^0}{\partial y\partial x^2}}_{\text{t(18.2.8)}}+\underbrace{2\frac{\partial N_{xy}}{\partial y}\frac{\partial^2 w^0}{\partial y\partial x}}_{\text{t(18.2.9)}}+\underbrace{2N_{xy}\frac{\partial^3 w^0}{\partial y^2\partial x}}_{\text{t(18.2.10)}}+\underbrace{\frac{\partial N_{yy}}{\partial y}\frac{\partial^2 w^0}{\partial y^2}}_{\text{t(18.2.11)}}+\underbrace{N_{yy}\frac{\partial^3 w^0}{\partial y^3}}_{\text{t(18.2.12)}}\right)\right]
\end{aligned}
\tag{2.87}
$$

Replacing the forces N_{xx}, N_{xy} and N_{yy} by the constitutive relations as mentioned in (2.39) and applying the Galerkin method by the multiplication of (2.87) by the approximation functions and subsequently integrating by parts, one obtains for each term several other subterms, for which the method will be individually resolved.

$$
t(18.2.1.1)=\frac{8b}{a^4}A_{11}\int_{-1}^{1}\frac{\partial f_{i\xi}}{\partial\xi}\frac{\partial^2 g_{j\xi}}{\partial\xi^2}\frac{\partial^2 f_{k\xi}}{\partial\xi^2}\mathrm{d}\xi\int_{-1}^{1}f_{i\eta}g_{j\eta}f_{k\eta}\mathrm{d}\eta q^u(j)q^w(k) \tag{2.88}
$$

$$
t(18.2.1.2)=\frac{8b}{a^5}A_{11}\int_{-1}^{1}\frac{\partial f_{i\xi}}{\partial\xi}\left[\frac{\partial^2 f_{j\xi}}{\partial\xi^2}\frac{\partial f_{k\xi}}{\partial\xi}+\frac{\partial f_{j\xi}}{\partial\xi}\frac{\partial^2 f_{k\xi}}{\partial\xi^2}\right]\frac{\partial^2 f_{l\xi}}{\partial\xi^2}\mathrm{d}\xi\int_{-1}^{1}f_{i\eta}f_{j\eta}f_{k\eta}f_{l\eta}\mathrm{d}\eta q^w(l)\,q^w(k)q^w(j) \tag{2.89}
$$

$$
t(18.2.1.3)=\frac{8}{a^3}A_{12}\int_{-1}^{1}\frac{\partial f_{i\xi}}{\partial\xi}\frac{\partial g_{j\xi}}{\partial\xi}\frac{\partial^2 f_{k\xi}}{\partial\xi^2}\mathrm{d}\xi\int_{-1}^{1}f_{i\eta}\frac{\partial g_{j\eta}}{\partial\eta}f_{k\eta}\mathrm{d}\eta q^v(j)q^w(k) \tag{2.90}
$$

$$
t(18.2.1.4)=\frac{8}{ba^3}A_{12}\int_{-1}^{1}\frac{\partial f_{i\xi}}{\partial\xi}\left[\frac{\partial f_{j\xi}}{\partial\xi}f_{k\xi}+f_{j\xi}\frac{\partial f_{k\xi}}{\partial\xi}\right]\frac{\partial^2 f_{l\xi}}{\partial\xi^2}\mathrm{d}\xi\int_{-1}^{1}f_{i\eta}\frac{\partial f_{j\eta}}{\partial\eta}\frac{\partial f_{k\eta}}{\partial\eta}f_{l\eta}\mathrm{d}\eta q^w(l)\,q^w(k)q^w(j) \tag{2.91}
$$

$$
t(18.2.2.1)=\frac{8b}{a^4}A_{11}\int_{-1}^{1}\frac{\partial f_{i\xi}}{\partial\xi}\frac{\partial g_{j\xi}}{\partial\xi}\frac{\partial^3 f_{k\xi}}{\partial\xi^3}\mathrm{d}\xi\int_{-1}^{1}f_{i\eta}g_{j\eta}f_{k\eta}\mathrm{d}\eta q^u(j)q^w(k) \tag{2.92}
$$

$$
t(18.2.2.2)=\frac{8b}{a^5}A_{11}\int_{-1}^{1}\frac{\partial f_{i\xi}}{\partial\xi}\frac{\partial f_{j\xi}}{\partial\xi}\frac{\partial f_{k\xi}}{\partial\xi}\frac{\partial^3 f_{l\xi}}{\partial\xi^3}\mathrm{d}\xi\int_{-1}^{1}f_{i\eta}f_{j\eta}f_{k\eta}f_{l\eta}\mathrm{d}\eta q^w(l)q^w(k)q^w(j) \tag{2.93}
$$

$$
t(18.2.2.3)=\frac{8}{a^3}A_{12}\int_{-1}^{1}\frac{\partial f_{i\xi}}{\partial\xi}g_{j\xi}\frac{\partial^3 f_{k\xi}}{\partial\xi^3}\mathrm{d}\xi\int_{-1}^{1}f_{i\eta}\frac{\partial g_{j\eta}}{\partial\eta}f_{k\eta}\mathrm{d}\eta q^v(j)q^w(k) \tag{2.94}
$$

$$
t(18.2.2.4)=\frac{8}{ba^3}A_{12}\int_{-1}^{1}\frac{\partial f_{i\xi}}{\partial\xi}f_{j\xi}f_{k\xi}\frac{\partial^3 f_{l\xi}}{\partial\xi^3}\mathrm{d}\xi\int_{-1}^{1}f_{i\eta}\frac{\partial f_{j\eta}}{\partial\eta}\frac{\partial f_{k\eta}}{\partial\eta}f_{l\eta}\mathrm{d}\eta q^w(l)q^w(k)q^w(j) \tag{2.95}
$$

$$t(18.2.3.1) = \frac{16}{ba^2} A_{33} \int_{-1}^{1} \frac{\partial f_{i\xi}}{\partial \xi} \frac{\partial g_{j\xi}}{\partial \xi} \frac{\partial f_{k\xi}}{\partial \xi} \mathrm{d}\xi \int_{-1}^{1} f_{i\eta} \frac{\partial g_{j\eta}}{\partial \eta} \frac{\partial f_{k\eta}}{\partial \eta} \mathrm{d}\eta q^u(j) q^w(k) \tag{2.96}$$

$$t(18.2.3.2) = \frac{16}{a^3} A_{33} \int_{-1}^{1} \frac{\partial f_{i\xi}}{\partial \xi} \frac{\partial^2 g_{j\xi}}{\partial \xi^2} \frac{\partial f_{k\xi}}{\partial \xi} \mathrm{d}\xi \int_{-1}^{1} f_{i\eta} g_{j\eta} \frac{\partial f_{k\eta}}{\partial \eta} \mathrm{d}\eta q^v(j) q^w(k) \tag{2.97}$$

$$t(18.2.3.3) = \frac{32}{ba^3} A_{33} \int_{-1}^{1} \frac{\partial f_{i\xi}}{\partial \xi} \left[\frac{\partial^2 f_{j\xi}}{\partial \xi^2} f_{k\xi} + \frac{\partial f_{j\xi}}{\partial \xi} \frac{\partial f_{k\xi}}{\partial \xi} \right] \frac{\partial f_{l\xi}}{\partial \xi} \mathrm{d}\xi \int_{-1}^{1} f_{i\eta} f_{j\eta} \frac{\partial f_{k\eta}}{\partial \eta} \frac{\partial f_{l\eta}}{\partial \eta} \mathrm{d}\eta q^w(l) q^w(k) q^w(j) \tag{2.98}$$

$$t(18.2.4.1) = \frac{16}{a^2 b} A_{33} \int_{-1}^{1} \frac{\partial f_{i\xi}}{\partial \xi} g_{j\xi} \frac{\partial^2 f_{k\xi}}{\partial \xi^2} \mathrm{d}\xi \int_{-1}^{1} f_{i\eta} \frac{\partial g_{j\eta}}{\partial \eta} \frac{\partial f_{k\eta}}{\partial \eta} \mathrm{d}\eta q^u(j) q^w(k) \tag{2.99}$$

$$t(18.2.4.2) = \frac{16}{a^3} A_{33} \int_{-1}^{1} \frac{\partial f_{i\xi}}{\partial \xi} \frac{\partial g_{j\xi}}{\partial \xi} \frac{\partial^2 f_{k\xi}}{\partial \xi^2} \mathrm{d}\xi \int_{-1}^{1} f_{i\eta} g_{j\eta} \frac{\partial f_{k\eta}}{\partial \eta} \mathrm{d}\eta q^v(j) q^w(k) \tag{2.100}$$

$$t(18.2.4.3) = \frac{32}{a^3 b} A_{33} \int_{-1}^{1} \frac{\partial f_{i\xi}}{\partial \xi} \frac{\partial f_{j\xi}}{\partial \xi} f_{k\xi} \frac{\partial^2 f_{l\xi}}{\partial \xi^2} \mathrm{d}\xi \int_{-1}^{1} f_{i\eta} f_{j\eta} \frac{\partial f_{k\eta}}{\partial \eta} \frac{\partial f_{l\eta}}{\partial \eta} \mathrm{d}\eta q^w(l) q^w(k) q^w(j) \tag{2.101}$$

$$t(18.2.5.1) = \frac{8}{a^2 b} A_{12} \int_{-1}^{1} \frac{\partial f_{i\xi}}{\partial \xi} \frac{\partial^2 g_{j\xi}}{\partial \xi^2} f_{k\xi} \mathrm{d}\xi \int_{-1}^{1} f_{i\eta} g_{j\eta} \frac{\partial^2 f_{k\eta}}{\partial \eta^2} \mathrm{d}\eta q^u(j) q^w(k) \tag{2.102}$$

$$t(18.2.5.2) = \frac{8}{a^3 b} A_{12} \int_{-1}^{1} \frac{\partial f_{i\xi}}{\partial \xi} \left[\frac{\partial^2 f_{k\xi}}{\partial \xi^2} \frac{\partial f_{k\xi}}{\partial \xi} + \frac{\partial f_{j\xi}}{\partial \xi} \frac{\partial^2 f_{k\xi}}{\partial \xi^2} \right] f_{l\xi} \mathrm{d}\xi \int_{-1}^{1} f_{i\eta} f_{j\eta} f_{k\eta} \frac{\partial^2 f_{l\eta}}{\partial \eta^2} \mathrm{d}\eta q^w(l) q^w(k) q^w(j) \tag{2.103}$$

$$t(18.2.5.3) = \frac{8}{ab^2} A_{22} \int_{-1}^{1} \frac{\partial f_{i\xi}}{\partial \xi} \frac{\partial g_{j\xi}}{\partial \xi} f_{k\xi} \mathrm{d}\xi \int_{-1}^{1} f_{i\eta} \frac{\partial g_{j\eta}}{\partial \eta} \frac{\partial^2 f_{k\eta}}{\partial \eta^2} \mathrm{d}\eta q^v(j) q^w(k) \tag{2.104}$$

$$t(18.2.5.4) = \frac{8}{ab^3} A_{22} \int_{-1}^{1} \frac{\partial f_{i\xi}}{\partial \xi} \left[\frac{\partial f_{j\xi}}{\partial \xi} f_{k\xi} + f_{j\xi} \frac{\partial f_{k\xi}}{\partial \xi} \right] f_{l\xi} \mathrm{d}\xi \int_{-1}^{1} f_{i\eta} \frac{\partial f_{j\eta}}{\partial \eta} \frac{\partial f_{k\eta}}{\partial \eta} \frac{\partial^2 f_{l\eta}}{\partial \eta^2} \mathrm{d}\eta q^w(l) q^w(k) q^w(j) \tag{2.105}$$

$$t(18.2.6.1) = \frac{8}{a^2 b} A_{12} \int_{-1}^{1} \frac{\partial f_{i\xi}}{\partial \xi} \frac{\partial g_{j\xi}}{\partial \xi} \frac{\partial f_{k\xi}}{\partial \xi} \mathrm{d}\xi \int_{-1}^{1} f_{i\eta} g_{j\eta} \frac{\partial^2 f_{k\eta}}{\partial \eta^2} \mathrm{d}\eta q^u(j) q^w(k) \tag{2.106}$$

$$t(18.2.6.2) = \frac{8}{a^3 b} A_{12} \int_{-1}^{1} \frac{\partial f_{i\xi}}{\partial \xi} \frac{\partial f_{j\xi}}{\partial \xi} \frac{\partial f_{k\xi}}{\partial \xi} \frac{\partial f_{l\xi}}{\partial \xi} \mathrm{d}\xi \int_{-1}^{1} f_{i\eta} f_{j\eta} f_{k\eta} \frac{\partial^2 f_{l\eta}}{\partial \eta^2} \mathrm{d}\eta q^w(l) q^w(k) q^w(j) \tag{2.107}$$

$$t(18.2.6.3) = \frac{8}{ab^2} A_{22} \int_{-1}^{1} \frac{\partial f_{i\xi}}{\partial \xi} g_{j\xi} \frac{\partial f_{k\xi}}{\partial \xi} \mathrm{d}\xi \int_{-1}^{1} f_{i\eta} \frac{\partial g_{j\eta}}{\partial \eta} \frac{\partial^2 f_{k\eta}}{\partial \eta^2} \mathrm{d}\eta q^v(j) q^w(k) \tag{2.108}$$

$$t(18.2.6.4) = \frac{8}{ab^3} A_{22} \int_{-1}^{1} \frac{\partial f_{i\xi}}{\partial \xi} f_{j\xi} f_{k\xi} \frac{\partial f_{l\xi}}{\partial \xi} \mathrm{d}\xi \int_{-1}^{1} f_{i\eta} \frac{\partial f_{j\eta}}{\partial \eta} \frac{\partial f_{k\eta}}{\partial \eta} \frac{\partial^2 f_{l\eta}}{\partial \eta^2} \mathrm{d}\eta q^w(l) q^w(k) q^w(j) \tag{2.109}$$

$$t(18.2.7.1) = \frac{8}{a^2 b} A_{11} \int_{-1}^{1} f_{i\xi} \frac{\partial g_{j\xi}}{\partial \xi} \frac{\partial^2 f_{k\xi}}{\partial \xi^2} \mathrm{d}\xi \int_{-1}^{1} \frac{\partial f_{i\eta}}{\partial \eta} \frac{\partial g_{j\eta}}{\partial \eta} f_{k\eta} \mathrm{d}\eta q^u(j) q^w(k) \tag{2.110}$$

$$t(18.2.7.2) = \frac{8}{a^3 b} A_{11} \int_{-1}^{1} f_{i\xi} \frac{\partial f_{j\xi}}{\partial \xi} \frac{\partial f_{k\xi}}{\partial \xi} \frac{\partial^2 f_{l\xi}}{\partial \xi^2} \mathrm{d}\xi \int_{-1}^{1} \frac{\partial f_{i\eta}}{\partial \eta} \left[\frac{\partial f_{j\eta}}{\partial \eta} f_{k\eta} + f_{j\eta} \frac{\partial f_{k\eta}}{\partial \eta} \right] f_{l\eta} \mathrm{d}\eta q^w(l) q^w(k) q^w(j) \tag{2.111}$$

$$t(18.2.7.3) = \frac{8}{b^2 a} A_{12} \int_{-1}^{1} f_{i\xi} g_{j\xi} \frac{\partial^2 f_{k\xi}}{\partial \xi^2} \mathrm{d}\xi \int_{-1}^{1} \frac{\partial f_{i\eta}}{\partial \eta} \frac{\partial^2 g_{j\eta}}{\partial \eta^2} f_{k\eta} \mathrm{d}\eta q^v(j) q^w(k) \tag{2.112}$$

$$t(18.2.7.4) = \frac{8}{b^3 a} A_{12} \int_{-1}^{1} f_{i\xi} f_{j\xi} f_{k\xi} \frac{\partial^2 f_{l\xi}}{\partial \xi^2} \mathrm{d}\xi \int_{-1}^{1} \frac{\partial f_{i\eta}}{\partial \eta} \left[\frac{\partial^2 f_{k\eta}}{\partial \eta^2} \frac{\partial f_{k\eta}}{\partial \eta} + \frac{\partial f_{j\eta}}{\partial \eta} \frac{\partial^2 f_{k\eta}}{\partial \eta^2} \right] f_{l\eta} \mathrm{d}\eta q^w(l) q^w(k) q^w(j) \tag{2.113}$$

$$t(18.2.8.1) = \frac{8}{b a^2} A_{11} \int_{-1}^{1} f_{i\xi} \frac{\partial g_{j\xi}}{\partial \xi} \frac{\partial^2 f_{k\xi}}{\partial \xi^2} \mathrm{d}\xi \int_{-1}^{1} \frac{\partial f_{i\eta}}{\partial \eta} g_{j\eta} \frac{\partial f_{k\eta}}{\partial \eta} \mathrm{d}\eta q^u(j) q^w(k) \tag{2.114}$$

$$t(18.2.8.2) = \frac{8}{a^3 b} A_{11} \int_{-1}^{1} f_{i\xi} \frac{\partial f_{j\xi}}{\partial \xi} \frac{\partial f_{k\xi}}{\partial \xi} \frac{\partial^2 f_{l\xi}}{\partial \xi^2} \mathrm{d}\xi \int_{-1}^{1} \frac{\partial f_{i\eta}}{\partial \eta} f_{j\eta} f_{k\eta} \frac{\partial f_{l\eta}}{\partial \eta} \mathrm{d}\eta q^w(l) q^w(k) q^w(j) \tag{2.115}$$

$$t(18.2.8.3) = \frac{8}{b a^2} A_{12} \int_{-1}^{1} f_{i\xi} g_{j\xi} \frac{\partial^2 f_{k\xi}}{\partial \xi^2} \mathrm{d}\xi \int_{-1}^{1} \frac{\partial f_{i\eta}}{\partial \eta} \frac{\partial g_{j\eta}}{\partial \eta} \frac{\partial f_{k\eta}}{\partial \eta} \mathrm{d}\eta q^v(j) q^w(k) \tag{2.116}$$

$$t(18.2.8.4) = \frac{8}{b^3 a} A_{12} \int_{-1}^{1} f_{i\xi} f_{j\xi} f_{k\xi} \frac{\partial^2 f_{l\xi}}{\partial \xi^2} \mathrm{d}\xi \int_{-1}^{1} \frac{\partial f_{i\eta}}{\partial \eta} \frac{\partial f_{j\eta}}{\partial \eta} \frac{\partial f_{k\eta}}{\partial \eta} \frac{\partial f_{l\eta}}{\partial \eta} \mathrm{d}\eta q^w(l) q^w(k) q^w(j) \tag{2.117}$$

$$t(18.2.9.1) = \frac{16}{b^3} A_{33} \int_{-1}^{1} f_{i\xi} g_{j\xi} \frac{\partial f_{k\xi}}{\partial \xi} \mathrm{d}\xi \int_{-1}^{1} \frac{\partial f_{i\eta}}{\partial \eta} \frac{\partial^2 g_{j\eta}}{\partial \eta^2} \frac{\partial f_{k\eta}}{\partial \eta} \mathrm{d}\eta q^u(j) q^w(k) \tag{2.118}$$

$$t(18.2.9.2) = \frac{16}{a b^2} A_{33} \int_{-1}^{1} f_{i\xi} \frac{\partial g_{j\xi}}{\partial \xi} \frac{\partial f_{k\xi}}{\partial \xi} \mathrm{d}\xi \int_{-1}^{1} \frac{\partial f_{i\eta}}{\partial \eta} \frac{\partial g_{j\eta}}{\partial \eta} \frac{\partial f_{k\eta}}{\partial \eta} \mathrm{d}\eta q^v(j) q^w(k) \tag{2.119}$$

$$t(18.2.9.3) = \frac{32}{a b^3} A_{33} \int_{-1}^{1} f_{i\xi} \frac{\partial f_{j\xi}}{\partial \xi} f_{k\xi} \frac{\partial f_{l\xi}}{\partial \xi} \mathrm{d}\xi \int_{-1}^{1} \frac{\partial f_{i\eta}}{\partial \eta} \left[\frac{\partial f_{j\eta}}{\partial \eta} \frac{\partial f_{k\eta}}{\partial \eta} + f_{j\eta} \frac{\partial^2 f_{k\eta}}{\partial \eta^2} \right] \frac{\partial f_{l\eta}}{\partial \eta} \mathrm{d}\eta q^w(l) q^w(k) q^w(j) \tag{2.120}$$

$$t(18.2.10.1) = \frac{16}{b^3} A_{33} \int_{-1}^{1} f_{i\xi} g_{j\xi} \frac{\partial f_{k\xi}}{\partial \xi} \mathrm{d}\xi \int_{-1}^{1} \frac{\partial f_{i\eta}}{\partial \eta} \frac{\partial g_{j\eta}}{\partial \eta} \frac{\partial^2 f_{k\eta}}{\partial \eta^2} \mathrm{d}\eta q^u(j) q^w(k) \tag{2.121}$$

$$t(18.2.10.2) = \frac{16}{b^2 a} A_{33} \int_{-1}^{1} f_{i\xi} \frac{\partial g_{j\xi}}{\partial \xi} \frac{\partial f_{k\xi}}{\partial \xi} \mathrm{d}\xi \int_{-1}^{1} \frac{\partial f_{i\eta}}{\partial \eta} g_{j\eta} \frac{\partial^2 f_{k\eta}}{\partial \eta^2} \mathrm{d}\eta q^v(j) q^w(k) \tag{2.122}$$

$$t(18.2.10.3) = \frac{32}{b^3 a} A_{33} \int_{-1}^{1} f_{i\xi} \frac{\partial f_{j\xi}}{\partial \xi} f_{k\xi} \frac{\partial f_{l\xi}}{\partial \xi} \mathrm{d}\xi \int_{-1}^{1} \frac{\partial f_{i\eta}}{\partial \eta} f_{j\eta} \frac{\partial f_{k\eta}}{\partial \eta} \frac{\partial^2 f_{l\eta}}{\partial \eta^2} \mathrm{d}\eta q^w(l) q^w(k) q^w(j) \tag{2.123}$$

$$t(18.2.11.1) = \frac{8}{b^3} A_{12} \int_{-1}^{1} f_{i\xi} \frac{\partial g_{j\xi}}{\partial \xi} f_{k\xi} \mathrm{d}\xi \int_{-1}^{1} \frac{\partial f_{i\eta}}{\partial \eta} \frac{\partial g_{j\eta}}{\partial \eta} \frac{\partial^2 f_{k\eta}}{\partial \eta^2} \mathrm{d}\eta q^u(j) q^w(k) \tag{2.124}$$

$$t(18.2.11.2) = \frac{8}{b^3 a} A_{12} \int_{-1}^{1} f_{i\xi} \frac{\partial f_{j\xi}}{\partial \xi} \frac{\partial f_{k\xi}}{\partial \xi} f_{l\xi} \mathrm{d}\xi \int_{-1}^{1} \frac{\partial f_{i\eta}}{\partial \eta} \left[\frac{\partial f_{i\eta}}{\partial \eta} f_{k\eta} + f_{j\eta} \frac{\partial f_{k\eta}}{\partial \eta} \right] \frac{\partial^2 f_{l\eta}}{\partial \eta^2} \mathrm{d}\eta q^w(l) q^w(k) q^w(j) \tag{2.125}$$

$$t(18.2.11.3) = \frac{8a}{b^4} A_{22} \int_{-1}^{1} f_{i\xi} g_{j\xi} f_{k\xi} \mathrm{d}\xi \int_{-1}^{1} \frac{\partial f_{i\eta}}{\partial \eta} \frac{\partial^2 g_{j\eta}}{\partial \eta^2} \frac{\partial^2 f_{k\eta}}{\partial \eta^2} \mathrm{d}\eta q^v(j) q^w(k) \tag{2.126}$$

$$t(18.2.11.4) = \frac{8a}{b^5} A_{22} \int_{-1}^{1} f_{i\xi} f_{j\xi} f_{k\xi} f_{l\xi} \mathrm{d}\xi \int_{-1}^{1} \frac{\partial f_{i\eta}}{\partial \eta} \left[\frac{\partial^2 f_{j\eta}}{\partial \eta^2} \frac{\partial f_{k\eta}}{\partial \eta} + \frac{\partial f_{j\eta}}{\partial \eta} \frac{\partial^2 f_{k\eta}}{\partial \eta^2} \right] \frac{\partial^2 f_{l\eta}}{\partial \eta^2} \mathrm{d}\eta q^w(l) q^w(k) q^w(j) \tag{2.127}$$

$$t(18.2.12.1) = \frac{8}{b^3} A_{12} \int_{-1}^{1} f_{i\xi} \frac{\partial g_{j\xi}}{\partial \xi} f_{k\xi} \mathrm{d}\xi \int_{-1}^{1} \frac{\partial f_{i\eta}}{\partial \eta} g_{j\eta} \frac{\partial^3 f_{k\eta}}{\partial \eta^3} \mathrm{d}\eta q^u(j) q^w(k) \tag{2.128}$$

$$t(18.2.12.2) = \frac{8}{ab^3} A_{12} \int_{-1}^{1} f_{i\xi} \frac{\partial f_{j\xi}}{\partial \xi} \frac{\partial f_{k\xi}}{\partial \xi} f_{l\xi} \mathrm{d}\xi \int_{-1}^{1} \frac{\partial f_{i\eta}}{\partial \eta} f_{j\eta} f_{k\eta} \frac{\partial^3 f_{l\eta}}{\partial \eta^3} \mathrm{d}\eta q^w(l) q^w(k) q^w(j) \tag{2.129}$$

$$t(18.2.12.3) = \frac{8a}{b^4} A_{22} \int_{-1}^{1} f_{i\xi} g_{j\xi} f_{k\xi} \mathrm{d}\xi \int_{-1}^{1} \frac{\partial f_{i\eta}}{\partial \eta} \frac{\partial g_{j\eta}}{\partial \eta} \frac{\partial^3 f_{k\eta}}{\partial \eta^3} \mathrm{d}\eta q^v(j) q^w(k) \tag{2.130}$$

$$t(18.2.12.4) = \frac{8a}{b^5} A_{22} \int_{-1}^{1} f_{i\xi} f_{j\xi} f_{k\xi} f_{l\xi} \mathrm{d}\xi \int_{-1}^{1} \frac{\partial f_{i\eta}}{\partial \eta} \frac{\partial f_{j\eta}}{\partial \eta} \frac{\partial f_{k\eta}}{\partial \eta} \frac{\partial^3 f_{l\eta}}{\partial \eta^3} \mathrm{d}\eta q^w(l) q^w(k) q^w(j) \tag{2.131}$$

Rewriting the equations of motion in the matrix form after the application of the Galerkin method, one obtains a set of algebraic equations (discretized in space) but still with non-linear terms in time continuous variables $q(t)$:

$$\begin{bmatrix} 0 & 0 & 0 \\ 0 & 0 & 0 \\ 0 & 0 & [M_{ww}] \end{bmatrix} \begin{Bmatrix} \{\ddot{q}^u\} \\ \{\ddot{q}^v\} \\ \{\ddot{q}^w\} \end{Bmatrix} + \left\{ \begin{bmatrix} [K^1_{uu}] & [K^1_{uv}] & 0 \\ [K^1_{vu}] & [K^1_{vv}] & 0 \\ 0 & 0 & [K^1_{ww}] \end{bmatrix} + \begin{bmatrix} 0 & 0 & [K^2_{uw}] \\ 0 & 0 & [K^2_{vw}] \\ 0 & 0 & 0 \end{bmatrix} \right.$$
$$\left. + \begin{bmatrix} 0 & 0 & 0 \\ 0 & 0 & 0 \\ [K^3_{wu}] & [K^3_{wv}] & 0 \end{bmatrix} + \begin{bmatrix} 0 & 0 & 0 \\ 0 & 0 & 0 \\ 0 & 0 & [K^4_{ww}] \end{bmatrix} - \mu \left(\begin{bmatrix} 0 & 0 & 0 \\ 0 & 0 & 0 \\ [K^5_{wu}] & [K^5_{wv}] & 0 \end{bmatrix} + \begin{bmatrix} 0 & 0 & 0 \\ 0 & 0 & 0 \\ 0 & 0 & [K^6_{ww}] \end{bmatrix} \right) \right\}$$
$$\begin{Bmatrix} \{q^u\} \\ \{q^v\} \\ \{q^w\} \end{Bmatrix} = \{0\} \tag{2.132}$$

The mass matrix has only one component $[M_{ww}]$ since the in-plane inertia terms were neglected. $\left[K^1\right]$ is the linear stiffness matrix, $\left[K^2\right]$ and $\left[K^3\right]$ are the first order non-linear stiffness matrices (linearly dependent on the generalized displacements), $\left[K^4\right]$ is the second-order non-linear stiffness matrix, $\left[K^5\right]$ and $\left[K^6\right]$ are first and second-order non-linear non-local stiffness matrices respectively. It should be noted that the complete stiffness matrix is a square matrix with the dimension $2pi^2 + po^2$. Writing the sub-matrices and the terms previously calculated from which they are derived (with the exclusion of the displacement and acceleration vectors with lowest indexes, such as $q^u(j), q^v(j), q^w(j)$ and $\ddot{q}^w(j)$, for the stiffness and mass matrices respectively):

- $[M_{ww}]$: $t(19) + t(20)$
- $\left[K^1_{uu}\right]$: $t(1) + t(5)$
- $\left[K^1_{uv}\right]$: $t(3) + t(6)$
- $\left[K^1_{vu}\right]$: $t(8) + t(12)$
- $\left[K^1_{vv}\right]$: $t(10) + t(13)$
- $\left[K^1_{ww}\right]$: $t(15) + t(16) + t(17)$
- $\left[K^2_{uw}\right]$: $t(2) + t(4) + t(7)$
- $\left[K^2_{vw}\right]$: $t(9) + t(11) + t(14)$
- $\left[K^3_{wu}\right]$: $t(18.1.1) + t(18.1.5) + t(18.1.8) + t(18.1.11)$
- $\left[K^3_{wv}\right]$: $t(18.1.3) + t(18.1.6) + t(18.1.9) + t(18.1.13)$
- $\left[K^4_{ww}\right]$: $t(18.1.2) + t(18.1.4) + t(18.1.7) + t(18.1.10) + t(18.1.12) + t(18.1.14)$
- $\left[K^5_{wu}\right]$: $t(18.2.1.1) + t(18.2.2.1) + t(18.2.3.1) + t(18.2.4.1) + t(18.2.5.1) + t(18.2.6.1) + t(18.2.7.1) + t(18.2.8.1) + t(18.2.9.1) + t(18.2.10.1) + t(18.2.11.1) + t(18.2.12.1)$
- $\left[K^5_{wv}\right]$: $t(18.2.1.3) + t(18.2.2.3) + t(18.2.3.2) + t(18.2.4.2) + t(18.2.5.3) + t(18.2.6.3) + t(18.2.7.3) + t(18.2.8.3) + t(18.2.9.2) + t(18.2.10.2) + t(18.2.11.3) + t(18.2.12.3)$
- $\left[K^6_{ww}\right]$: $t(18.2.1.2) + t(18.2.1.4) + t(18.2.2.2) + t(18.2.2.4) + t(18.2.3.3) + t(18.2.4.3) + t(18.2.5.2) + t(18.2.5.4) + t(18.2.6.2) + t(18.2.6.4) + t(18.2.7.2) + t(18.2.7.4) + t(18.2.8.2) + t(18.2.8.4) + t(18.2.9.3) + t(18.2.10.3) + t(18.2.11.2) + t(18.2.11.4) + t(18.2.12.2) + t(18.2.12.4)$

2.6 Harmonic Balance Method

Time domain integration methods, such as Wilson-Theta, Newmark and central finite difference methods, can be applied to solve the non-linear differential equations. However, these are not particularly suitable to study frequency domain stationary solutions. Moreover, the conversion of the equations of motion into the frequency domain permits the posterior determination of turning and bifurcation points by the application of continuation methods, which will be explained ahead.

According to [10] and [54], the application of the harmonic balance method allows the reduction of a system of continuous non-linear differential equations in the time domain to a frequency domain problem by assuming a periodic solution in the form of a Fourier series, where each sinusoidal function that comprises the linear combination corresponds to a harmonic of the fundamental frequency. This assumed solution is posteriorly substituted in the equations of motion and the coefficients of equal harmonics are compared (hence the name harmonic balance method). Unlike perturbation methods, which rely on a small parameter and are consequently confined to weakly non-linear systems, the harmonic balance method is applicable to any non-linear problem without exception. Moreover, the latter is also advantageous for its simplicity, easy implementation and for the convergence of the

assumed solution to the exact periodic one (for smooth systems). The main disadvantage lies in the necessity for an appropriate selection of harmonics in the solution.

Rewriting (2.132) in terms of in-plane and out-of-plane displacements:

$$\begin{cases} \left[K_p^1\right]\{q^p\} + \left[K^2\right]\{q^b\} = \{0\} \\ [M_b]\left\{\ddot{q}^b\right\} + \left[K_b^1\right]\{q^b\} + \left[K^{3+5}\right]\{q^p\} + \left[K^{4+6}\right]\{q^b\} = \{0\} \end{cases} \tag{2.133}$$

where the $\left[K_p^1\right]$ and $\left[K_b^1\right]$ denote the in-plane and out-of-plane components of the matrix $\left[K^1\right]$ respectively; $[M_b]$ corresponds to the out-of-plane mass matrix; $\left[K^{3+5}\right]$ is equivalent to the assemblage of the first order non-linear local and non-local matrices $\left(\left[K^3\right];\mu\left[K^5\right]\right)$; $\left[K^{4+6}\right]$ follows the same logic with second order non-linear local and non-local matrices and $\{q^p\}$ and $\{q^b\}$ designate the in-plane and out-of-plane generalized displacement vectors respectively. Solving the first equation of (2.133) with respect to $\{q^p\}$:

$$\{q^p\} = -\left[K_p^1\right]^{-1}\left[K^2\right]\left\{q^b\right\} \tag{2.134}$$

And substituting (2.134) in the second equation of (2.133) one can write:

$$[M_b]\left\{\ddot{q}^b\right\} + \left(\left[K_b^1\right] - \left[K^{3+5}\right]\left[K_p^1\right]^{-1}\left[K^2\right] + \left[K^{4+6}\right]\right)\left\{q^b\right\} = \{0\} \tag{2.135}$$

Since $\left[K^{3+5}\right]$ and $\left[K^2\right]$ are both first order polynomial functions of $\left\{q^b\right\}$ and the matrix $\left[K^{4+6}\right]$ is a second order polynomial function, $\left(-\left[K^{3+5}\right]\left[K_p^1\right]^{-1}\left[K^2\right] + \left[K^{4+6}\right]\right)\{q^b\}$ is a third order function of $\left\{q^b\right\}$. It can now be seen that the equations of motion are of undamped *Duffing* type, which generically can be written as:

$$[M]\{\ddot{q}(t)\} + [K_L]\{q(t)\} + [K_{NL}(q(t))]\{q(t)\} = \{0\} \tag{2.136}$$

where $[M]$ in this case would be the out-of-plane mass matrix $[M_b]$; $[K_L]$ corresponds to the out-of-plane stiffness matrix $\left[K_b^1\right]$ and $[K_{NL}]$ represents $\left(-\left[K^{3+5}\right]\left[K_p^1\right]^{-1}\left[K^2\right] + \left[K^{4+6}\right]\right)$ which, as it was mentioned before, is a function of the out-of-plane generalized displacements.

Because the system's non-linearity is cubic, only odd harmonics are considered in the Fourier series for the assumed solution [54]:

$$\left\{q^b(t)\right\} = \sum_{i=1,3}^{2k-1} \{w_{ci}\}\cos(i\omega t) + \{w_{si}\}\sin(i\omega t) \tag{2.137}$$

The sine term can be neglected since the system is undamped and for this model only one harmonic will be taken into account. This consideration, however, can lead to significant errors if the existence of internal resonance is verified. As mentioned before, this phenomena occurs when the natural frequencies of a multiple degrees of freedom system become commensurable, which causes coupling of the normal modes resulting in

multi-mode, multi-frequency response [42]. With the consideration of a single harmonic, the assumed solution can be rewritten for this case as follows:

$$\left\{q^b(t)\right\} = \{w_{c1}\}\cos(\omega t) \tag{2.138}$$

And the second derivative of the out-of-plane generalized displacement vector is:

$$\left\{\ddot{q}^b(t)\right\} = -\omega^2\{w_{c1}\}\cos(\omega t) \tag{2.139}$$

Rewriting (2.136) and substituting with the assumed solution (2.138) and its second derivative (2.139):

$$\left(-\omega^2[M]\cos(\omega t) + [K_L]\cos(\omega t) + [K_{NL}(\{w_{c1}\})]\cos^3(\omega t)\right)\{w_{c1}\} = \{0\} \tag{2.140}$$

The term $\cos^3(\omega t)$ can be written as:

$$\cos^3(\omega t) = \frac{3}{4}\cos(\omega t) + \frac{1}{4}\cos(3\omega t) \tag{2.141}$$

Substituting (2.141) in (2.140) and neglecting $\frac{1}{4}\cos(3\omega t)$ due to the consideration of a single harmonic:

$$\left(-\omega^2[M]\cos(\omega t) + [K_L]\cos(\omega t) + \frac{3}{4}[K_{NL}(\{w_{c1}\})]\cos(\omega t)\right)\{w_{c1}\} = \{0\} \tag{2.142}$$

which after the cosine elimination one finally obtains an eigenvalue-type problem:

$$\left\{F\left(\{w_{c1}\},\omega^2\right)\right\} = \left(-\omega^2[M] + [K_L] + \frac{3}{4}[K_{NL}(\{w_{c1}\})]\right)\{w_{c1}\} = \{0\} \tag{2.143}$$

It should be noted that the equation (2.143) has no analytical solution and can only be solved through numerical methods. One viable option for solving the non-linear problem and obtaining the FRF or the backbone curve is the application of Newton-Raphson's method integrated in an external loop where for each fixed frequency, the values of the vector $\{w_{c1}\}_i$ are predictions to the solution and subsequently corrected by the method, until convergence is achieved. This process would then be repeated for another fixed value of frequency. Since this analysis is for free vibration, for the first prediction of the first solution, the linear mode of vibration can be used.

2.7 Continuation Method

Unlike Newton-Raphson's method, continuation methods are able to pass turning points, bifurcation points and follow secondary branches of solutions. In other words, regions of multiple solutions that may exist in the context of non-linear vibrations would be much harder to find if the Newton-Raphson's method was to be applied. However, there are various similarities between methods as the continuation method version presented in this work integrates the latter with the addition of an "arc-length" constraint equation [55]. To obtain the backbone curve, the transverse displacement vector $\{w_{c1}\}$ (which will be written solely as $\{w\}$ for a matter of convenience), is incremented in an external loop. In this loop, a predictor or approximation to the solution is defined considering the two last points of the backbone curve $\left(\{w\}_i, \omega_i^2\right)$ and $\left(\{w\}_{i-1}, \omega_{i-1}^2\right)$, (note that a vector is needed in order to determine the direction in which the method must proceed). The following steps are considered in [54]:

$$\{w\}_{i+1} = \{w\}_i + \Delta\{w\}_{i+1} \tag{2.144a}$$

$$\Delta\{w\}_{i+1} = \left(\{w\}_i - \{w\}_{i-1}\right) \frac{dwaux}{w_m} \tag{2.144b}$$

where $dwaux$ designates the amplitude of the first increment vector $\Delta\{w\}_{i+1}$ and w_m is the difference between amplitudes of consecutive transverse displacement vectors $\left(\{w\}_i - \{w\}_{i-1}\right)$. Analogously, for the prediction to the solution of the natural frequencies:

$$\omega_{i+1}^2 = \omega_i^2 + \Delta\omega_0^2 \tag{2.145a}$$

$$\Delta\omega_0^2 = \pm \frac{s}{\sqrt{\left(\{\delta w\}_1^T \{\delta w\}_1\right)}} \tag{2.145b}$$

The sign of the previous increment is used and can only be changed if the determinant of the Jacobian matrix $[J]$ also changed its sign. The determination of the vector $\{\delta w\}_1$ will be derived from the equations established in the internal loop, using the last known frequency of the curve. The parameter s denotes the arc-length between two successive points of the backbone curve and is obtained by restraining that distance to a fixed value using a constraint equation:

$$s^2 = \left\| \Delta\{w\}_{i+1} \right\|^2 \tag{2.146}$$

The approximated solution for the amplitude vector and for the natural frequency is corrected in the internal loop by the application of Newton-Raphson's method. From equation (2.143) one obtains:

$$[J]\{\delta w\} - [M]\{w\}_{i+1}\delta\omega^2 = -\{F\} \tag{2.147}$$

where $[J]$ is the Jacobian of $\{F\}$ defined by:

$$[J] = \frac{\partial \{F\}}{\partial \{w\}} \tag{2.148}$$

It should be noted that unlike strict Newton-Raphson's method, where only the static part of the left subexpression is considered, thus reducing the problem to one equation of one unknown (amplitude vector), equation (2.147) has the frequency of vibration as an unknown as well. This is the reason why continuation methods are able to pass turning points, permitting a much better characterization of non-linear systems if multiple solutions are to occur, granted that an adequate arc-length s is chosen and that the constraint equation (2.146) is added in order to solve the two variable problem. So, despite the benefits and the improved description of the non-linear vibration behaviour, continuation methods require greater computational effort, one of the reasons being the necessity for an extra equation.

From equation (2.146) one can rewrite $\{\delta w\}$ as:

$$\{\delta w\} = \delta\omega^2 \{\delta w\}_1 + \{\delta w\}_2 \tag{2.149}$$

where $\{\delta w\}_1$ and $\{\delta w\}_2$ result from the following equations derived from (2.147):

$$[J] \{\delta w\}_1 = [M] \{w\}_{i+1} \tag{2.150a}$$
$$[J] \{\delta w\}_2 = -\{F\} \tag{2.150b}$$

The solutions of the vectors $\{\delta w\}_1$ and $\{\delta w\}_2$ expressed above should be obtained by solving the system of equations (2.150) and not by the inversion of $[J]$ since the latter may lead to an increased number of operations and to considerably larger numerical round-off errors. After determining both $\{\delta w\}_1$ and $\{\delta w\}_2$ and calculating $\{\delta w\}$ one can correct the value of the amplitude vector $\{w\}_{i+1}$ considering:

$$\{w\}_{i+1} = \{w\}_i + \Delta \{w\}_{i+1} \tag{2.151a}$$
$$\Delta \{w\}_{i+1} = \Delta \{w\}_{i+1}^{previous} + \{\delta w\} \tag{2.151b}$$

Note that the superscript *previous* refers to the previous iteration of the internal loop, whereas i is the index of the external loop. Substituting $\Delta \{w\}_{i+1}$ from equation (2.151b) into the constraint equation (2.146) one arrives at:

$$a_1 \left(\delta\omega^2\right)^2 + a_2 \delta\omega^2 + a_3 = 0 \tag{2.152}$$

where each constant a_1, a_2, a_3 can be written as follows:

$$a_1 = \{\delta w\}_1^T \{\delta w\}_1 \tag{2.153a}$$

$$a_2 = 2\left(\Delta \{w\}_{i+1}^{previous} + \{\delta w\}_2\right)^T \{\delta w\}_1 \tag{2.153b}$$

$$a_3 = \left(\Delta \{w\}_{i+1}^{previous} + \{\delta w\}_2\right)^T \left(\Delta \{w\}_{i+1}^{previous} + \{\delta w\}_2\right) - s^2 \tag{2.153c}$$

It should be mentioned that equation (2.152) has two solutions. Therefore, in order to avoid a return to an already determined region of the backbone curve, the angle between the incremental amplitude vector of the previous and present iteration must be positive, thus generating a new point in the curve. If both angles are positive, the appropriate root is determined by comparison with the linear solution.

For the correction of the natural frequencies, a similar procedure to the one applied to the amplitude vector is adopted:

$$\omega_{i+1}^2 = \omega_i^2 + \Delta\omega_{i+1}^2 \tag{2.154a}$$

$$\Delta\omega_{i+1}^2 = \left(\Delta\omega_{i+1}^2\right)_{previous} + \delta\omega^2 \tag{2.154b}$$

The iterations of the internal loop are repeated until convergence is achieved. The criterion for satisfiable convergence is defined by three errors:

$$\left|\frac{\delta\omega^2}{\omega_{i+1}^2}\right| < error_1 \tag{2.155a}$$

$$\frac{\|\{\delta w\}\|}{\left\|\{w\}_{i+1}\right\|} < error_2 \tag{2.155b}$$

$$\|\{F\}\| < error_3 \tag{2.155c}$$

If the number of iterations necessary to achieve convergence or the difference $\omega_{i+1} - \omega_i$ is larger than the desired value, the arc-length s and the amplitude of the first increment vector $dwaux$ are reduced. This procedure is also applied in case the solution of equation (2.152) is complex.

2.8 Conclusions

In this chapter, a thin-plate model based on Kirchhoff plate theory, applicable to both isotropic and orthotropic materials, with inclusion of small-scale effect by the consideration of non-local constitutive relations proposed by Eringen, was devised. The equations of motion were established after the application of Hamilton's principle as were posteriorly discretized in space coordinates by the Galerkin method. After obtaining a system of equations in the weak formulation, the harmonic balance method was employed converting a time domain problem to a frequency domain system of algebraic equations. A single harmonic was considered and therefore the periodic response of the plate was in fact considered harmonic in nature. Lastly, an arc-length continuation method, which allows one to solve the non-linear resulting equations of motion, was presented.

Chapter 3

Numerical Results

3.1 Introduction

In this chapter the model developed previously will be verified and various cases will be analysed. This chapter is divided in two main sections, the first referring to the linear eigenvalue problem typically encountered in the study of linear vibrations and the second dealing with the non-linear problem. This division was purposely done as it follows the sequence of this work, since after the implementation of the model, the geometrical non-linear terms were discarded and the linear natural frequencies and mode shapes were calculated. Only after the validation of the linear model was the non-linear problem addressed. It is worth mentioning that for both linear and non-linear sections, both local and non-local cases were analysed.

3.2 Linear Analysis

To validate the model formulated in the previous chapter, the linear eigenvalue-type problem was first considered. Since all non-linear matrices (those that depend either linearly or quadratically on the transverse displacement vector) are dismissed, only the linear stiffness matrix $\left[K^1\right]$ and the mass matrix $[M]$ are considered. Consequently, the stiffness matrices affected by the non-local parameter are not taken into account due to their non-linearity, reducing the influence of the small-scale effect solely to the mass matrix. Henceforth, this reduced model will be referred as the linear model.

In this section convergence of the eigenvalue-type problem will be discussed for different boundary conditions, the linear natural frequencies and mode shapes will be analysed for different non-local parameters and its influence will be verified for various plate length's and boundary conditions. A comparison between an isotropic linear model and orthotropic one will also be performed for a single layer graphene sheet.

3.2.1 Convergence and Validation of the Linear Model

The first four linear natural frequencies of a fully clamped (CCCC) and pinned (SSSS) square plate with the non-local parameter set to zero were calculated in *Maple 2015* software and compared with the results by A.W. Leissa in [56]. Different numbers of out-of-plane shape functions were used in order to study the convergence of the linear model

and the respective relative error was calculated. The fully clamped and pinned boundary conditions are expressed below:

- CCCC ($u^0 = v^0 = w^0 = \frac{\partial w^0}{\partial x} = \frac{\partial w^0}{\partial y} = 0$ along $x = 0, a$; $y = 0, b$)
- SSSS ($u^0 = v^0 = w^0 = \frac{\partial w^0}{\partial y} = 0$ along $x = 0, a$; $u^0 = v^0 = w^0 = \frac{\partial w^0}{\partial x} = 0$ along $y = 0, b$)

The plate considered is an isotropic linear model (neglecting the geometric non-linearity associated with Von Kármán strains) of a square graphene sheet with the following elastic and geometric properties from [57]:

Table 3.1: Isotropic square SLGS properties with $\mu = 0$ [57]

E [TPa]	a [nm]	h [nm]	ν	ρ [kg/m^3]	μ [nm^2]
1.06	10	0.34	0.25	2250	0

Table 3.2: Linear natural frequencies [THz] of square SLGS - CCCC

	po	ω_{11}	error (%)	ω_{12}, ω_{21}	error (%)	ω_{22}	error (%)
Sol. by Leissa	-	0.12601	-	0.25701	-	0.37895	-
	3	0.12603	0.016	0.25977	1.074	0.38026	0.346
Model	5	0.12601	0	0.25707	0.023	0.37909	0.037
	7	0.12601	0	0.25701	0	0.37895	0
	9	0.12601	0	0.25701	0	0.37895	0

Table 3.3: Linear natural frequencies [THz] of square SLGS - SSSS

	po	ω_{11}	error (%)	ω_{12}, ω_{21}	error (%)	ω_{22}	error (%)
Sol. by Leissa	-	0.06912	-	0.17280	-	0.27649	-
	3	0.06913	0.014	0.20558	18.970	0.32413	17.23
Model	5	0.06912	0	0.17330	0.289	0.27722	0.264
	7	0.06912	0	0.17281	0.006	0.27649	0
	9	0.06912	0	0.17280	0	0.27649	0

In Table 3.2 the first four linear natural frequencies are calculated for a fully clamped graphene sheet. It can be seen that the solutions obtained with the linear model are in good agreement with the solutions from [56] (when using a minimum of 5 out-of-plane shape functions the relative errors are well below 1%). Convergence of the linear natural frequencies can be confirmed since from $po = 7$ to $po = 9$ the results obtained were identical.

In Table 3.3 the natural frequencies are calculated for a pinned plate. Convergence is verified and the results obtained are in excellent agreement with the exact solution, leading to relative errors of almost 0% when using a minimum of 7 out-of-plane shape

functions (except for ω_{12}, ω_{21}). An important aspect to take into account is the considerably lower value of the linear natural frequencies of a pinned plate than that of a fully clamped one, which can be justified by the higher stiffness of the latter, since not only the displacements but also the rotations around the edges are restrained, thus increasing the in-plane membrane stresses.

To verify and analyse the influence of the non-local parameter on the linear natural frequencies, a pinned square isotropic plate (SSSS) which properties (dimensionless) are presented in Table 3.4, is considered. The solutions were obtained with $po = 5$ and $po = 7$ and were posteriorly compared with a classical plate model considering Eringen's non-local elasticity theory from [58] which can be observed in Table 3.5.

Table 3.4: Isotropic square plate properties [58]

E	a	h	ν	ρ
30×10^6	10	1	0.3	1

Table 3.5: Linear natural frequencies $\bar{\omega} = \omega h\sqrt{\frac{\rho}{G}}$ of a square plate - SSSS with varying non-local parameter

	μ	Classical [58]	Model ($po = 5$)	error (%)	Model ($po = 7$)	error (%)
	0	0.0963	0.0963	0	0.0963	0
	1	0.0880	0.0880	0	0.0880	0
$\bar{\omega}_{11}$	2	0.0816	0.0816	0	0.0816	0
	3	0.0763	0.0763	0	0.0763	0
	4	0.0720	0.0720	0	0.0720	0
	5	0.0683	0.0683	0	0.0683	0
	0	0.3853	0.3863	0.26	0.3853	0
	1	0.2880	0.2887	0.24	0.2880	0
$\bar{\omega}_{22}$	2	0.2399	0.2404	0.21	0.2399	0
	3	0.2099	0.2103	0.19	0.2099	0
	4	0.1889	0.1893	0.21	0.1889	0
	5	0.1732	0.1736	0.23	0.1732	0
	0	0.8669	0.8770	1.17	0.8670	0.01
	1	0.5202	0.5252	0.96	0.5203	0.02
$\bar{\omega}_{33}$	2	0.4063	0.4100	0.91	0.4063	0
	3	0.3446	0.3477	0.90	0.3446	0
	4	0.3045	0.3072	0.89	0.3045	0
	5	0.2757	0.2782	0.91	0.2758	0.04

In Table 3.5 it can be verified that an increase in the value of the non-local parameter decreases the linear natural frequencies, which can be explained by the increase in the inertia of the plate. Note that if non-linearity was being considered, the non-local parameter would also affect the stiffness of the system leading to an increase in the effective non-linear natural frequencies (this phenomena will be discussed ahead). It can be verified that even with 5 out-of-plane functions the results obtained are very accurate for $\bar{\omega}_{11}$ despite variation in the non-local parameter. In fact, different values of the non-local parameter have no apparent correlation with the accuracy of the model, as there is no visible tendency of the relative error and the disparity between the model and the solution proposed in [58] is relatively arbitrary, given that the same number of shape functions is being used. For $\bar{\omega}_{22}$ and $\bar{\omega}_{33}$ the results obtained with 7 shape functions had relative errors of approximately 0% (except a few which are all below 0.05%).

The first linear natural frequency, in [THz], was also compared with the results obtained with a continuum linear isotropic non-local model and a molecular dynamics simulation, referred to as MD for abbreviation, for different lengths of a square plate from [11]. The natural frequency was calculated for a single layer graphene sheet with two different configurations (armchair and zig-zag) and for distinct boundary conditions (pinned and fully clamped) using a set of five shape functions for the out-of-plane displacements ($po = 5$). The elastic and geometric properties considered are presented in Table 3.6. Note that depending on the graphene configuration, the geometry of the plate and the boundary conditions, the adequate value for the non-local parameter varies. In fact, the estimation of the appropriate non-local parameter is a debatable subject and atomistic models or even experimental procedures are generally used to extrapolate it. In the four different cases studied below, the values used for the non-local parameter are proposed in [11].

Table 3.6: Isotropic square SLGS properties [11]

E [TPa]	h [nm]	ν	ρ [kg/m^3]
1	0.34	0.16	2250

Table 3.7: First linear natural frequency [THz] of zig-zag SSSS SLGS for different values of a ($\mu = 1.41$ nm^2)

MD [11]	Difference (%)	Model [11]	Difference (%)	Model	a [nm]
0.0587725	5.04	0.0584221	4.47	0.0558072	10
0.0157524	0.26	0.0164593	4.548	0.0157107	20
0.0070655	1.37	0.0075049	4.56	0.00716255	30

Table 3.8: First linear natural frequency [THz] of zig-zag CCCC SLGS for different values of a ($\mu = 0.87$ nm^2)

MD [11]	Difference (%)	Model [11]	Difference (%)	Model	a [nm]
0.1146223	3.68	0.1141898	3.31	0.1104043	10
0.0306219	4.14	0.0306486	4.23	0.0293533	20
0.0132953	0.67	0.0138166	4.41	0.0132066	30

Table 3.9: First linear natural frequency [THz] of armchair SSSS SLGS for different values of a ($\mu = 1.34$ nm^2)

MD [11]	Difference (%)	Model [11]	Difference (%)	Model	a [nm]
0.0595014	4.9	0.0592359	4.48	0.0565847	10
0.0158141	0.22	0.0165309	4.55	0.0157791	20
0.0070712	1.5	0.0075201	4.56	0.00717709	30

Table 3.10: First linear natural frequency [THz] of armchair CCCC SLGS for different values of a ($\mu = 0.71$ nm^2)

MD [11]	Difference (%)	Model [11]	Difference (%)	Model	a [nm]
0.1162438	2.47	0.1160658	2.32	0.1133711	10
0.0307422	3.816	0.0307898	3.96	0.02956909	20
0.0133060	0.41	0.0138455	4.3	0.01325048	30

It can be verified that the relative difference between the linear model presented in this work and the molecular dynamics simulation is generally lower than that between the model and the results from [11]. Although the agreement between solutions is not particularly good for some cases (some relative errors are up to 5%) it is necessary to take under consideration the fact that neither the model nor the molecular dynamics simulation are exact solutions. It is worth mentioning that armchair sheets have slightly higher linear natural frequencies than zig-zag sheets, which is clearly observable when comparing both molecular configurations for the same boundary condition (Table 3.7, Table 3.8 and Table 3.9, Table 3.10). Perhaps more importantly, the influence of boundary conditions should be noted, which seems to considerably affect the natural frequencies and shows to become less relevant with the increase in the size of the sheet. In fact, one may say that chirality is almost negligible when compared to the effect of boundary conditions on the natural frequencies. As it was indicated before, an increase in the non-local parameter results in lower linear natural frequencies, hence the higher values for the armchair configuration, particularly for sheets with a smaller length where the small-scale effect has greater influence, as will be demonstrated ahead.

3.2.2 Size and non-local effects

The influence of the plate's length was evaluated for the first linear natural frequency and for ω_{22} (fourth linear natural frequency for the square plate case) considering different values of the non-local parameter. Three cases were analysed: A pinned isotropic square plate $a = b = 10$, a pinned isotropic rectangular plate with $b = 10$ and a pinned isotropic rectangular plate with $b = 50$ (for the two rectangular cases only a was varied). The plate's properties were the same considered in Table 3.4. For all cases, 5 out-of-plane shape functions were used. Regardless of the plate's geometry or non-local parameter, the increase in the size of the plate results in a decrease in the linear natural frequencies.

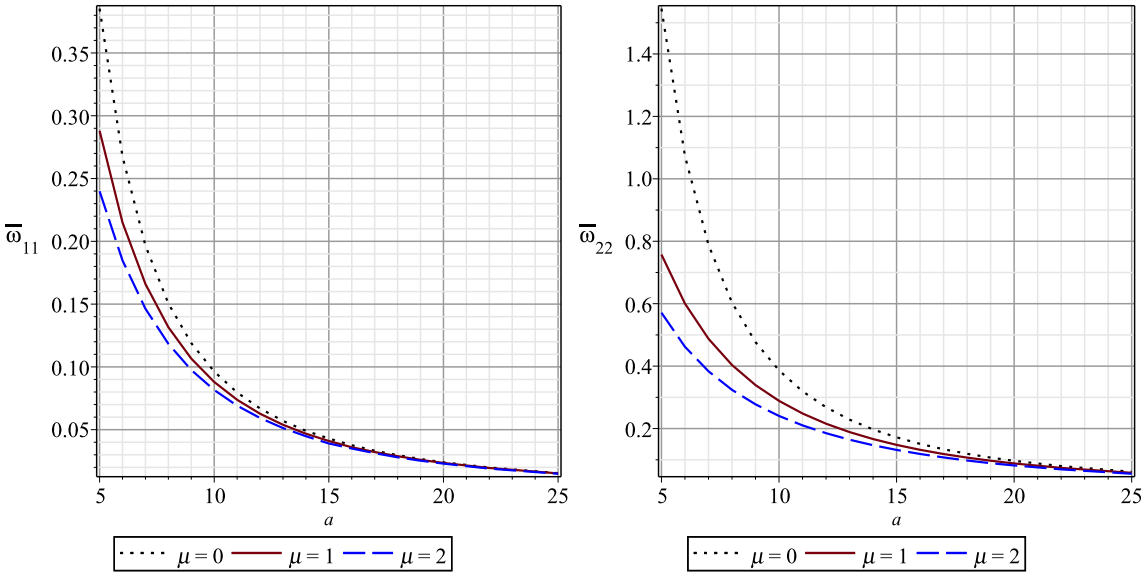

(a) $\bar{\omega}_{11}$ (b) $\bar{\omega}_{22}$

Figure 3.1: Variation in linear natural frequencies of a square plate - SSSS with a for different values of non-local parameter

It can be observed that for both subfigure 3.1a and 3.1b the linear natural frequencies vary considerably for $a = 5$ to around $a = 10$ for different values of the non-local parameter. This dispersion becomes less accentuated as the length of the square plate is increased, which implies that the small-scale effect is less pronounced for larger plates. Indeed, for a considerably larger external length than the internal characteristic length [35], Eringen's non-local elasticity is reduced to the classic elasticity theory developed by Hooke, thus the small-scale effect becomes nonexistent. It should be noted that the difference between natural frequencies for the same plate's length and varying non-local parameter is significantly greater for the fourth natural frequency than the first. In other words, the small-scale effect has greater influence on higher natural frequencies and higher modes of vibration seeing that the "effective" length, denoted "L_e", is half of the nominal length "L_n" for the case of the fourth mode of vibration (since in this case there is a vibration node in each direction). On the other hand, for the first mode, the nominal length coincides with the "effective" one, as illustrated in Figure 3.2. Evidently for the shorter "effective" length, the small-scale effect has greater influence. It should be mentioned that the illustration in Figure 3.2 corresponds to a fully clamped plate and does not represent

the plate studied in Figure 3.1.

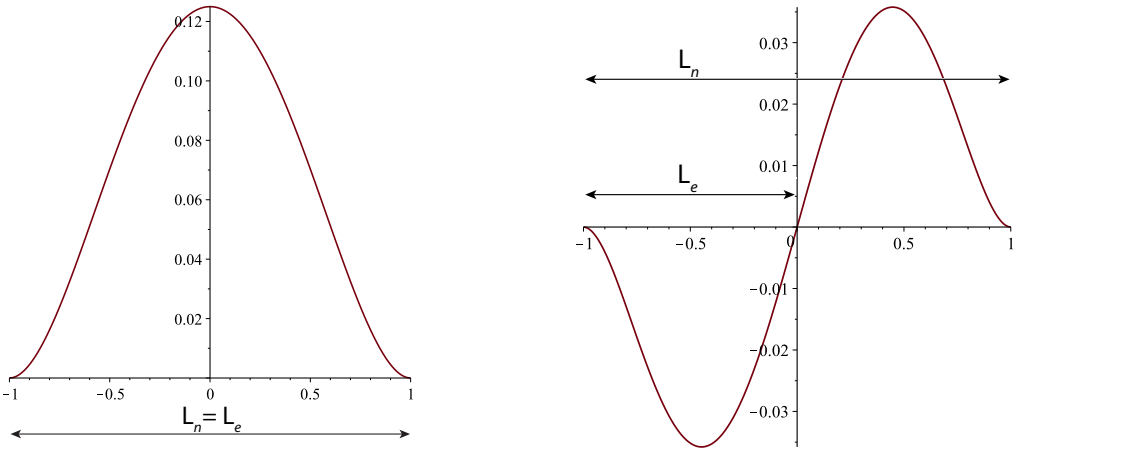

(a) Section of the first mode of vibration $y = 0$ (b) Section of the fourth mode of vibration $x = y$

Figure 3.2: Nominal L_n and "effective" L_e lengths

In Figure 3.3 the first rectangular plate, with $b = 10$ is analysed. Contrarily to the square plate, where the values of the linear natural frequencies gradually converge with the increase of the plate's length, in this case, in spite of the length of the plate, there is still a considerable dispersion between curves for different non-local parameters. One can conclude that increasing only one of the sides' length is not enough to suppress the size-effect since, although it might become less significant in the direction of the larger side, it still cannot be neglected in the smaller one.

However, in Figure 3.4 the convergence of the linear natural frequencies for a considerable length a is prominent. In this case, despite considering a rectangular plate as well, the constant length b is very large, as opposed to Figure 3.3. As a matter of fact, the first rectangular plate further deviates from a square plate after $a = 10$, which results in an increasingly larger aspect ratio where the smaller side emphasises the small-scale effect. The second rectangular plate is the opposite in what concerns the evolution of the aspect ratio, approaching a square plate as a is increased. As a result, the small-scale effect only attributed to length a, since b is already quite large, only reduces with its increase, provoking a behaviour in the natural frequencies similar to the one observed in the case of a square plate.

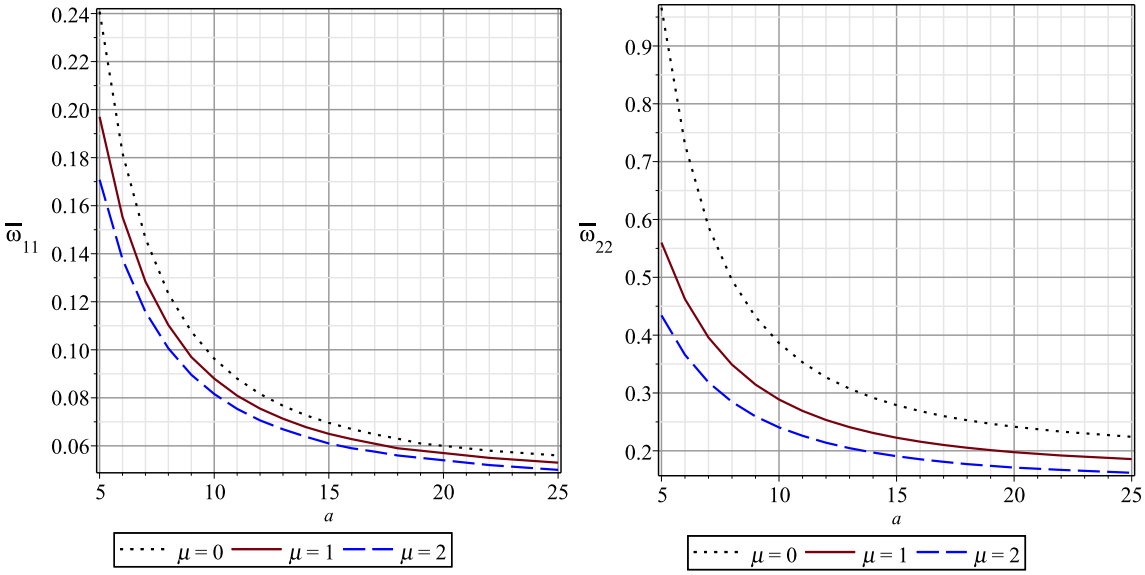

(a) $\bar{\omega}_{11}$ (b) $\bar{\omega}_{22}$

Figure 3.3: Variation in linear natural frequencies of a rectangular plate $b = 10$ - SSSS with a for different values of non-local parameter

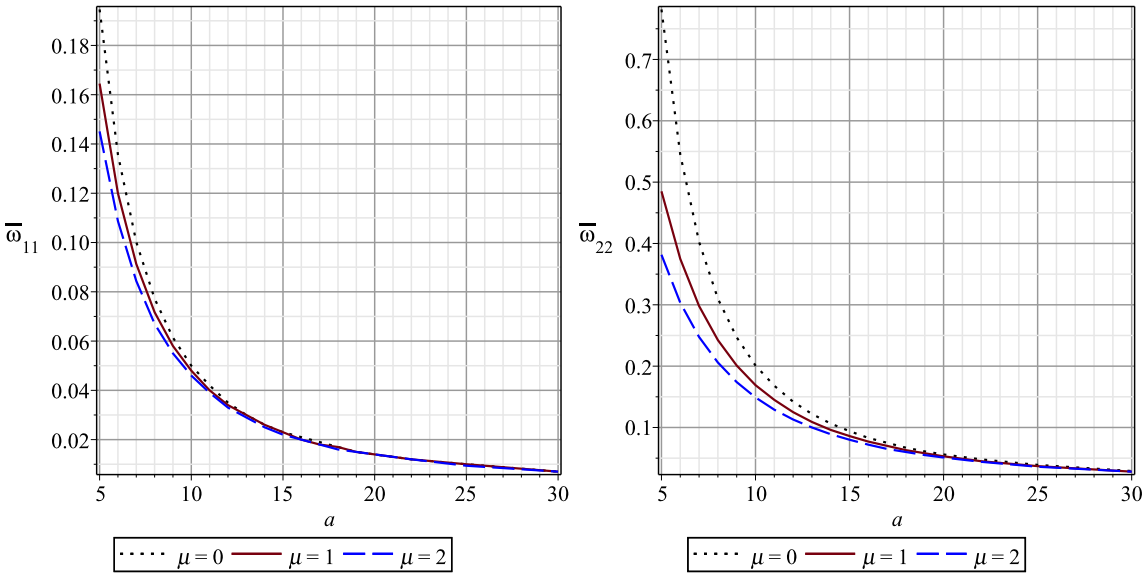

(a) $\bar{\omega}_{11}$ (b) $\bar{\omega}_{22}$

Figure 3.4: Variation in linear natural frequencies of a rectangular plate $b = 50$ - SSSS with a for different values of non-local parameter

In Figure 3.5 the effect of the non-local parameter was studied for different boundary conditions (SSSS and CCCC). A square isotropic plate was considered and the first and fourth linear natural frequencies were calculated for both boundary conditions, varying the non-local parameter. The geometric and elastic properties of the plate were the same as those used in Table 3.4 and five shape functions were used for both in-plane and out-

of-plane displacements.

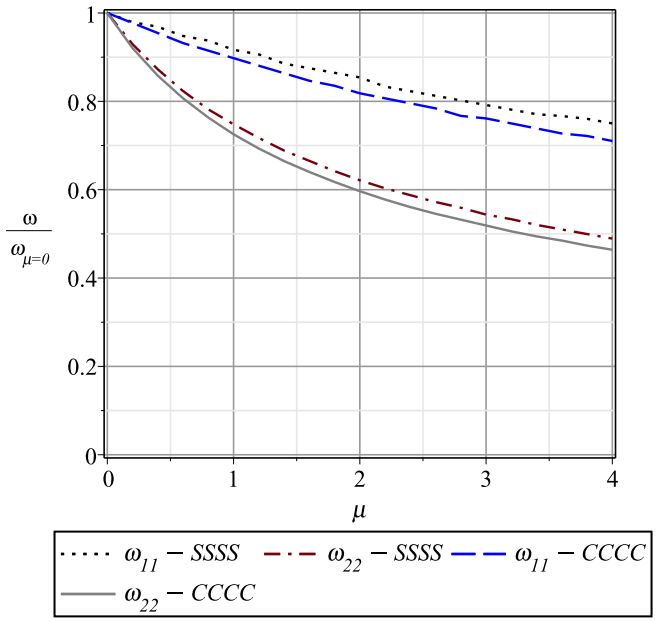

Figure 3.5: Variation of the ratio $\frac{\omega}{\omega_{\mu=0}}$ of a square isotropic plate with μ for different boundary conditions

It can be observed that the small-scale effect has greater influence on fully clamped plates than pinned ones since the variation in the ratio of the linear natural frequencies and the respective linear local ($\mu = 0$) natural frequency is bigger for the first case. One possible explanation for the slight difference in these ratios might be the marginally smaller "effective" length of the fully clamped plate, where the edges of the plate are not allowed to rotate and subsequently have zero slope near the edges (reducing the length of the plate that is effectively moved during a period of vibration). This smaller "effective" length is responsible for the higher influence of the small-scale effect on the fully clamped plate. In addition, the fourth linear natural frequency shows larger variation than the first, which, as mentioned before, reflects greater influence of the small-scale effect on higher natural frequencies.

The influence of the small-scale effect on the linear mode shapes was also evaluated for the same isotropic square plate considering different boundary conditions. It was verified that the small-scale effect had no influence on the linear mode shapes for the case of the pinned plate and these remained unaltered for considerably large variations of the non-local parameter. For the case of the fully clamped plate, the variation in mode shapes was more significant for higher modes of vibration, which was expected. For high values of the non-local parameter, the disparity in mode shapes decreased and from a given value (depending on the mode of vibration) the increase in the parameter did not yield any further variation. Only the fully clamped case is presented and the first, second, fourth and fifth mode can be visualized in Figure 3.6. The representation of the mode shapes was purposely done in the $y = 0$ plane for the first, second and fifth mode and in the $y = x$ plane for the fourth mode since a three-dimensional plot of overlapping mode shapes would not be very clear. It should be noted that for the first, second and fourth mode, the shape

correspondent to $\mu = 4$ was not considered since it was almost indistinguishable from $\mu = 3$.

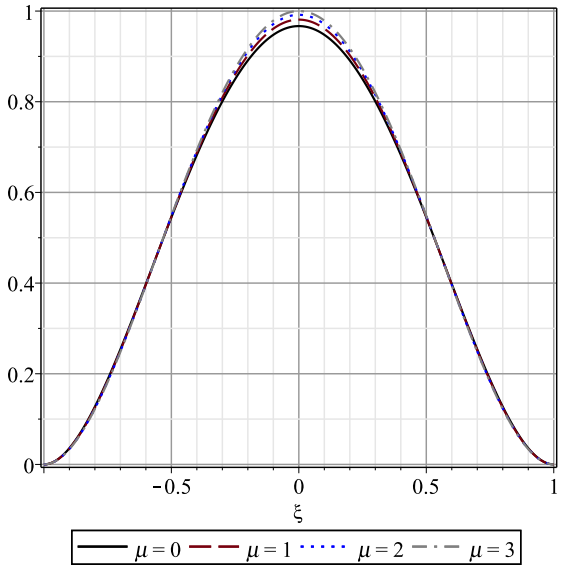

(a) 1st - $y = 0$ plane

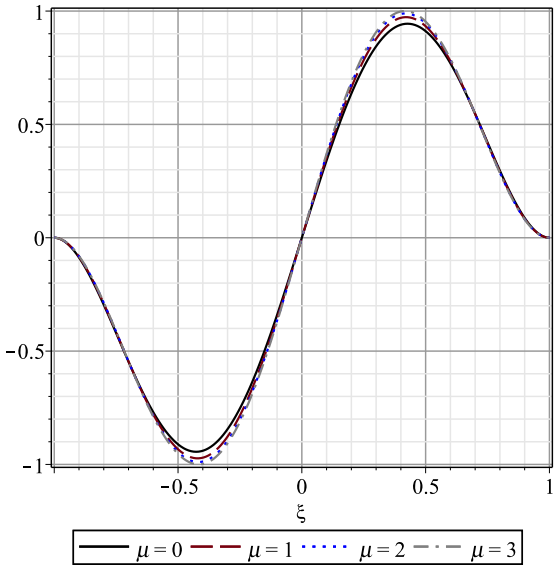

(b) 2nd - $y = 0$ plane

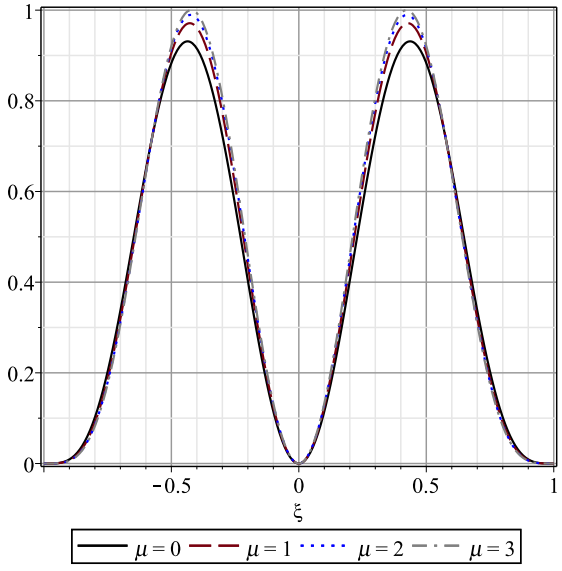

(c) 4th - $y = x$ plane

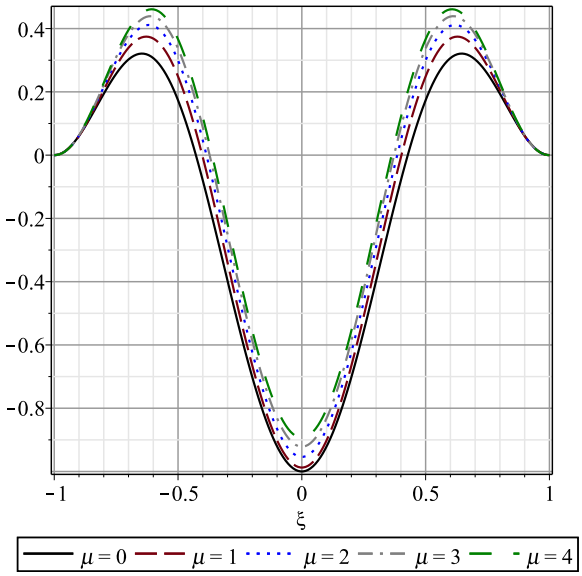

(d) 5th - $y = 0$ plane

Figure 3.6: Sections of modes shapes of a square isotropic plate for different values of μ - CCCC

3.2.3 Isotropic and Orthotropic Models

In the presented model, both isotropic and orthotropic materials can be considered. For the particular case of single layer graphene sheets, both approaches have been done in the past and good results have been obtained with both isotropic and orthotropic modelling. However, the selection of an accurate Young's modulus is necessary for the simplified isotropic formulations to be consistent with the results achieved by more complex orthotropic ones. In this section, a comparison between the first and fourth linear natural frequencies was conducted for a square single layer graphene sheet considering orthotropic and isotropic elastic properties, with varying non-local parameter. The results were obtained using a set of five shape functions for the out-of-plane displacements and both pinned and fully clamped boundary conditions were studied. The orthotropic material properties are proposed in [59] and are presented in Table 3.11. For the isotropic model, the Young's modulus was the average between E_1 and E_2, corresponding to 1676.5 [GPa], the Poisson ratio was set to 0.3 and the remaining properties were unchanged.

Table 3.11: Square orthotropic SLGS properties

E_1 [GPa]	E_2 [GPa]	G_{12} [GPa]	a [nm]	h [nm]	ν_{12}	ρ [kg/m^3]
1765	1588	678.85	10	0.34	0.3	2500

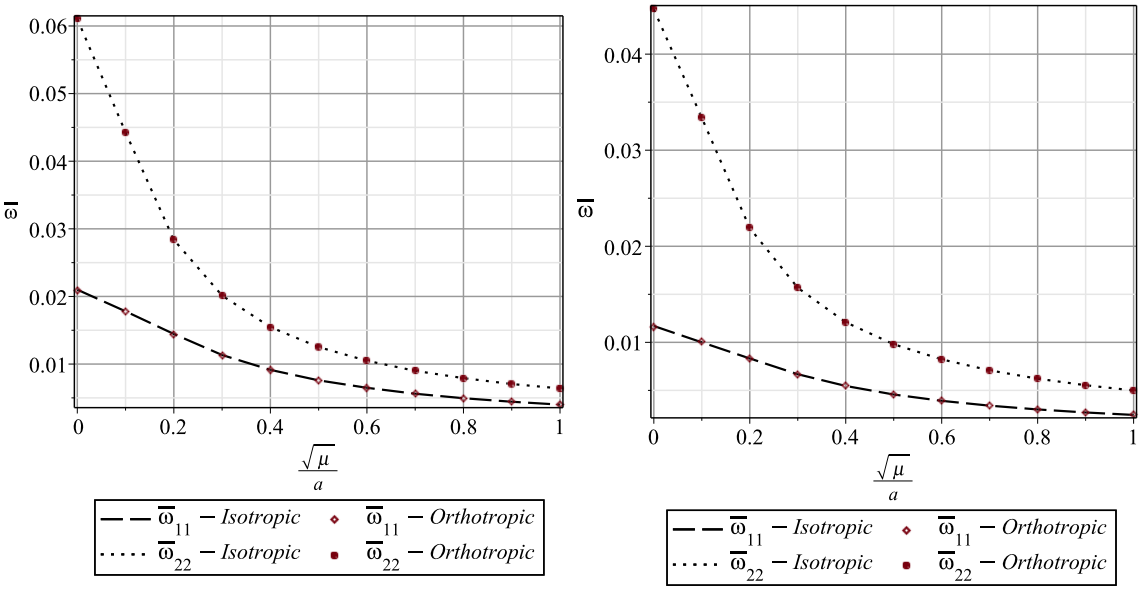

(a) Fully Clamped - CCCC

(b) Pinned - SSSS

Figure 3.7: First and fourth linear natural frequencies of a square SLGS for different μ with isotropic and orthotropic models

From Figure 3.7a it can be concluded that given an adequate value for the Young's modulus (in this case, the average of the two orthotropic moduli), the results for the linear natural frequencies using an isotropic model are in very good agreement with the orthotropic alternative, for either pinned and fully clamped edges, and for different values of the non-local parameter.

A second comparison between the isotropic and orthotropic model was performed and the linear mode shapes of the same square single layer graphene sheet were investigated using the values $\sqrt{\mu}/a = 0$ and $\sqrt{\mu}/a = 1$ for the non-local parameter in the case of a fully clamped sheet. For the pinned sheet case, since variation in the non-local parameter has no influence on the linear mode shapes (as it was previously verified), the parameter was set to zero. The first, second and fourth mode shapes are displayed for the fully clamped and pinned sheet in Figure 3.8 and Figure 3.9 respectively.

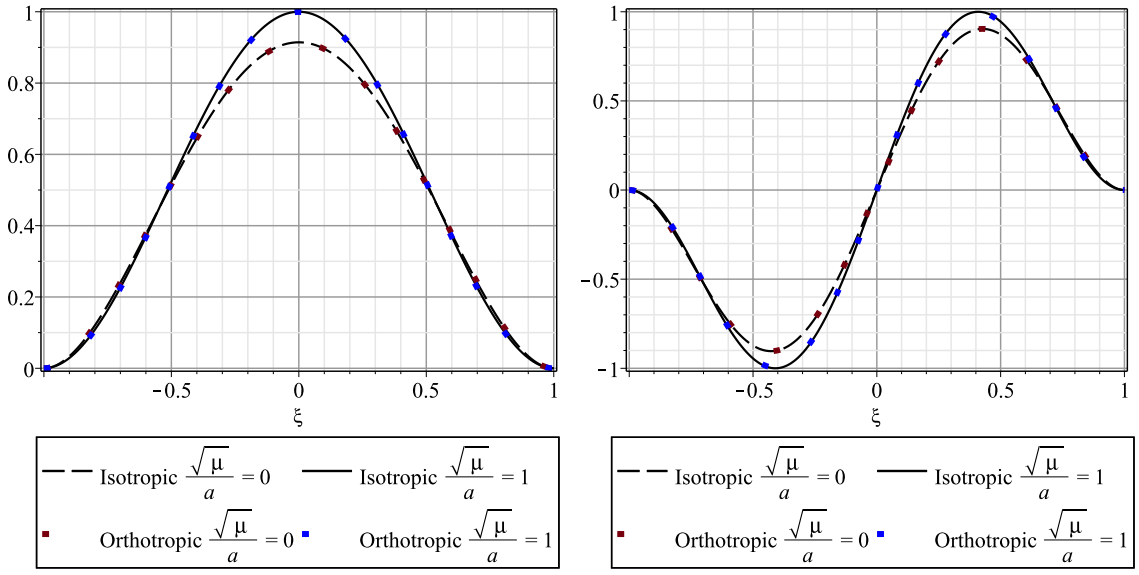

(a) 1st Mode shape - CCCC

(b) 2nd Mode shape - CCCC

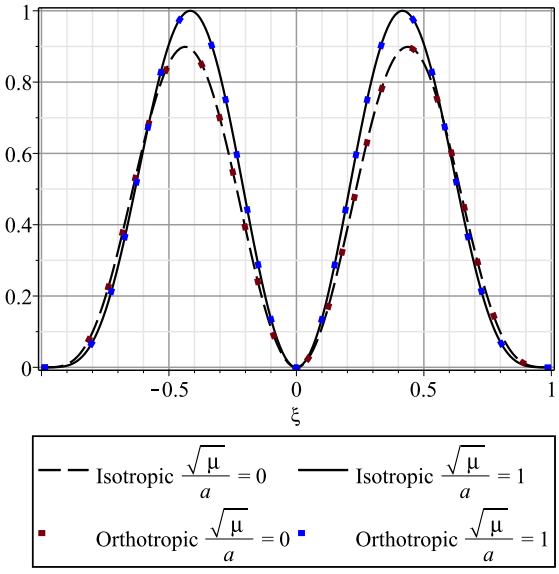

(c) 4th Mode shape - CCCC

Figure 3.8: Sections of first, second and fourth linear mode shapes of a square CCCC SLGS for different $\sqrt{\mu}/a$ with isotropic and orthotropic models

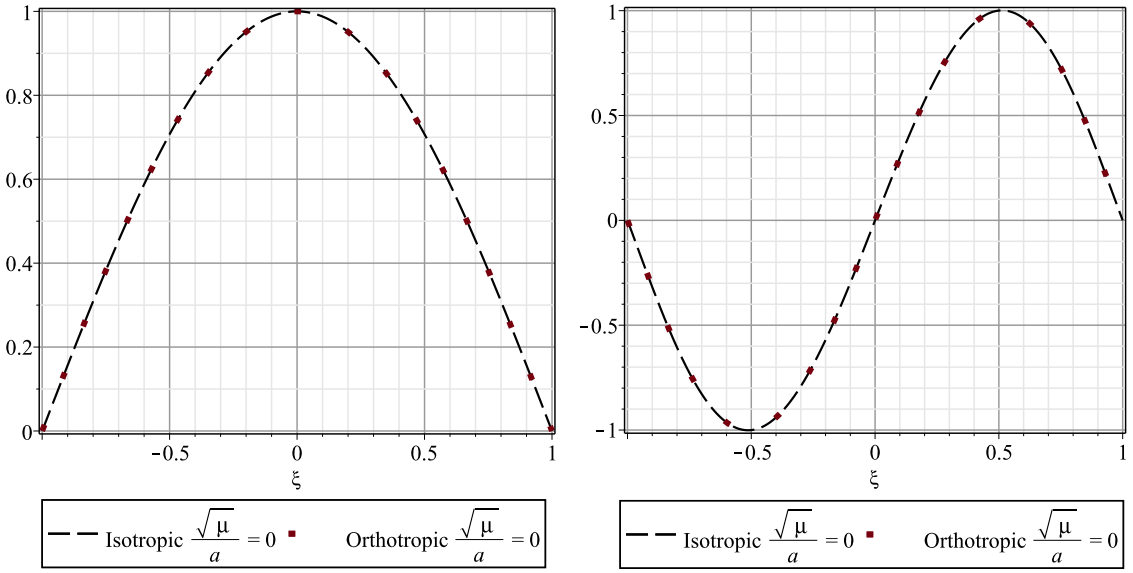

(a) 1st Mode shape - SSSS

(b) 2nd Mode shape - SSSS

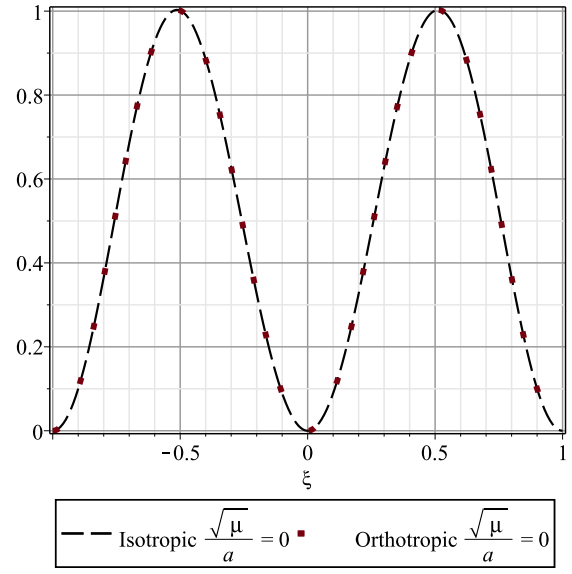

(c) 4th Mode shape - SSSS

Figure 3.9: Sections of first, second and fourth linear mode shapes of a square SSSS SLGS with $\sqrt{\mu}/a = 0$ using isotropic and orthotropic models

From Figures 3.8 and 3.9 one may conclude that the solutions obtained with both isotropic and orthotropic models are in very good agreement for fully clamped and pinned sheets. As a consequence, both models are equally valid despite the boundary conditions. Variation in the non-local parameter for the case of the fully clamped sheet is also irrelevant in the sense that both models present very close results for either $\sqrt{\mu}/a = 0$ or $\sqrt{\mu}/a = 1$.

3.2.4 Linear Mode Shapes of SLGS

In this section the three-dimensional plot of the linear mode shapes of a square single layer graphene sheet will be presented. The properties of the sheet are the same used in Table 3.11 and the non-linear behaviour of the same graphene sheet will be studied in chapter 4 (the linear natural frequencies of the simply supported case are also presented in Table 4.1). The first four mode shapes for both fully clamped and pinned boundary conditions considering the non-local parameter $\mu = 0$ are demonstrated in Figure 3.10 and Figure 3.11 respectively (only $\mu = 0$ was considered since the influence of the small-scale effect on the linear mode shapes was already studied and is not very clear using three-dimensional plots).

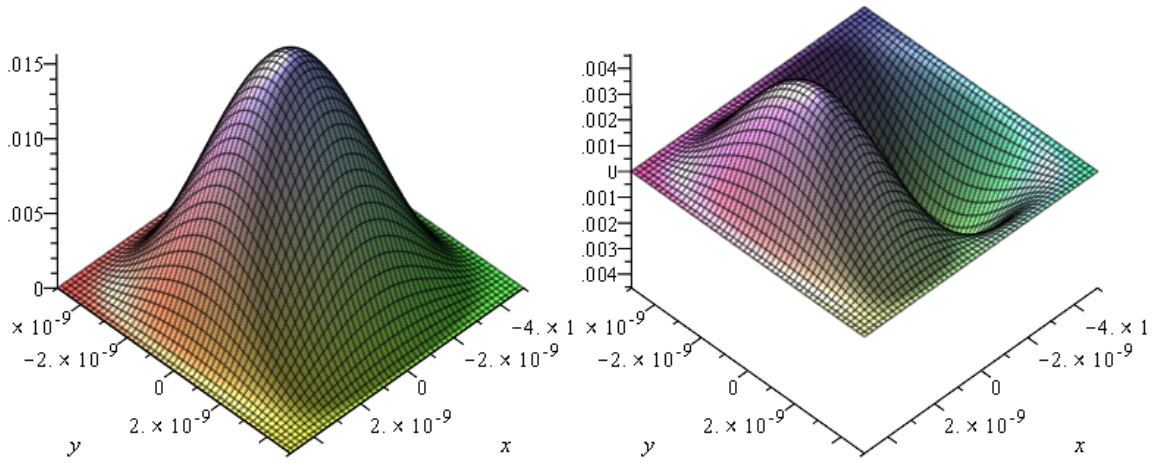

(a) 1st Mode shape (1,1)

(b) 2nd Mode shape (2,1)

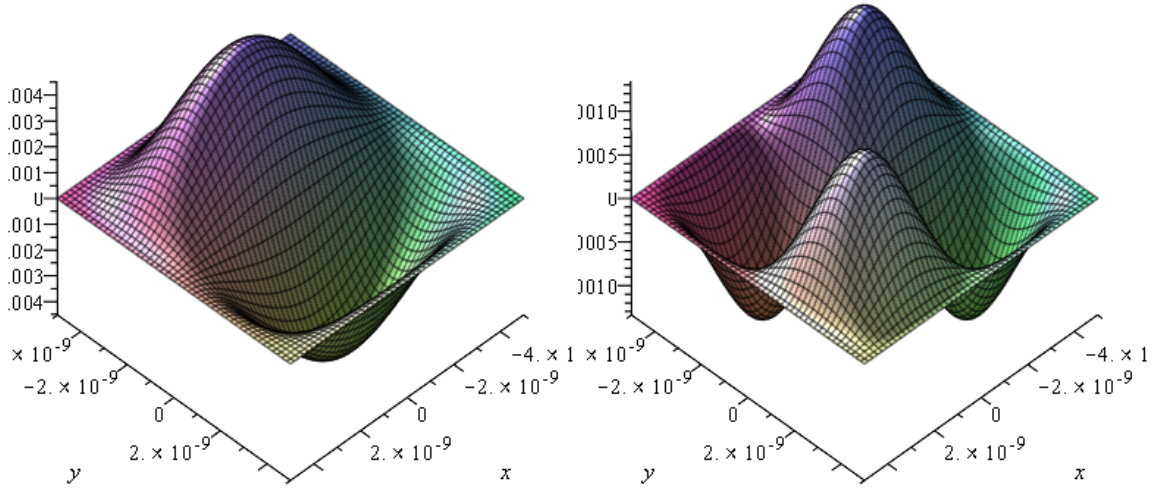

(c) 3rd Mode shape (1,2)

(d) 4th Mode shape (2,2)

Figure 3.10: Linear mode shapes of square CCCC SLGS with $\mu = 0$

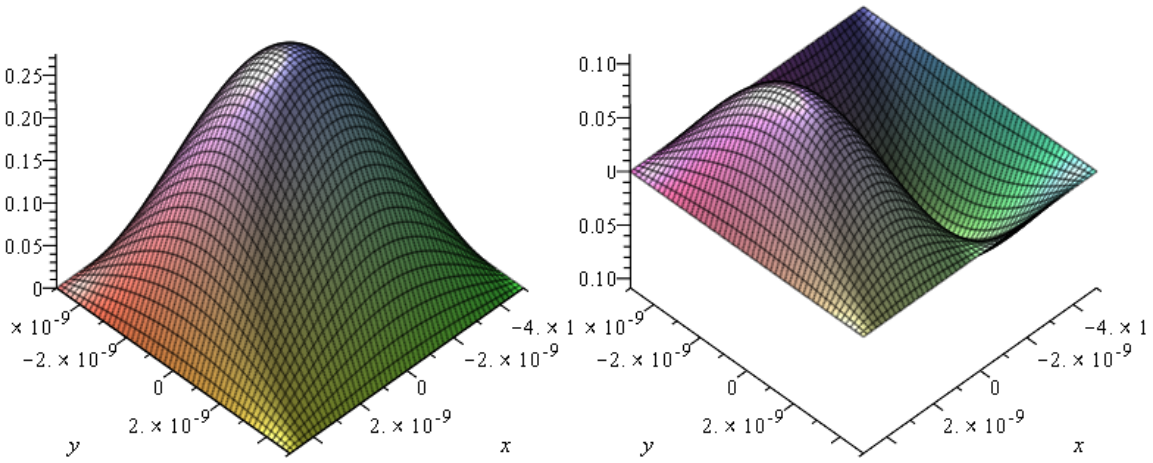

(a) 1st Mode shape (1,1)

(b) 2nd Mode shape (2,1)

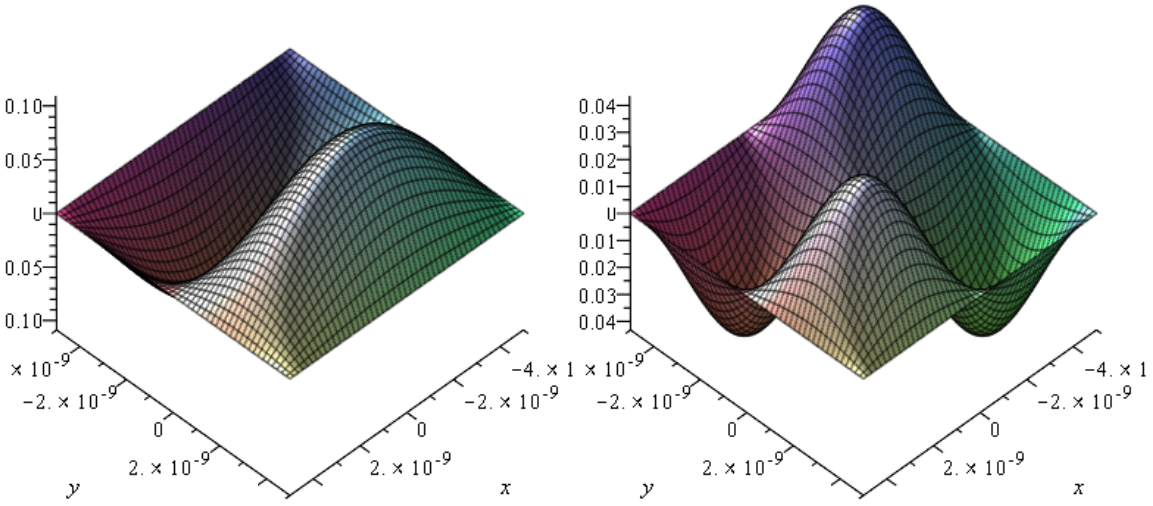

(c) 3rd Mode shape (1,2)

(d) 4th Mode shape (2,2)

Figure 3.11: Linear mode shapes of square SSSS SLGS with $\mu = 0$

3.3 Non-Linear Analysis

In this subchapter the non-linear model was verified. Firstly, only the local stiffness matrices were considered in the non-linear model to validate the particular case $\mu = 0$. The verification of the non-linear model with varying non-local parameter and the particular case of single layer graphene sheets will be carried out afterwards.

3.3.1 Local Non-Linear Validation

Since several non-linear geometric mathematical formulations have been developed in the past for thin plates, it is convenient to study this simpler case in order to guarantee the validity and accuracy of the model. Note that for this case, the model is not the most adequate to describe nanoplates or in particular, graphene sheets, seeing that the small-scale effect is not being taken into account, therefore the results obtained are for macroscopic plates and do not serve any other purpose besides the validation of the model.

For both pinned and fully clamped plates, it should be noted that out-of-plane shape functions yield little effect on convergence of the solutions when compared to in-plane functions [9]. Due to this and since larger sets of out-of-plane shape functions imply a higher computational effort than in-plane shape functions, only two cases were studied with the latter varying from 5 to 7. Different combinations were verified and results did not improve from the solution (3,7). In Table 3.13 the ratio between the non-linear natural frequencies and the linear ones $\frac{\omega}{\omega_l}$ is compared with those obtained in [60] for a pinned isotropic rectangular plate, the properties of which can be observed in Table 3.12. It is also compared with the results obtained by other procedures such as the elliptic function (E.F), perturbation method (P.M) and the finite element method, all presented and referenced in [60]. The results for the present model were obtained considering two different sets of shape functions, as it was mentioned previously: $po = 3, pi = 5$ and $po = 3, pi = 7$. The shape functions used were only the out-of-plane symmetric ones whilst for the in-plane displacements both symmetric and anti-symmetric must be considered. The ratio between non-linear and linear natural frequencies is calculated for different values of W/h, which designates the ratio between the amplitude of vibration at $x = y = 0$ and the thickness of the plate. Note that W is determined at $x = y = 0$, with $t = 0s$, after solving the non-linear equations expressed in (2.143) by the application of the arc-length continuation method, and given that only one harmonic is being considered, $W = w_{c1}$. Since the points of the backbone curve obtained by the model are not perfectly coincident with the amplitude ratios given in [60], linear interpolations had to be conducted, possibly leading to slight deviances (note that the increment used in the model was rather small).

Table 3.12: Properties of an isotropic rectangular plate [60]

E [MPa]	a [mm]	b [mm]	h [mm]	ν	ρ [kg/m^3]
205800	20	10	0.1	0.3	7800

Table 3.13: Ratio $\frac{\omega}{\omega_l}$ of an isotropic rectangular SSSS plate calculated with perturbation method (P.M), finite element method (F.E.M), elliptic function (E.F) and with the present model

W/h	E.F [60]	P.M [60]	F.E.M [60]	Model [60]	Model (3,5)	Model (3,7)
0.2	1.0241	1.0241	1.0168	1.0254	1.0259	1.0259
0.4	1.0927	1.0933	1.0658	1.0975	1.0954	1.0957
0.6	1.1975	1.1998	1.1439	1.2072	1.2061	1.2059
0.8	1.3292	1.3347	1.2467	1.3447	1.3489	1.3488
1	1.4808	1.4903	1.3701	1.5023	1.5181	1.5175

The points mentioned in Table 3.13 (particularly those obtained with the elliptic function and with the model developed in [60] are displayed below in Figure 3.12 with the full backbone curve achieved by the present model for comparison:

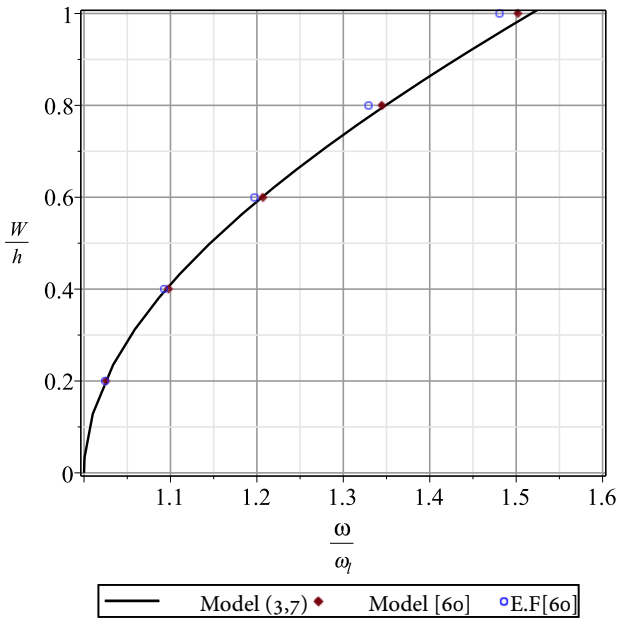

Figure 3.12: Isotropic rectangular SSSS plate backbone curve validation

The results obtained seem to be in good agreement with the model proposed by M.S. Sarma [60] and with the solutions from the elliptic function. It can be verified in Table 3.13 that the largest disparity occurs for the results obtained with the finite element method and the remaining methods present relatively close results to those obtained by the model developed in this work. In addition, hardening spring effect is clearly visible since a rise in the amplitude of vibration leads to an increase in the non-dimensional natural frequencies by effectively stiffening the plate.

In Table 3.15 the ratio between linear and non-linear natural frequencies is calculated for a fully clamped square isotropic plate with the following geometric and elastic properties proposed in [9]:

Table 3.14: Isotropic square plate properties [9]

E [Pa]	a [m]	h [mm]	ν	ρ [kg/m^3]
21×10^{10}	0.1	2	0.3	7800

The results were obtained, again, with two different sets of shape functions ($po = 3, pi = 5$ and $po = 3, pi = 7$) but considering both symmetric and anti-symmetric terms for both in-plane and out-of-plane shape functions. These were posteriorly compared with the results given in [9], where a non-linear plate model is proposed by Han and Petyt and experimental results by Benamar [61] are presented as well.

Table 3.15: Ratio $\frac{\omega}{\omega_l}$ of an isotropic square CCCC plate calculated with present model and compared with results by Han, Petyt and Benamar [9,61]

W/h	Benamar [61]	Han and Petyt [9]	Model (3,5)	Model (3,7)
0.2	1.0083	1.0068	1.0083	1.0079
0.4	1.0283	1.0271	1.0320	1.0307
0.6	1.0617	1.0600	1.0669	1.0640
0.8	1.1065	1.1047	1.1141	1.1104
1	1.1591	1.1599	1.1716	1.1660
1.5	1.3423	1.3355	1.3519	1.3457

In Figure 3.13 the full backbone curve is displayed for the fully clamped plate considered in Table 3.13 with both (3,5) and (3,7) shape functions. The values obtained numerically by Han and Petyt and experimentally by Benamar can also be visualized.

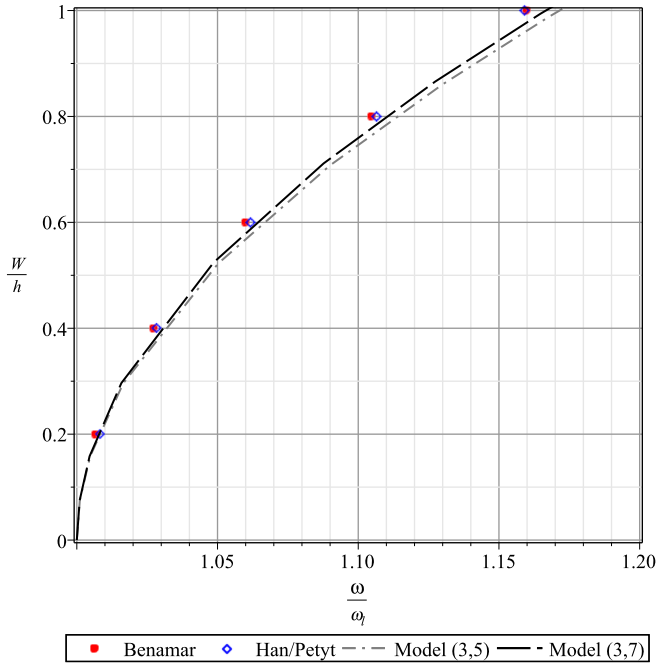

Figure 3.13: Isotropic square CCCC plate backbone curve validation

It is worth mentioning the conceptual difference between the mathematical formulation of the model proposed by Han and Petyt, where non-linear matrix $\left[K^3\right]$ is approximated as $\left[K^3\right] = 2\left[K^2\right]^T$, and the model developed in this work. The sets of shape functions used also differ. While in the model presented in this work both symmetric and anti-symmetric in-plane shape functions were used, in [9], only anti-symmetric in-plane shape functions were considered. According to [54], both symmetric and anti-symmetric in-plane shape functions must be considered since the middle-plane longitudinal displacements u^0 and v^0 are anti-symmetric with respect to one axis and symmetric with respect to the other one:

$$u^0(x,y) = u^0(x,-y) = -u^0(-x,y) \tag{3.1a}$$

$$v^0(x,y) = v^0(-x,y) = -v^0(x,-y) \tag{3.1b}$$

Therefore, the consideration by Han and Petyt is not entirely correct.

3.3.2 Verification of Non-Local Non-Linear Model

In this sub-section the non-local non-linear model will be analysed and the results obtained for the backbone curves will be compared with more than one reference, considering different boundary conditions and different non-local parameters.

Firstly, a rectangular single-layer armchair graphene sheet was considered according to E.Jomehzadeh and A.Saidi in [8]. The sheet's elastic and geometric properties are presented in Table 3.16 and the results were obtained with a set of 7 in-plane and 3 out-of-plane shape functions, using an orthotropic model. Both fully clamped and pinned sheets were considered and the results were subsequently compared with those in [8], which can be observed in Figure 3.14. For the case of the pinned sheet only symmetric out-of-plane shape functions were used, whereas in the fully clamped case both symmetric and anti-symmetric were considered. The in-plane shape functions were the same (symmetric and anti-symmetric) for the two cases.

Table 3.16: Orthotropic rectangular armchair SLGS properties [8]

E_1 [TPa]	E_2 [TPa]	G_{12} [TPa]	a [nm]	b [nm]	h [nm]	ν_{12}	ρ [kg/m^3]	μ [nm^2]
2.424	2.473	1.039	9.519	4.844	0.129	0.197	6316	0.67^2

A second comparison was conducted, also considering the results provided in [8] for a zig-zag single layer graphene sheet. In this case, the set of shape functions used in the model was exactly the same as in the previous case and again, both fully clamped and pinned boundary conditions were studied. The properties of the SLGS are shown in Table 3.17 and the results obtained can be observed in Figure 3.15.

Table 3.17: Orthotropic rectangular zig-zag SLGS properties [8]

E_1 [TPa]	E_2 [TPa]	G_{12} [TPa]	a [nm]	b [nm]	h [nm]	ν_{12}	ρ [kg/m^3]	μ [nm^2]
2.145	2.097	0.938	9.496	4.877	0.145	0.223	5624	0.47^2

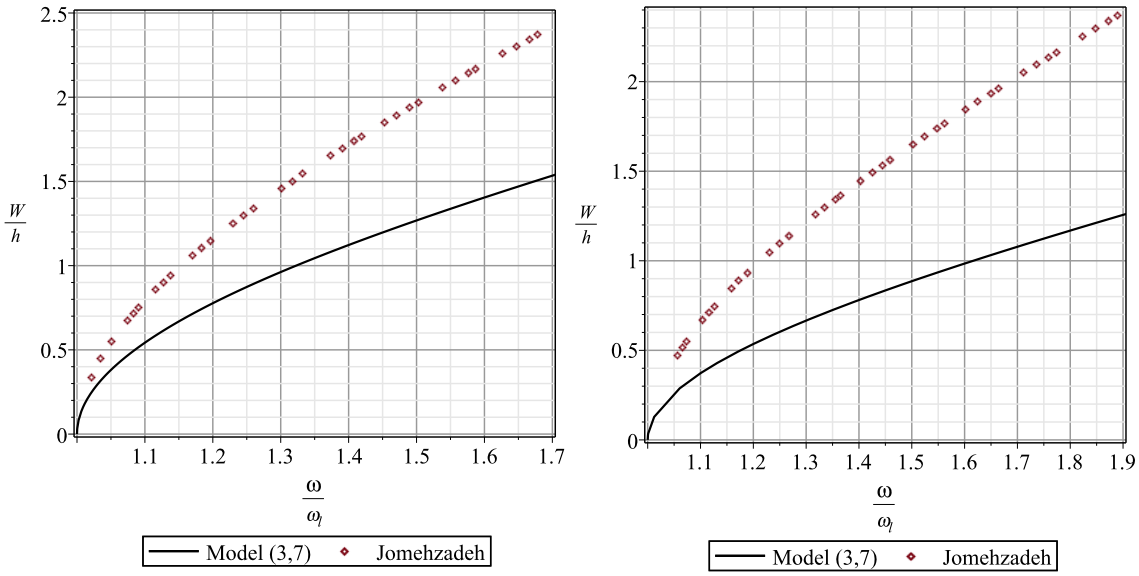

(a) CCCC (b) SSSS

Figure 3.14: Backbone curves - armchair SLGS

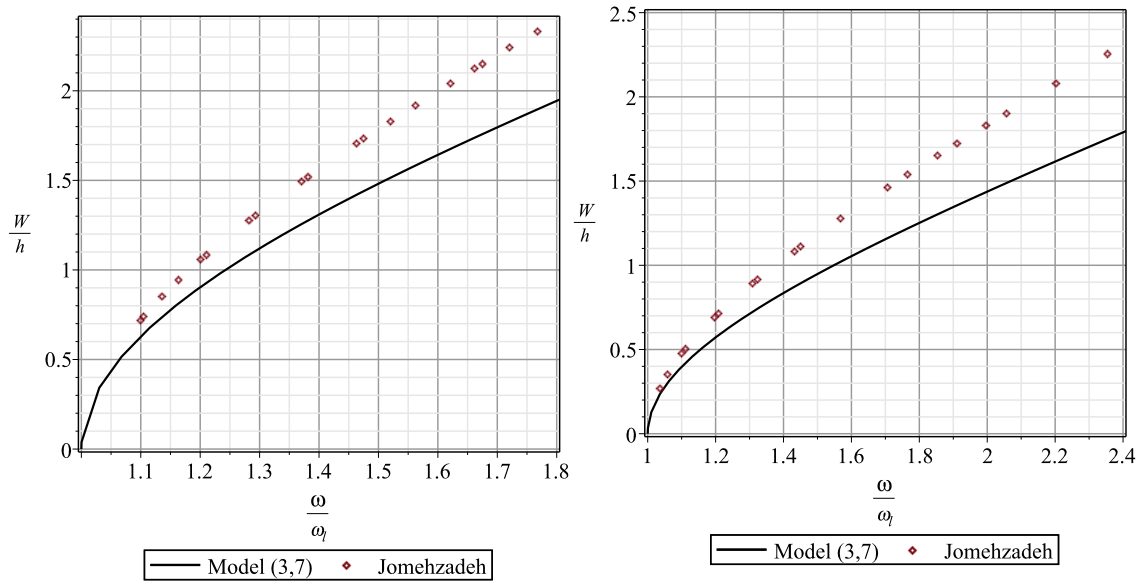

(a) CCCC (b) SSSS

Figure 3.15: Backbone curves - zig-zag SLGS

It can be observed from Figure 3.14 and Figure 3.15 that the results obtained with the model developed in chapter 2 are not in agreement with [8], particularly in the case of the armchair configuration. For zig-zag single layer graphene sheets, both pinned and fully clamped, the results are much closer to those obtained by Jomehzadeh. The reason behind the greater disparity for the case of the armchair sheet is the higher correspondent

non-local parameter. In fact, the model has been proved to accurately depict the plate's behaviour without the consideration of the small-scale effect and consequently, for larger values of the non-local parameter, the results obtained further diverge from other non-local models.

Despite the inaccuracy of the proposed model for higher values of the non-local parameter, it is worth mentioning that hardening spring effect is greater for the case of pinned plates than fully clamped ones, regardless of the small-scale effect. This tendency is visible even for the results obtained.

The model was compared with another reference by A.Farajpour et al. [43] for further robustness of the analysis. In this case, a square piezoelectric nanoplate with the following properties was considered: $a = b = 50$ nm, $h = 5$ nm, c_{11} =132 GPa, $c_{12} = 71$ GPa, $c_{13} =$ 73 GPa, $c_{33} = 115$ GPa and $c_{66} = 30.5$ GPa. It should be noted that the determination of the elasticity matrix from the given coefficients c_{ij} is detailed in [43]. The results were obtained for different values of the non-local parameter represented in this case by its dimensionless value $\mu = \frac{e_0 a_i}{a}$, and compared with the results from [43], which are referred for abbreviation as "F" and can be visualized in Figure 3.16.

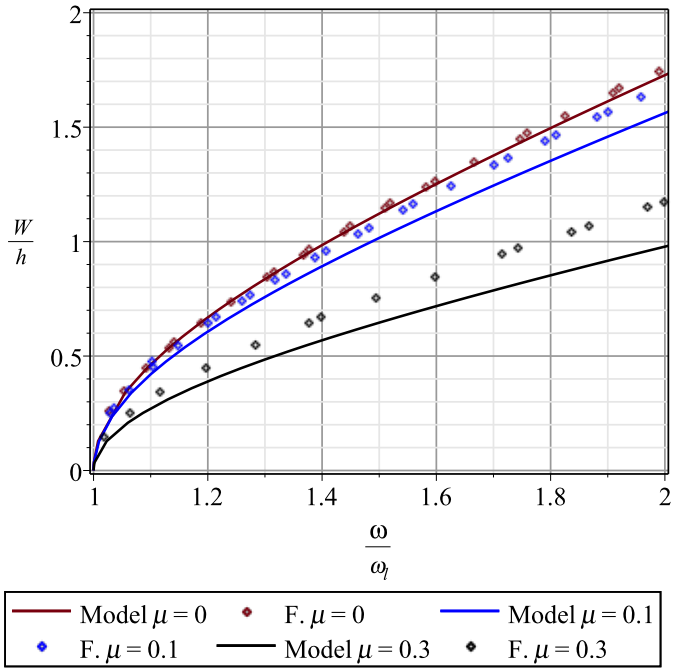

Figure 3.16: SSSS - Comparison of the backbone curves for different μ and the results obtained by Farajpour (F.) [43]

As mentioned before, the increasing disparity in the results obtained by the model and those proposed by A.Farajpour with the rise in the non-local parameter is clearly observable in Figure 3.16. The inaccuracy of the model to describe non-local non-linear sheets is a result of the approximation assumed in (2.39). However, one aspect worth mentioning despite the validity of the model is the higher hardening-spring effect for higher values of the non-local parameter. In fact, since the small-scale effect is only attributed to non-linear stiffness, besides its influence in inertia terms, the hardening-spring effect resultant from this increased non-linear stiffness is consequently greater.

It should be noted, however, that the models proposed in [8, 43] have a considerably distinct mathematical formulation, compared to the model presented in chapter 2. Both [43] and [8] do not use a finite element method approach and only one function for the transverse displacement is considered. Consequently, modes of vibration must be studied individually and certain non-linear behaviour such as mode interaction cannot be studied. Moreover, these models use an additional compatibility equation and an additional stress function variable. The equations of motion are obtained after the employment of the Galerkin method and the posterior application of either the harmonic balance method or a multiple scale method for [8] and [43] respectively. Lastly, the equations can be solved analytically without resorting to any type of numerical procedure. In chapter 4, the formulation and results of a similar model can be visualized.

3.4 Conclusions

In this chapter the linear and non-linear model were analysed and the results obtained were compared with different references. In the linear case, convergence was verified and both local and non-local results proved to be in good agreement with the solutions presented in the literature. The influence of the small-scale effect and the size of the plate on the linear natural frequencies was studied.

In the first case, the increase in the non-local parameter resulted in a reduction of the linear natural frequencies due to the rise in the inertia of the sheet. Increasing size also resulted in smaller values of the linear natural frequencies and decreasing influence of the small-scale effect. In addition, higher frequencies of vibration were shown to be more affected by the non-local parameter due to the smaller "effective" length of the plate. This phenomenon also justifies the slight difference in the influence of the small-scale effect on fully clamped and pinned sheets, which seems to be greater in the former case as a result of zero slope near the edges and consequently shorter "effective" length.

The influence of the small-scale effect on the linear mode shapes was observed for the case of a fully clamped plate and, as expected, the higher modes of vibration were the most affected by the variation in the non-local parameter. The shape of a given mode seems to stabilize from a certain value of the parameter, remaining unaltered for higher non-local parameters. For the case of a pinned plate, change in the non-local parameter does not yield any effect in the linear mode shapes.

The first and fourth linear natural frequencies were compared using an isotropic and orthotropic square single layer graphene sheet, for different boundary conditions and with varying non-local parameter, showing very little difference. In addition, the first, second and fourth linear mode shapes were also investigated for both fully clamped and pinned boundary conditions and the results obtained with the isotropic and orthotropic models

were very close. Therefore, it was concluded that if an adequate Young's modulus is used, an isotropic model is a perfectly valid simplification of a SLGS.

The non-linear model was first validated for the particular case of $\mu = 0$ and the results obtained are in very good agreement with other non-linear local models. For the non-local non-linear case, the difference between the backbone curves obtained with the presented model and other proposed models from the literature is considerable. In fact, for higher values of the non-local parameter this disparity further increases, which might be attributed to the approximation done in the mathematical formulation in (2.39). However, despite the erroneous results, the tendency of greater hardening-spring effect for higher values of the non-local parameter was observed and it was also found that pinned plates have higher hardening ratios than fully clamped ones.

Chapter 4

Non-Local, Non-Linear Model based on Airy Stress Function

4.1 Introduction

In this chapter a new non-local non-linear model was formulated since the results obtained with the model presented in chapter 3 were not particularly good, especially for high values of the non-local parameter. In the previous model, neglecting several terms of $\mathcal{L}(\aleph)$ in (2.39) was a necessity considering the difficulty in the application of Eringen's non-local theory to coupled forces and displacements. The formulation presented in this chapter avoids coupled stress and displacements by using a scalar potential function, known as Airy stress function, which can be expressed in terms of displacements only, therefore not requiring any type of approximation. Moreover, the Airy stress function can be obtained analytically after defining a particular solution of the non-homogeneous differential equation of compatibility.

Two different formulations were implemented in this chapter, where in the first, the p-version finite element method was not applied since only one transverse displacement function was used, neglecting in-plane displacements. Within this approach, the backbone curves of a nano-plate were compared and validated. The backbone curves were obtained considering one and three harmonics and the influence of each individual harmonic was verified considering different values of the non-local parameter. It should be noted that for the formulation with three harmonics the continuation method was employed to solve the non-linear equations of motion whereas for one harmonic only, the solution for the natural frequencies was obtained analytically. The influence of the small-scale effect was then studied for different non-linear modes of vibration using three harmonics and the Airy stress function and its derivatives (in-plane forces) were plotted for each mode of a single layer graphene sheet.

In the second approach, more than one function was used for the transverse displacement and a set of Airy stress shape functions was also considered. The Galerkin method was applied to both the equation of motion and the equation of compatibility and the p-version finite element method was employed. After the discretization of the time domain continuous equations of motion into frequency domain algebraic ones by the harmonic balance method, the continuation method was used to solve the system of non-linear equations. However, due to time limitations, no results were obtained and only the corre-

spondent mathematical formulation is presented.

4.2 Mathematical Formulation

In this section the two distinct mathematical formulations mentioned before will be discussed in detail. Firstly, the single transverse displacement function approach will be considered according to [43,62] and lastly, the p-version finite element model will be taken into account.

4.2.1 Single function model

Considering once again the third equation of motion already presented in (2.33) and neglecting the first two equations in terms of in-plane displacements one has:

$$-D_{11}\frac{\partial^4 w^0}{\partial x^4} - 2\left(D_{12}+2D_{33}\right)\frac{\partial^4 w^0}{\partial x^2\partial y^2} - D_{22}\frac{\partial^4 w^0}{\partial y^4} + \mathcal{L}\left(\aleph\right) = (1-\mu\nabla^2)\rho h\ddot{w}^0 \tag{4.1}$$

which, considering in-plane inertia null so that $\aleph$ is given by equation (2.17), can be rewritten as:

$$\begin{aligned} &D_{11}\frac{\partial^4 w^0}{\partial x^4} + 2\left(D_{12}+2D_{33}\right)\frac{\partial^4 w^0}{\partial x^2\partial y^2} + D_{22}\frac{\partial^4 w^0}{\partial y^4} - \left(1-\mu\nabla^2\right)\left(N_{xx}\frac{\partial^2 w^0}{\partial x^2} + 2N_{xy}\frac{\partial^2 w^0}{\partial x\partial y}\right. \\ &\left.+N_{yy}\frac{\partial^2 w^0}{\partial y^2}\right) = -\left(1-\mu\nabla^2\right)\rho h\ddot{w}^0 \end{aligned} \tag{4.2}$$

Defining a potential stress function, or Airy stress function $\Phi = h\phi$ so that its second order derivatives can represent the membrane forces, one has:

$$N_{xx} = \frac{\partial^2\Phi}{\partial y^2} \tag{4.3a}$$

$$N_{yy} = \frac{\partial^2\Phi}{\partial x^2} \tag{4.3b}$$

$$N_{xy} = -\frac{\partial^2\Phi}{\partial x\partial y} \tag{4.3c}$$

and subsequently substituting with the membrane forces - stress function relations above in (4.2) one can write the equation of motion as a function of transverse displacement and stress function:

$$\begin{aligned} &D_{11}\frac{\partial^4 w^0}{\partial x^4} + 2\left(D_{12}+2D_{33}\right)\frac{\partial^4 w^0}{\partial x^2\partial y^2} + D_{22}\frac{\partial^4 w^0}{\partial y^4} \\ &-\left(1-\mu\nabla^2\right)\left(\frac{\partial^2\Phi}{\partial y^2}\frac{\partial^2 w^0}{\partial x^2} - 2\frac{\partial^2\Phi}{\partial x\partial y}\frac{\partial^2 w^0}{\partial x\partial y} + \frac{\partial^2\Phi}{\partial x^2}\frac{\partial^2 w^0}{\partial y^2}\right) = -\left(1-\mu\nabla^2\right)\rho h\ddot{w}^0 \end{aligned} \tag{4.4}$$

It should be noted, however, that this fourth order partial differential equation in terms of transverse displacement and stress function cannot be solved and an additional equation is evidently needed. A compatibility equation must be added and can be easily obtained by eliminating the in-plane displacements u^0 and v^0 from the strain field or strain-displacement relations, expressing the in-plane strain components in terms of Airy stress function instead.

Considering the middle-plane in-plane strains components (not dependent on z) from equations (2.2a) to (2.2c) one has:

$$\varepsilon_{xx}^0 = \frac{\partial u^0}{\partial x} + \frac{1}{2}\left(\frac{\partial w^0}{\partial x}\right)^2 \tag{4.5a}$$

$$\varepsilon_{yy}^0 = \frac{\partial v^0}{\partial y} + \frac{1}{2}\left(\frac{\partial w^0}{\partial y}\right)^2 \tag{4.5b}$$

$$\gamma_{xy}^0 = \frac{\partial u^0}{\partial y} + \frac{\partial v^0}{\partial x} + \frac{\partial w^0}{\partial x}\frac{\partial w^0}{\partial y} \tag{4.5c}$$

Calculating the second order derivatives of the in-plane strain components presented in (4.5):

$$\frac{\partial^2 \varepsilon_{xx}^0}{\partial y^2} = \frac{\partial^3 u^0}{\partial y^2 \partial x} + \frac{\partial^3 w^0}{\partial y^2 \partial x}\frac{\partial w^0}{\partial x} + \left(\frac{\partial^2 w^0}{\partial y \partial x}\right)^2 \tag{4.6a}$$

$$\frac{\partial^2 \varepsilon_{yy}^0}{\partial x^2} = \frac{\partial^3 v^0}{\partial x^2 \partial y} + \frac{\partial^3 w^0}{\partial x^2 \partial y}\frac{\partial w^0}{\partial y} + \left(\frac{\partial^2 w^0}{\partial x \partial y}\right)^2 \tag{4.6b}$$

$$\frac{\partial^2 \gamma_{xy}^0}{\partial x \partial y} = \frac{\partial^3 u^0}{\partial x \partial y^2} + \frac{\partial^3 v^0}{\partial y \partial x^2} + \frac{\partial^3 w^0}{\partial y \partial x^2}\frac{\partial w^0}{\partial y} + \frac{\partial^2 w^0}{\partial x \partial y}\frac{\partial^2 w^0}{\partial x \partial y} + \frac{\partial^2 w^0}{\partial x^2}\frac{\partial^2 w^0}{\partial y^2} + \frac{\partial w^0}{\partial x}\frac{\partial^3 w^0}{\partial x \partial y^2} \tag{4.6c}$$

By adding equations (4.6a) and (4.6b) and subtracting equation (4.6c) it is possible to finally obtain the compatibility equation in terms of in-plane strains and transverse displacement only by eliminating the in-plane displacements:

$$\frac{\partial^2 \varepsilon_{xx}^0}{\partial y^2} + \frac{\partial^2 \varepsilon_{yy}^0}{\partial x^2} - \frac{\partial^2 \gamma_{xy^0}}{\partial x \partial y} = \left(\frac{\partial^2 w^0}{\partial x \partial y}\right)^2 - \frac{\partial^2 w^0}{\partial x^2}\frac{\partial^2 w^0}{\partial y^2} \tag{4.7}$$

In order to replace the strains by membrane forces the constitutive non-local relation displayed in (2.25) is used:

$$\begin{Bmatrix} N_{xx} \\ N_{yy} \\ N_{xy} \end{Bmatrix} - \mu\nabla^2 \begin{Bmatrix} N_{xx} \\ N_{yy} \\ N_{xy} \end{Bmatrix} = \begin{bmatrix} A_{11} & A_{12} & 0 \\ A_{12} & A_{22} & 0 \\ 0 & 0 & A_{33} \end{bmatrix} \begin{Bmatrix} \varepsilon_{xx}^0 \\ \varepsilon_{yy}^0 \\ \gamma_{xy}^0 \end{Bmatrix} \tag{4.8}$$

Solving equation (4.8) with respect to the in-plane strains by the inversion of the coefficients matrix one obtains:

$$\left\{ \begin{array}{c} \varepsilon^0_{xx} \\ \varepsilon^0_{yy} \\ \gamma^0_{xy} \end{array} \right\} = \left[\begin{array}{ccc} S_{11} & S_{12} & 0 \\ S_{12} & S_{22} & 0 \\ 0 & 0 & S_{33} \end{array} \right] \left\{ \left\{ \begin{array}{c} \varepsilon^0_{xx} \\ \varepsilon^0_{yy} \\ \gamma^0_{xy} \end{array} \right\} - \mu\nabla^2 \left\{ \begin{array}{c} \varepsilon^0_{xx} \\ \varepsilon^0_{yy} \\ \gamma^0_{xy} \end{array} \right\} \right\} \tag{4.9}$$

where the matrix $[S_{ij}]$ is the inverse of $[A_{ij}]$. The relations expressed in (4.9) can be written as a system of equations:

$$\varepsilon^0_{xx} = S_{11}\left(1-\mu\nabla^2\right)N_{xx} + S_{12}\left(1-\mu\nabla^2\right)N_{yy} \tag{4.10a}$$
$$\varepsilon^0_{yy} = S_{12}\left(1-\mu\nabla^2\right)N_{xx} + S_{22}\left(1-\mu\nabla^2\right)N_{yy} \tag{4.10b}$$
$$\gamma^0_{xy} = S_{33}\left(1-\mu\nabla^2\right)N_{xy} \tag{4.10c}$$

Substituting the strains relations from (4.10) in the compatibility equation (4.7) one obtains:

$$\begin{aligned} &\left(1-\mu\nabla^2\right)\left[S_{11}\frac{\partial^2 N_{xx}}{\partial y^2} + S_{12}\left(\frac{\partial^2 N_{yy}}{\partial y^2} + \frac{\partial^2 N_{xx}}{\partial x^2}\right) + S_{22}\frac{\partial^2 N_{xy}}{\partial x^2} - S_{33}\frac{\partial^2 N_{xy}}{\partial x \partial y}\right] \\ &= \left(\frac{\partial^2 w^0}{\partial x \partial y}\right)^2 - \frac{\partial^2 w^0}{\partial x^2}\frac{\partial^2 w^0}{\partial y^2} \end{aligned} \tag{4.11}$$

Considering the relations established in (4.3) between the membrane forces and the Airy stress function and posteriorly calculating the fourth order derivatives:

$$\frac{\partial^2 N_{xx}}{\partial y^2} = \frac{\partial^4 \Phi}{\partial y^4} \tag{4.12a}$$
$$\frac{\partial^2 N_{xx}}{\partial x^2} = \frac{\partial^4 \Phi}{\partial x^2 \partial y^2} \tag{4.12b}$$
$$\frac{\partial^2 N_{yy}}{\partial y^2} = \frac{\partial^4 \Phi}{\partial y^2 \partial x^2} \tag{4.12c}$$
$$\frac{\partial^2 N_{yy}}{\partial x^2} = \frac{\partial^4 \Phi}{\partial x^4} \tag{4.12d}$$
$$\frac{\partial^2 N_{xy}}{\partial x \partial y} = -\frac{\partial^4 \Phi}{\partial x^2 \partial y^2} \tag{4.12e}$$

Finally, after substituting (4.12) in (4.11) one obtains the compatibility equation as a function of stress potential and transverse displacement:

$$\left(1-\mu\nabla^2\right)\left[S_{11}\frac{\partial^4 \Phi}{\partial y^4} + \left(2S_{12}+S_{33}\right)\frac{\partial^4 \Phi}{\partial x^2 \partial y^2} + S_{22}\frac{\partial^4 \Phi}{\partial x^4}\right] = \left(\frac{\partial^2 w^0}{\partial x \partial y}\right)^2 - \frac{\partial^2 w^0}{\partial x^2}\frac{\partial^2 w^0}{\partial y^2} \tag{4.13}$$

It should be noted that in this model both the compatibility and motion equation are considered non-local. However, certain models proposed in the literature do not include Eringen's non-local theory in the compatibility equation, which is therefore assumed to be local, only applying non-local elasticity in the equation of motion [8, 15, 63].

In this chapter, only simply supported plates with movable edges will be studied since the exact solution of the transverse displacement is known, easily allowing the determination of the Airy stress function. For the case of a fully clamped plate, the solution of the compatibility equation would be much more complex seeing that the transverse displacement cannot be represented by simple first degree sinusoidal functions without committing a certain error (it is only possible to obtain an approximation of the transverse displacement). For abbreviation, simply supported plates with movable edges will be referred as SSSS plates hereafter. The boundary conditions in terms of Airy stress function are expressed below [8, 15, 43]:

$$x = \pm\frac{a}{2} : \frac{\partial^2\Phi}{\partial x \partial y} = 0, \int_{-\frac{b}{2}}^{\frac{b}{2}} \frac{\partial^2\Phi}{\partial y^2}\mathrm{d}y = 0 \tag{4.14a}$$

$$y = \pm\frac{b}{2} : \frac{\partial^2\Phi}{\partial x \partial y} = 0, \int_{-\frac{a}{2}}^{\frac{a}{2}} \frac{\partial^2\Phi}{\partial x^2}\mathrm{d}x = 0 \tag{4.14b}$$

It is clear from equations (4.14) that the average membrane shear stress is zero in all edges and that the total normal in-plane force is null in its respective axis.

For the transverse displacement of a SSSS plate in the first mode of vibration the exact solution is known to be [8, 15, 43, 62]:

$$w^0(x, y, t) = q^w(t)\cos(\alpha x)\cos(\beta y) \tag{4.15}$$

Whilst in the second and fourth mode the solution takes the following forms, respectively:

$$w^0(x, y, t) = q^w(t)\sin(\alpha x)\cos(\beta y) \tag{4.16}$$

$$w^0(x, y, t) = q^w(t)\sin(\alpha x)\sin(\beta y) \tag{4.17}$$

where α and β can be defined as:

$$\alpha = \frac{n\pi}{a} \tag{4.18a}$$

$$\beta = \frac{m\pi}{b} \tag{4.18b}$$

The indexes n and m are (1,1), (2,1) and (2,2) for the first, second and fourth mode of vibration respectively.

In this formulation, the Galerkin method is only applied to the equation of motion so it is necessary to determine the Airy stress potential as a function of transverse displacement

in order to reduce this equation to one unknown variable only. Substituting (4.15) in the compatibility equation (4.13), the following relation for the first mode is obtained:

$$\begin{aligned}&\left(1-\mu\nabla^2\right)\left[S_{11}\frac{\partial^4\Phi}{\partial y^4}+\left(2S_{12}+S_{33}\right)\frac{\partial^4\Phi}{\partial x^2\partial y^2}+S_{22}\frac{\partial^4\Phi}{\partial x^4}\right]=\\&-\frac{1}{2}\left(q^w(t)\right)^2\alpha^2\beta^2\left(\cos\left(2\alpha x\right)+\cos\left(2\beta y\right)\right)\end{aligned}\tag{4.19}$$

Defining the particular solution of the non-homogeneous compatibility equation above as:

$$\Phi=A_1\cos\left(2\alpha x\right)+A_2\cos\left(2\beta y\right)\tag{4.20}$$

And substituting (4.20) in (4.19), the coefficients A_1 and A_2 can be determined by comparison of the left and right-hand sides of the resulting equation:

$$\begin{aligned}&\left[16S_{11}A_2\beta^4\cos\left(2\beta y\right)+16S_{22}A_1\alpha^4\cos\left(2\alpha x\right)\right]-\mu\left[-64S_{22}A_1\alpha^6\cos\left(2\alpha x\right)\right.\\&\left.-64S_{11}A_2\beta^6\cos\left(2\beta y\right)\right]=-\frac{1}{2}\left(q^w(t)\right)^2\alpha^2\beta^2\left(\cos\left(2\alpha x\right)+\cos\left(2\beta y\right)\right)\end{aligned}\tag{4.21}$$

From which one obtains:

$$A_1=-\frac{\left(q^w(t)\right)^2}{32S_{22}}\left(\frac{ma}{nb}\right)^2\left(\frac{1}{1+\left(4n^2\pi^2\mu\right)/a^2}\right)\tag{4.22a}$$

$$A_2=-\frac{\left(q^w(t)\right)^2}{32S_{11}}\left(\frac{nb}{ma}\right)^2\left(\frac{1}{1+\left(4m^2\pi^2\mu\right)/b^2}\right)\tag{4.22b}$$

It should be noted that the solution of A_1 and A_2 slightly changes for the case of the second and fourth mode of vibration since the transverse displacement function is defined with different sinusoid products. For the second mode, the introduction of a sine term in the transverse displacement results in a positive coefficient A_1 and analogously, for the fourth mode, both coefficients A_1 and A_2 are positive.

From the equation of motion (4.4) it is possible to define $\mathcal{L}_w$ as follows:

$$\begin{aligned}\mathcal{L}_w=&D_{11}\frac{\partial^4w^0}{\partial x^4}+2\left(D_{12}+2D_{33}\right)\frac{\partial^4w^0}{\partial x^2\partial y^2}+D_{22}\frac{\partial^4w^0}{\partial y^4}\\&-\left(1-\mu\nabla^2\right)\left(\frac{\partial^2\Phi}{\partial y^2}\frac{\partial^2w^0}{\partial x^2}-2\frac{\partial^2\Phi}{\partial x\partial y}\frac{\partial^2w^0}{\partial x\partial y}+\frac{\partial^2\Phi}{\partial x^2}\frac{\partial^2w^0}{\partial y^2}\right)+\left(1-\mu\nabla^2\right)\rho h\ddot{w}^0\end{aligned}\tag{4.23}$$

By substituting Φ and w^0 in (4.23) by the particular solution (4.20) with the coefficients (4.22) and by (4.15), (4.16) or (4.17) depending on the mode of vibration that is intended to be studied respectively, it is finally possible to apply the Galerkin method in order to determine the mass, linear and non-linear stiffness terms.

$$\int_{-\frac{b}{2}}^{\frac{b}{2}} \int_{-\frac{a}{2}}^{\frac{a}{2}} \cos(\alpha x)\cos(\beta y)\mathcal{L}_w \mathrm{d}x\mathrm{d}y \tag{4.24a}$$

$$\int_{-\frac{b}{2}}^{\frac{b}{2}} \int_{-\frac{a}{2}}^{\frac{a}{2}} \sin(\alpha x)\cos(\beta y)\mathcal{L}_w \mathrm{d}x\mathrm{d}y \tag{4.24b}$$

$$\int_{-\frac{b}{2}}^{\frac{b}{2}} \int_{-\frac{a}{2}}^{\frac{a}{2}} \sin(\alpha x)\sin(\beta y)\mathcal{L}_w \mathrm{d}x\mathrm{d}y \tag{4.24c}$$

It should be taken into account that the procedure varies according to the mode of interest, since the spatial component of the transverse displacement is distinct for each mode. In (4.24) the method applied to the first, second and fourth mode of vibration is demonstrated respectively.

From the application of the Galerkin method, a *Duffing* type equation is obtained:

$$M\ddot{q}^w(t) + K_L q^w(t) + K_{NL}\left(q^w(t)\right)^3 = 0 \tag{4.25}$$

Defining $q^w(t)$ with only one harmonic in order to apply the harmonic balance method (it should be mentioned that for this formulation the harmonic balance method can be solved analytically for the consideration of one harmonic since only one transverse displacement function is being used):

$$q^w(t) = w_{c1}\cos\left(\omega t\right) \tag{4.26}$$

and posteriorly substituting in equation (4.25):

$$-M\omega^2 w_{c1}\cos\left(\omega t\right) + K_L w_{c1}\cos\left(\omega t\right) + K_{NL} w_{c1}^3 \cos^3\left(\omega t\right) = 0 \tag{4.27}$$

Replacing $\cos^3\left(\omega t\right)$ by its Fourier expansion and neglecting the higher harmonics in equation (4.27):

$$-M\omega^2 w_{c1}\cos\left(\omega t\right) + K_L w_{c1}\cos\left(\omega t\right) + K_{NL} w_{c1}^3 \frac{3}{4}\cos\left(\omega t\right) = 0 \tag{4.28}$$

Which after the elimination of the cosines becomes:

$$-M\omega^2 w_{c1} + K_L w_{c1} + \frac{3}{4} K_{NL} w_{c1}^3 = 0 \tag{4.29}$$

The root of the equation above permits the direct determination of the backbone curve of the simply supported plate:

$$\omega = \sqrt{\frac{\frac{3}{4}K_{NL}w_{c1}^2 + K_L}{M}} \tag{4.30}$$

If more harmonics are considered, the analytical solution above is not applicable. In this case, for every generalized displacement, the number of equations to solve is multiplied by the number of harmonics considered and numerical methods must be employed to find adequate solutions. Considering the first three odd harmonics, since only free vibration is being studied, the transverse displacement $q^w(t)$ can be written as:

$$q^w(t) = w_{c1}\cos(\omega t) + w_{c3}\cos(3\omega t) + w_{c5}\cos(5\omega t) \tag{4.31}$$

where each component corresponds to the individual contribution of the first, third and fifth harmonic in the total transverse displacement respectively. As a consequence, instead of one *Duffing* type equation, there is now a system of three coupled equations:

$$\left(-\omega^2 \begin{bmatrix} M & 0 & 0 \\ 0 & 9M & 0 \\ 0 & 0 & 25M \end{bmatrix} + \begin{bmatrix} K_L & 0 & 0 \\ 0 & K_L & 0 \\ 0 & 0 & K_L \end{bmatrix} + \begin{bmatrix} K_{NL11} & K_{NL12} & K_{NL13} \\ K_{NL12} & K_{NL22} & K_{NL23} \\ K_{NL13} & K_{NL23} & K_{NL33} \end{bmatrix}\right) \begin{Bmatrix} w_{c1} \\ w_{c3} \\ w_{c5} \end{Bmatrix} = \{0\} \tag{4.32}$$

Each quadratic term of the non-linear stiffness matrix can be calculated as follows:

$$K_{NL11} = \frac{3}{4}K_{NL}w_{c1}w_{c1} + \frac{1}{4}K_{NL}w_{c1}w_{c3} + \frac{1}{2}K_{NL}w_{c3}w_{c3} + \frac{1}{4}K_{NL}w_{c3}w_{c5} + \frac{1}{2}K_{NL}w_{c5}w_{c5} \tag{4.33a}$$

$$K_{NL12} = \frac{1}{4}K_{NL}w_{c1}w_{c1} + \frac{1}{2}K_{NL}w_{c1}w_{c3} + \frac{1}{4}K_{NL}w_{c1}w_{c5} + \frac{1}{4}K_{NL}w_{c3}w_{c5} \tag{4.33b}$$

$$K_{NL13} = \frac{1}{4}K_{NL}w_{c1}w_{c3} + \frac{1}{2}K_{NL}w_{c1}w_{c5} + \frac{1}{4}K_{NL}w_{c3}w_{c3} \tag{4.33c}$$

$$K_{NL22} = \frac{1}{2}K_{NL}w_{c1}w_{c1} + \frac{1}{4}K_{NL}w_{c1}w_{c5} + \frac{3}{4}K_{NL}w_{c3}w_{c3} + \frac{1}{2}K_{NL}w_{c5}w_{c5} \tag{4.33d}$$

$$K_{NL23} = \frac{1}{4}K_{NL}w_{c1}w_{c1} + \frac{1}{4}K_{NL}w_{c1}w_{c3} + \frac{1}{2}K_{NL}w_{c3}w_{c5} \tag{4.33e}$$

$$K_{NL33} = \frac{1}{2}K_{NL}w_{c1}w_{c1} + \frac{1}{2}K_{NL}w_{c3}w_{c3} + \frac{3}{4}K_{NL}w_{c5}w_{c5} \tag{4.33f}$$

To solve the system of *Duffing* type equations in (4.32) the continuation method is employed and for every harmonic, each amplitude w_{c1}, w_{c3} and w_{c5} is calculated as a function of the frequency ω. The total transverse displacement W at $x = y = 0$ and with $t = 0s$ is given by the sum of each of these individual amplitudes (all positive), so, rewriting w_{c1}, w_{c3} and w_{c5} as W_1, W_3 and W_5, W is given by:

$$W = q^w(t = 0s) = W_1 + W_3 + W_5 \tag{4.34}$$

4.2.2 *p*-Version Finite Element Model

In this formulation, the Galerkin method is applied not only to the equation of motion but also to the compatibility equation. The particular solution of the non-homogeneous compatibility equation is not defined and consequently the Airy stress function remains an unknown. In fact, a set of shape functions is used for both the Airy potential and the transverse displacement and the p-version finite element method is employed. The non-linear time continuous equations are then discretized by the application of the harmonic balance method and the resulting system of algebraic equations is solved by the arc-length continuation method.

The Airy stress function and the middle-plane transverse displacement can be defined as the product of combinations of shape functions $t_r(\xi)t_s(\eta)$, $f_r(\xi)f_s(\eta)$ and the time continuous variables $q^{\Phi}_{rs}(t)$, $q^{w}_{rs}(t)$ respectively:

$$\left\{ \begin{array}{c} \Phi\left(\xi,\eta,t\right) \\ w^0\left(\xi,\eta,t\right) \end{array} \right\} = \left\{ \begin{array}{l} \sum\limits_{r=1}^{pt}\sum\limits_{s=1}^{pt} t_r\left(\xi\right) t_s\left(\eta\right) q^{\Phi}_{rs}\left(t\right) \\ \sum\limits_{r=1}^{po}\sum\limits_{s=1}^{po} f_r\left(\xi\right) f_s\left(\eta\right) q^{w}_{rs}\left(t\right) \end{array} \right. \tag{4.35}$$

Applying the Galerkin method and considering $\mathcal{L}_w$ from (4.23) using natural coordinates:

$$\frac{a}{2}\frac{b}{2}\int_{-1}^{1}\int_{-1}^{1} t_r\left(\xi\right) t_s\left(\eta\right) \mathcal{L}_{\Phi}\left(\xi,\eta,t\right) \mathrm{d}\xi\mathrm{d}\eta \tag{4.36a}$$

$$\frac{a}{2}\frac{b}{2}\int_{-1}^{1}\int_{-1}^{1} f_r\left(\xi\right) f_s\left(\eta\right) \mathcal{L}_{w}\left(\xi,\eta,t\right) \mathrm{d}\xi\mathrm{d}\eta \tag{4.36b}$$

Considering the compatibility equation from (4.13) and defining $\mathcal{L}_{\Phi}$ by moving all the terms to the left-hand side:

$$\begin{aligned} \mathcal{L}_{\Phi} = {} & \underbrace{S_{11}\frac{\partial^4\Phi}{\partial y^4}}_{\mathrm{t}(21)} + \underbrace{\left(2S_{12}+S_{33}\right)\frac{\partial^4\Phi}{\partial x^2\partial y^2}}_{\mathrm{t}(22)} + \underbrace{S_{22}\frac{\partial^4\Phi}{\partial x^4}}_{\mathrm{t}(23)} - \underbrace{\mu\left(S_{11}+2S_{12}+S_{33}\right)\frac{\partial^6\Phi}{\partial x^2\partial y^4}}_{\mathrm{t}(24)} \\ & - \underbrace{\mu\left(S_{22}+2S_{12}+S_{33}\right)\frac{\partial^6\Phi}{\partial x^4\partial y^2}}_{\mathrm{t}(25)} - \underbrace{\mu S_{22}\frac{\partial^6\Phi}{\partial x^6}}_{\mathrm{t}(26)} - \underbrace{\mu S_{11}\frac{\partial^6\Phi}{\partial y^6}}_{\mathrm{t}(27)} - \underbrace{\left(\frac{\partial^2 w^0}{\partial x\partial y}\right)^2}_{\mathrm{t}(28)} + \underbrace{\frac{\partial^2 w^0}{\partial x^2}\frac{\partial^2 w^0}{\partial y^2}}_{\mathrm{t}(29)} \end{aligned} \tag{4.37}$$

Writing each resulting term of (4.37) after the application of the Galerkin method, as demonstrated in (4.36a) for the case of the compatibility equation, and considering the indexes from (2.48) in order to take into account all possible products between shape functions:

$$t(21) = S_{11}\frac{4a}{b^3}\int_{-1}^{1} t_{i\xi}t_{j\xi}\mathrm{d}\xi \int_{-1}^{1} \frac{\partial^2 t_{i\eta}}{\partial\eta^2}\frac{\partial^2 t_{j\eta}}{\partial\eta^2}\mathrm{d}\eta q^{\Phi}(j) \tag{4.38}$$

$$t(22) = (2S_{12} + S_{33})\frac{4}{ab}\int_{-1}^{1} \frac{\partial t_{i\xi}}{\partial\xi}\frac{\partial t_{j\xi}}{\partial\xi}\mathrm{d}\xi \int_{-1}^{1} \frac{\partial t_{i\eta}}{\partial\eta}\frac{\partial t_{j\eta}}{\partial\eta}\mathrm{d}\eta q^{\Phi}(j) \tag{4.39}$$

$$t(23) = S_{22}\frac{4b}{a^3}\int_{-1}^{1} \frac{\partial^2 t_{i\xi}}{\partial\xi^2}\frac{\partial^2 t_{j\xi}}{\partial\xi^2}\mathrm{d}\xi \int_{-1}^{1} t_{i\eta}t_{j\eta}\mathrm{d}\eta q^{\Phi}(j) \tag{4.40}$$

$$t(24) = \mu\,(S_{11} + 2S_{12} + S_{33})\frac{16}{ab^3}\int_{-1}^{1} \frac{\partial t_{i\xi}}{\partial\xi}\frac{\partial t_{j\xi}}{\partial\xi}\mathrm{d}\xi \int_{-1}^{1} \frac{\partial^2 t_{i\eta}}{\partial\eta^2}\frac{\partial^2 t_{j\eta}}{\partial\eta^2}\mathrm{d}\eta q^{\Phi}(j) \tag{4.41}$$

$$t(25) = \mu\,(S_{22} + 2S_{12} + S_{33})\frac{16}{ba^3}\int_{-1}^{1} \frac{\partial^2 t_{i\xi}}{\partial\xi^2}\frac{\partial^2 t_{j\xi}}{\partial\xi^2}\mathrm{d}\xi \int_{-1}^{1} \frac{\partial t_{i\eta}}{\partial\eta}\frac{\partial t_{j\eta}}{\partial\eta}\mathrm{d}\eta q^{\Phi}(j) \tag{4.42}$$

$$t(26) = \mu S_{22}\frac{16b}{a^5}\int_{-1}^{1} \frac{\partial^3 t_{i\xi}}{\partial\xi^3}\frac{\partial^3 t_{j\xi}}{\partial\xi^3}\mathrm{d}\xi \int_{-1}^{1} t_{i\eta}t_{j\eta}\mathrm{d}\eta q^{\Phi}(j) \tag{4.43}$$

$$t(27) = \mu S_{11}\frac{16a}{b^5}\int_{-1}^{1} t_{i\xi}t_{j\xi}\mathrm{d}\xi \int_{-1}^{1} \frac{\partial^3 t_{i\eta}}{\partial\eta^3}\frac{\partial^3 t_{j\eta}}{\partial\eta^3}\mathrm{d}\eta q^{\Phi}(j) \tag{4.44}$$

$$t(28) = -\frac{4}{ab}\int_{-1}^{1} t_{i\xi}\frac{\partial f_{j\xi}}{\partial\xi}\frac{\partial f_{k\xi}}{\partial\xi}\mathrm{d}\xi \int_{-1}^{1} t_{i\eta}\frac{\partial f_{j\eta}}{\partial\eta}\frac{\partial f_{k\eta}}{\partial\eta}\mathrm{d}\eta q^{w}(k)q^{w}(j) \tag{4.45}$$

$$t(29) = \frac{4}{ab}\int_{-1}^{1} t_{i\xi}\frac{\partial^2 f_{j\xi}}{\partial\xi^2}f_{k\xi}\mathrm{d}\xi \int_{-1}^{1} t_{i\eta}f_{j\eta}\frac{\partial^2 f_{k\eta}}{\partial\eta^2}\mathrm{d}\eta q^{w}(k)q^{w}(j) \tag{4.46}$$

Proceeding in a similar way and rewriting the terms of $\mathcal{L}_w$ one has:

$$\begin{aligned}
\mathcal{L}_w = {} & \underbrace{D_{11}\frac{\partial^4 w^0}{\partial x^4}}_{\text{-t(15)}} + \underbrace{2\,(D_{12}+2D_{33})\,\frac{\partial^4 w^0}{\partial x^2\partial y^2}}_{\text{-t(16)}} + \underbrace{D_{22}\frac{\partial^4 w^0}{\partial y^4}}_{\text{-t(17)}} + \left(\underbrace{1}_{\text{-t(19)}}\underbrace{-\mu\nabla^2}_{\text{-t(20)}}\right)\rho h\ddot{w}^0 \underbrace{-\frac{\partial^2\Phi}{\partial y^2}\frac{\partial^2 w^0}{\partial x^2}}_{\text{t(30)}} \\
& \underbrace{+2\frac{\partial^2\Phi}{\partial x\partial y}\frac{\partial^2 w^0}{\partial x\partial y}}_{\text{t(31)}} \underbrace{-\frac{\partial^2\Phi}{\partial x^2}\frac{\partial^2 w^0}{\partial y^2}}_{\text{t(32)}} + \mu\left(\underbrace{\frac{\partial^4\Phi}{\partial x^2\partial y^2}\frac{\partial^2 w^0}{\partial x^2}}_{\text{t(33)}} + \underbrace{2\frac{\partial^3\Phi}{\partial x\partial y^2}\frac{\partial^3 w^0}{\partial x^3}}_{\text{t(34)}} + \underbrace{\frac{\partial^2\Phi}{\partial y^2}\frac{\partial^4 w^0}{\partial x^4}}_{\text{t(35)}}\right. \\
& \underbrace{-2\frac{\partial^4\Phi}{\partial x^3\partial y}\frac{\partial^2 w^0}{\partial x\partial y}}_{\text{t(36)}} \underbrace{-4\frac{\partial^3\Phi}{\partial x^2\partial y}\frac{\partial^3 w^0}{\partial x^2\partial y}}_{\text{t(37)}} \underbrace{-2\frac{\partial^2\Phi}{\partial x\partial y}\frac{\partial^4 w^0}{\partial x^3\partial y}}_{\text{t(38)}} + \underbrace{\frac{\partial^4\Phi}{\partial x^4}\frac{\partial^2 w^0}{\partial y^2}}_{\text{t(39)}} + \underbrace{2\frac{\partial^3\Phi}{\partial x^3}\frac{\partial^3 w^0}{\partial x\partial y^2}}_{\text{t(40)}} \\
& \underbrace{+\frac{\partial^2\Phi}{\partial x^2}\frac{\partial^4 w^0}{\partial x^2\partial y^2}}_{\text{t(41)}} + \underbrace{\frac{\partial^4\Phi}{\partial y^4}\frac{\partial^2 w^0}{\partial x^2}}_{\text{t(42)}} + \underbrace{2\frac{\partial^3\Phi}{\partial y^3}\frac{\partial^3 w^0}{\partial y\partial x^2}}_{\text{t(43)}} + \underbrace{\frac{\partial^2\Phi}{\partial y^2}\frac{\partial^4 w^0}{\partial y^2\partial x^2}}_{\text{t(44)}} \underbrace{-2\frac{\partial^4\Phi}{\partial y^2\partial x\partial y}\frac{\partial^2 w^0}{\partial x\partial y}}_{\text{t(45)}} \\
& \left.\underbrace{-4\frac{\partial^3\Phi}{\partial y\partial x\partial y}\frac{\partial^3 w^0}{\partial y\partial x\partial y}}_{\text{t(46)}} \underbrace{-2\frac{\partial^2\Phi}{\partial x\partial y}\frac{\partial^4 w^0}{\partial y^2\partial x\partial y}}_{\text{t(47)}} + \underbrace{\frac{\partial^4\Phi}{\partial y^2\partial x^2}\frac{\partial^2 w^0}{\partial y^2}}_{\text{t(48)}} + \underbrace{2\frac{\partial^3\Phi}{\partial y\partial x^2}\frac{\partial^3 w^0}{\partial y^3}}_{\text{t(49)}} + \underbrace{\frac{\partial^2\Phi}{\partial x^2}\frac{\partial^4 w^0}{\partial y^4}}_{\text{t(50)}}\right)
\end{aligned} \tag{4.47}$$

Applying the Galerkin method, as demonstrated in (4.36b) to each term of $\mathcal{L}_w$ individually (note that the terms $t(15)$ to $t(20)$ will be omitted and can be observed in equations (2.66) to (2.70)):

$$t(30) = -\frac{4}{ab}\int_{-1}^{1} f_{i\xi} t_{j\xi} \frac{\partial^2 f_{k\xi}}{\partial \xi^2} \mathrm{d}\xi \int_{-1}^{1} f_{i\eta} \frac{\partial^2 t_{j\eta}}{\partial \eta^2} f_{k\eta} \mathrm{d}\eta q^w(k) q^\Phi(j) \tag{4.48}$$

$$t(31) = \frac{8}{ab}\int_{-1}^{1} f_{i\xi} \frac{\partial t_{j\xi}}{\partial \xi} \frac{\partial f_{k\xi}}{\partial \xi} \mathrm{d}\xi \int_{-1}^{1} f_{i\eta} \frac{\partial t_{j\eta}}{\partial \eta} \frac{\partial f_{k\eta}}{\partial \eta} \mathrm{d}\eta q^w(k) q^\Phi(j) \tag{4.49}$$

$$t(32) = -\frac{4}{ab}\int_{-1}^{1} f_{i\xi} \frac{\partial^2 t_{j\xi}}{\partial \xi^2} f_{k\xi} \mathrm{d}\xi \int_{-1}^{1} f_{i\eta} t_{j\eta} \frac{\partial^2 f_{k\eta}}{\partial \eta^2} \mathrm{d}\eta q^w(k) q^\Phi(j) \tag{4.50}$$

$$t(33) = \frac{16}{ba^3}\int_{-1}^{1} f_{i\xi} \frac{\partial^2 t_{j\xi}}{\partial \xi^2} \frac{\partial^2 f_{k\xi}}{\partial \xi^2} \mathrm{d}\xi \int_{-1}^{1} f_{i\eta} \frac{\partial^2 t_{j\eta}}{\partial \eta^2} f_{k\eta} \mathrm{d}\eta q^w(k) q^\Phi(j) \tag{4.51}$$

$$t(34) = \frac{32}{ba^3}\int_{-1}^{1} f_{i\xi} \frac{\partial t_{j\xi}}{\partial \xi} \frac{\partial^3 f_{k\xi}}{\partial \xi^3} \mathrm{d}\xi \int_{-1}^{1} f_{i\eta} \frac{\partial^2 t_{j\eta}}{\partial \eta^2} f_{k\eta} \mathrm{d}\eta q^w(k) q^\Phi(j) \tag{4.52}$$

$$t(35) = \frac{16}{ba^3}\int_{-1}^{1} \frac{\partial^2}{\partial \xi^2}\left(f_{i\xi} t_{j\xi}\right) \frac{\partial^2 f_{k\xi}}{\partial \xi^2} \mathrm{d}\xi \int_{-1}^{1} f_{i\eta} \frac{\partial^2 t_{j\eta}}{\partial \eta^2} f_{k\eta} \mathrm{d}\eta q^w(k) q^\Phi(j) \tag{4.53}$$

$$t(36) = -\frac{32}{ba^3}\int_{-1}^{1} f_{i\xi} \frac{\partial^3 t_{j\xi}}{\partial \xi^3} \frac{\partial f_{k\xi}}{\partial \xi} \mathrm{d}\xi \int_{-1}^{1} f_{i\eta} \frac{\partial t_{j\eta}}{\partial \eta} \frac{\partial f_{k\eta}}{\partial \eta} \mathrm{d}\eta q^w(k) q^\Phi(j) \tag{4.54}$$

$$t(37) = -\frac{64}{ba^3}\int_{-1}^{1} f_{i\xi} \frac{\partial^2 t_{j\xi}}{\partial \xi^2} \frac{\partial^2 f_{k\xi}}{\partial \xi^2} \mathrm{d}\xi \int_{-1}^{1} f_{i\eta} \frac{\partial t_{j\eta}}{\partial \eta} \frac{\partial f_{k\eta}}{\partial \eta} \mathrm{d}\eta q^w(k) q^\Phi(j) \tag{4.55}$$

$$t(38) = -\frac{32}{ba^3}\int_{-1}^{1} f_{i\xi} \frac{\partial t_{j\xi}}{\partial \xi} \frac{\partial^3 f_{k\xi}}{\partial \xi^3} \mathrm{d}\xi \int_{-1}^{1} f_{i\eta} \frac{\partial t_{j\eta}}{\partial \eta} \frac{\partial f_{k\eta}}{\partial \eta} \mathrm{d}\eta q^w(k) q^\Phi(j) \tag{4.56}$$

$$t(39) = \frac{16}{ba^3}\int_{-1}^{1} \frac{\partial^2}{\partial \xi^2}\left(f_{i\xi} f_{k\xi}\right) \frac{\partial^2 t_{j\xi}}{\partial \xi^2} \mathrm{d}\xi \int_{-1}^{1} f_{i\eta} t_{j\eta} \frac{\partial^2 f_{k\eta}}{\partial \eta^2} \mathrm{d}\eta q^w(k) q^\Phi(j) \tag{4.57}$$

$$t(40) = \frac{32}{ba^3}\int_{-1}^{1} f_{i\xi} \frac{\partial^3 t_{j\xi}}{\partial \xi^3} \frac{\partial f_{k\xi}}{\partial \xi} \mathrm{d}\xi \int_{-1}^{1} f_{i\eta} t_{j\eta} \frac{\partial^2 f_{k\eta}}{\partial \eta^2} \mathrm{d}\eta q^w(k) q^\Phi(j) \tag{4.58}$$

$$t(41) = \frac{16}{ba^3}\int_{-1}^{1} f_{i\xi} \frac{\partial^2 t_{j\xi}}{\partial \xi^2} \frac{\partial^2 f_{k\xi}}{\partial \xi^2} \mathrm{d}\xi \int_{-1}^{1} f_{i\eta} t_{j\eta} \frac{\partial^2 f_{k\eta}}{\partial \eta^2} \mathrm{d}\eta q^w(k) q^\Phi(j) \tag{4.59}$$

$$t(42) = \frac{16}{ab^3} f_{i\xi} t_{j\xi} \frac{\partial^2 f_{k\xi}}{\partial \xi^2} \mathrm{d}\xi \int_{-1}^{1} \frac{\partial^2}{\partial \eta^2}\left(f_{i\eta} f_{k\eta}\right) \frac{\partial^2 t_{j\eta}}{\partial \eta^2} \mathrm{d}\eta q^w(k) q^\Phi(j) \tag{4.60}$$

$$t(43) = \frac{32}{ab^3}\int_{-1}^{1} f_{i\xi} t_{j\xi} \frac{\partial^2 f_{k\xi}}{\partial \xi^2} \mathrm{d}\xi \int_{-1}^{1} f_{i\eta} \frac{\partial^3 t_{j\eta}}{\partial \eta^3} \frac{\partial f_{k\eta}}{\partial \eta} \mathrm{d}\eta q^w(k) q^\Phi(j) \tag{4.61}$$

$$t(44) = \frac{16}{ab^3}\int_{-1}^{1} f_{i\xi} t_{j\xi} \frac{\partial^2 f_{k\xi}}{\partial \xi^2} \mathrm{d}\xi \int_{-1}^{1} f_{i\eta} \frac{\partial^2 t_{j\eta}}{\partial \eta^2} \frac{\partial^2 f_{k\eta}}{\partial \eta^2} \mathrm{d}\eta q^w(k) q^\Phi(j) \tag{4.62}$$

$$t(45) = -\frac{32}{ab^3}\int_{-1}^{1} f_{i\xi} \frac{\partial t_{j\xi}}{\partial \xi} \frac{\partial f_{k\xi}}{\partial \xi} \mathrm{d}\xi \int_{-1}^{1} f_{i\eta} \frac{\partial^3 t_{j\eta}}{\partial \eta^3} \frac{\partial f_{k\eta}}{\partial \eta} \mathrm{d}\eta q^w(k) q^\Phi(j) \tag{4.63}$$

$$t(46) = -\frac{64}{ab^3}\int_{-1}^{1} f_{i\xi} \frac{\partial t_{j\xi}}{\partial \xi} \frac{\partial f_{k\xi}}{\partial \xi} \mathrm{d}\xi \int_{-1}^{1} f_{i\eta} \frac{\partial^2 t_{j\eta}}{\partial \eta^2} \frac{\partial^2 f_{k\eta}}{\partial \eta^2} \mathrm{d}\eta q^w(k) q^\Phi(j) \tag{4.64}$$

$$t(47) = -\frac{32}{ab^3}\int_{-1}^{1} f_{i\xi}\frac{\partial t_{j\xi}}{\partial \xi}\frac{\partial f_{k\xi}}{\partial \xi}\mathrm{d}\xi \int_{-1}^{1} f_{i\eta}\frac{\partial t_{j\eta}}{\partial \eta}\frac{\partial^3 f_{k\eta}}{\partial \eta^3}\mathrm{d}\eta q^w(k)q^\Phi(j) \tag{4.65}$$

$$t(48) = \frac{16}{ab^3}\int_{-1}^{1} f_{i\xi}\frac{\partial^2 t_{j\xi}}{\partial \xi^2}f_{k\xi}\mathrm{d}\xi \int_{-1}^{1} f_{i\eta}\frac{\partial^2 t_{j\eta}}{\partial \eta^2}\frac{\partial^2 f_{k\eta}}{\partial \eta^2}\mathrm{d}\eta q^w(k)q^\Phi(j) \tag{4.66}$$

$$t(49) = \frac{32}{ab^3}\int_{-1}^{1} f_{i\xi}\frac{\partial^2 t_{j\xi}}{\partial \xi^2}f_{k\xi}\mathrm{d}\xi \int_{-1}^{1} f_{i\eta}\frac{\partial t_{j\eta}}{\partial \eta}\frac{\partial^3 f_{k\eta}}{\partial \eta^3}\mathrm{d}\eta q^w(k)q^\Phi(j) \tag{4.67}$$

$$t(50) = \frac{16}{ab^3}\int_{-1}^{1} f_{i\xi}\frac{\partial^2 t_{j\xi}}{\partial \xi^2}f_{k\xi}\mathrm{d}\xi \int_{-1}^{1} \frac{\partial^2}{\partial \eta^2}\left(f_{i\eta}t_{j\eta}\right)\frac{\partial^2 f_{k\eta}}{\partial \eta^2}\mathrm{d}\eta q^w(k)q^\Phi(j) \tag{4.68}$$

Rewriting the equation of motion and the compatibility equation after the application of the Galerkin method as a system of algebraic equations (discretized in space) with the time continuous variables $q^\Phi(t)$ and $q^w(t)$ one has:

$$\begin{cases} [M_{ww}]\{\ddot{q}^w\} + \left[K^1_{ww}\right]\{q^w\} + \left[K^7_{ww}\right]\left\{q^\Phi\right\} + \mu\left[K^8_{ww}\right]\left\{q^\Phi\right\} = \{0\} \\ [X]\left\{q^\Phi\right\} + [Y]\{q^w\} = \{0\} \end{cases} \tag{4.69}$$

Both the out-of-plane mass matrix $[M_{ww}]$ and the out-of-plane linear stiffness matrix $\left[K^1_{ww}\right]$ have already been defined in chapter 2. The matrices $\left[K^7_{ww}\right]$ and $\left[K^8_{ww}\right]$ are first-order non-linear stiffness matrices and are both linearly dependent on the transverse displacement vector $\{q^w\}$. The matrices $[X]$ and $[Y]$ arise from the compatibility equation. The former does not depend on any time continuous variable while the latter is linearly dependent on the transverse displacement vector $\{q^w\}$. Writing the matrices and the terms previously calculated from which they are derived (with the exclusion of the Airy stress function vector and the acceleration vector, $q^\Phi(j)$ and $\ddot{q}^w(j)$):

- $[X]$: $t(21) + t(22) + t(23) + t(24) + t(25) + t(26) + t(27)$
- $[Y]$: $t(28) + t(29)$
- $\left[K^7_{ww}\right]$: $t(30) + t(31) + t(32)$
- $\left[K^8_{ww}\right]$: $t(33) + t(3) + t(35) + t(36) + t(37) + t(38) + t(39) + t(40) + t(41) + t(42) + t(43) + t(44) + t(45) + t(46) + t(47) + t(48) + t(49) + t(50)$

It is now possible to reduce the system of equations (4.69) by determining $\left\{q^\Phi\right\}$ as a function of the transverse displacement vector $\{q^w\}$. Solving the compatibility equation and posteriorly substituting into the equation of motion one finally has:

$$\begin{cases} [M_{ww}]\{\ddot{q}^w\} + \left[K^1_{ww}\right]\{q^w\} - \left[K^7_{ww}\right][X]^{-1}[Y]\{q^w\} - \mu\left[K^8_{ww}\right][X]^{-1}[Y]\{q^w\} = \{0\} \\ \left\{q^\Phi\right\} = -[X]^{-1}[Y]\{q^w\} \end{cases} \tag{4.70}$$

From the substitution performed in (4.70) a system of coupled *Duffing* type equations is obtained since the products $\left[K^7_{ww}\right][X]^{-1}[Y]\{q^w\}$ and $\mu\left[K^8_{ww}\right][X]^{-1}[Y]\{q^w\}$ are both third-order functions of $\{q^w\}$. The harmonic balance method can finally be employed in the same way as the formulation presented in chapter 2. To solve the resulting frequency-domain equations, the arc-length continuation method is used.

4.3 Numerical Results

In this section the single function model is validated considering one and three harmonics with varying non-local parameter in the first mode of vibration. The influence of each harmonic is also studied and the respective backbone curves are also represented for different values of the non-local parameter. Lastly, the particular case of a single layer graphene sheet is studied and the first, second and fourth mode backbone curves are presented for different non-local parameters. The Airy stress function and the resulting membrane forces are also demonstrated for each mode of vibration.

4.3.1 Model Validation

In order to validate the single function model presented in this chapter, a simply supported square magneto-electro-elastic nano-plate is considered, where the magnetic and electric potential is null. The plate's properties are the same as the ones used in the determination of the backbone curves in Figure 3.16, with the exception that in this case the plate is simply supported with movable edges. As mentioned before, the model was validated for the first mode of vibration and both one and three harmonics solutions are presented, as well as the solution proposed in [43], which was obtained by a multiple scale method. In Figure 4.1 the backbone curves are demonstrated for $\frac{\sqrt{\mu}}{a} = 0$, $\frac{\sqrt{\mu}}{a} = 0.1$, $\frac{\sqrt{\mu}}{a} = 0.2$ and $\frac{\sqrt{\mu}}{a} = 0.3$ respectively.

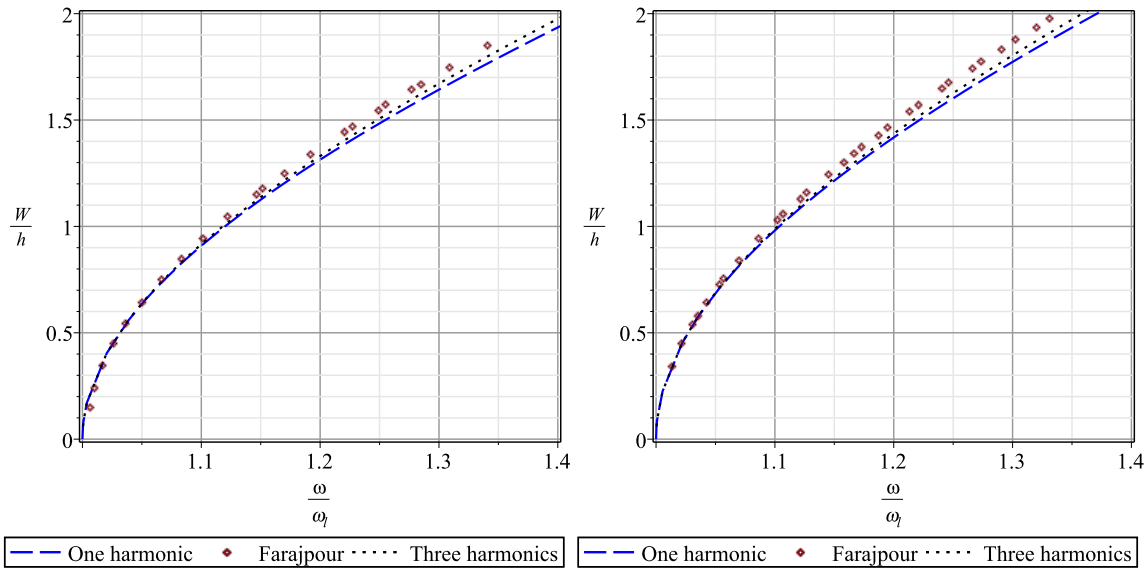

(a) $\frac{\sqrt{\mu}}{a} = 0$ (b) $\frac{\sqrt{\mu}}{a} = 0.1$

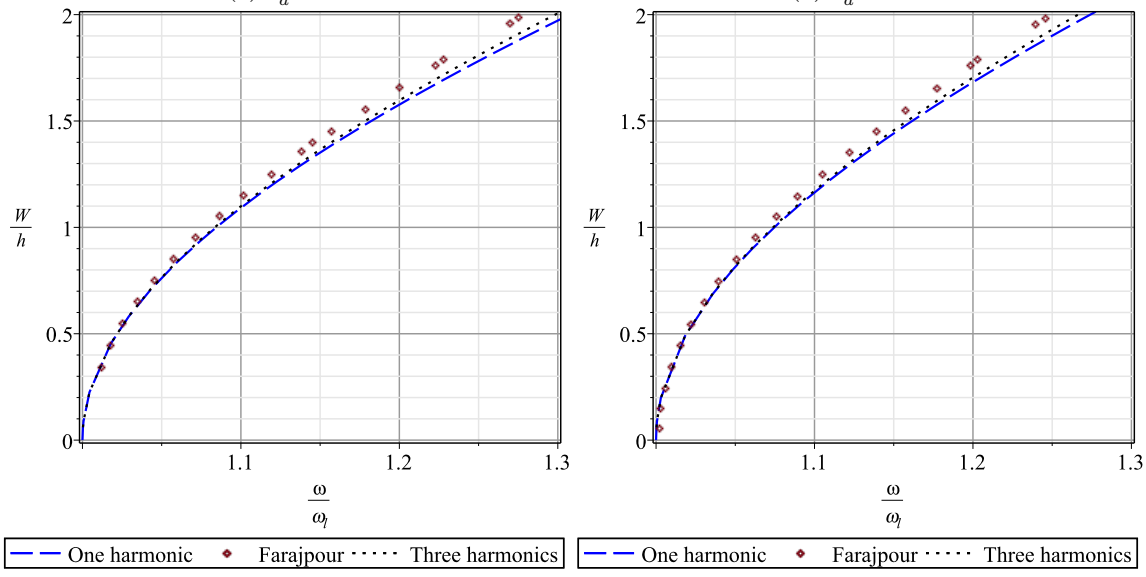

(c) $\frac{\sqrt{\mu}}{a} = 0.2$ (d) $\frac{\sqrt{\mu}}{a} = 0.3$

Figure 4.1: Backbone curves with one and three harmonics - orthotropic square SSSS plate with movable edges

From the observation of Figure 4.1 it is possible to conclude that the results are in very good agreement with the solution in [43]. The consideration of more harmonics brings the backbone curve slightly upper and approximates the solution of the model to the reference. It should be noted that the rather small difference between the model's backbone curve and the one presented in [43] might be related with the difference in the procedure adopted, which was a multiple scale method instead of a harmonic balance one, as it was mentioned before. In addition, it can be verified that for higher values of the non-local parameter, the contribution of higher harmonics becomes less influential in the total amplitude of vibration since the distance between the solution with one harmonic and the backbone curve attributed to three harmonics slightly diminishes.

4.3.2 Influence of the Small-Scale effect on Harmonics

To study the influence of the non-local parameter on the different harmonics, the respective backbone curves were plotted for different values of the parameter. The nano-plate considered is the same as the one used in the previous validation and its properties are stated next to Figure 3.16. Note that W_1, W_3 and W_5 refer to the amplitude of each respective individual harmonic at the centre of the plate ($x = y = 0$).

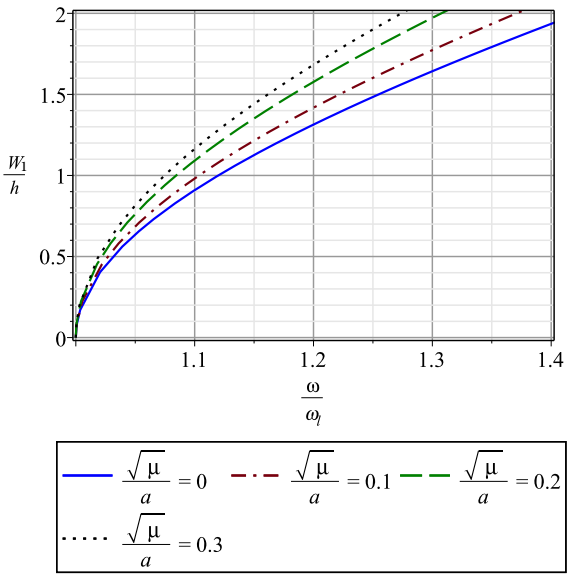

(a) First harmonic with W_1 at $x = y = 0$

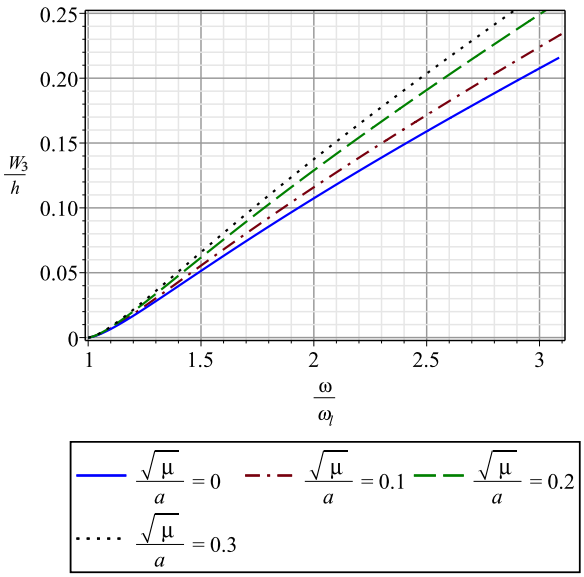

(b) Third harmonic with W_3 at $x = y = 0$

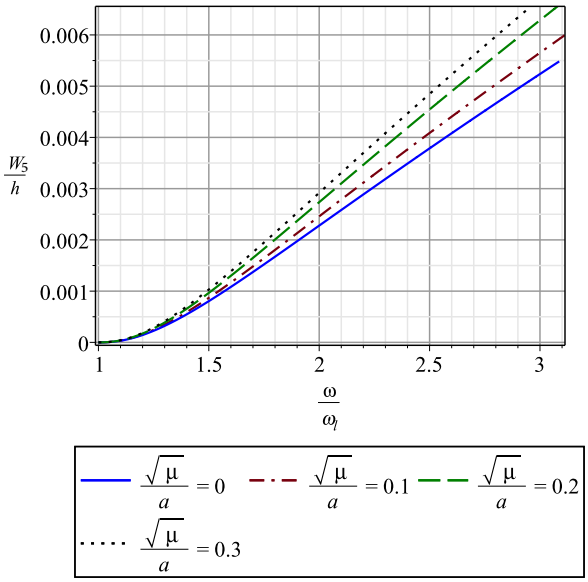

(c) Fifth harmonic with W_5 at $x = y = 0$

Figure 4.2: Backbone curves of first, third and fifth harmonics of square SSSS plate with varying non-local parameter

From Figure 4.2 it can be seen that the influence of the first harmonic is significantly greater than the third and fifth. In fact, the contribution of the fifth harmonic is almost negligible since the amplitude ratios W_5/h are well below 1% of the ratios of the first harmonic. It can also be concluded that the increase of the non-local parameter leads to less hardening spring effect in every harmonic backbone curve, which is rather counterintuitive since higher non-local parameters are generally associated with greater non-linearities. In fact, it was previously concluded that this was the case even for pinned plates. However, the added movable edges, besides free rotation, result in an opposite behaviour and for higher values of the non-local parameter, given a fixed amplitude of vibration, the respective frequency is lower. It was verified that for a simply supported plate with movable edges, a rise in the non-local parameter does indeed reduce the non-linear stiffness. It should be noted that inertia is still increased with a rise in the parameter seeing that it does not depend on transverse displacement and is therefore unaffected by boundary conditions.

4.3.3 Modes of vibration of SLGS

In this section, the effect of the non-local parameter on the non-linear modes of vibration of a square single layer graphene sheet will be studied, and the Airy stress function and the resulting membrane stresses will also be displayed. For this study, the graphene sheet considered has the orthotropic elastic properties from Table 3.11 as well as the same geometric properties and the results were obtained considering three harmonics. The modes studied are the first, second and fourth and for each of them the linear natural frequencies are also calculated. Note that the third mode is not studied since it is identical to the second but with the nodal line in $y = 0$ instead of $x = 0$. Besides the backbone curve associated with each mode, the three-dimensional plot of the stress function and the forces N_{xx} and N_{yy} are demonstrated for a given amplitude of vibration and non-local parameter.

In Table 4.1 the first, second and fourth linear natural frequencies of the single layer graphene sheet are calculated for different values of the non-local parameter.

In Figure 4.3 the first mode of vibration is studied and the backbone curves are plotted for the same values of non-local parameter as those used in the determination of the linear frequencies. The Airy stress function and its second order derivatives, N_{xx} and N_{yy}, are also plotted considering the non-local parameter null and an amplitude of vibration correspondent to a frequency ratio $\frac{\omega}{\omega_l}$ equal to 1.1 (variation in μ and W result in different maximums and minimums, but the shape of these functions remains unaltered).

In Figure 4.4 the second mode of vibration is studied and the Airy stress function and the resulting membrane forces are plotted considering a null non-local parameter as well, but in this case the point in the backbone curve has the frequency ratio $\frac{\omega}{\omega_l}$ of 1.2.

In Figure 4.5 the fourth mode of vibration is studied in the same fashion as the first mode, where the point selected of the backbone curve corresponds to a frequency ratio $\frac{\omega}{\omega_l}$ of 1.1 and the non-local parameter is also zero.

Table 4.1: Linear natural frequencies in [THz] of a square SSSS SLGS with movable edges

$\sqrt{\mu}/a$	0	0.2	0.4	0.6	0.8
ω_{11}	0.0884	0.0661	0.0434	0.0311	0.0239
ω_{21}	0.2239	0.1298	0.0751	0.0517	0.0392
ω_{22}	0.3537	0.1734	0.0958	0.0652	0.0493

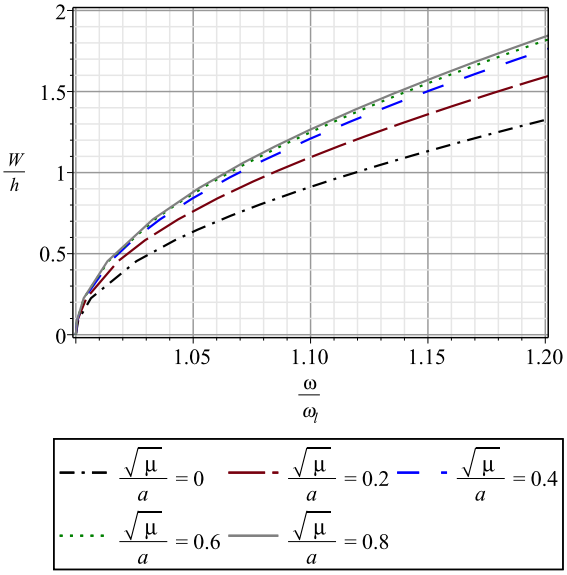

(a) Backbone curves for different $\frac{\sqrt{\mu}}{a}$

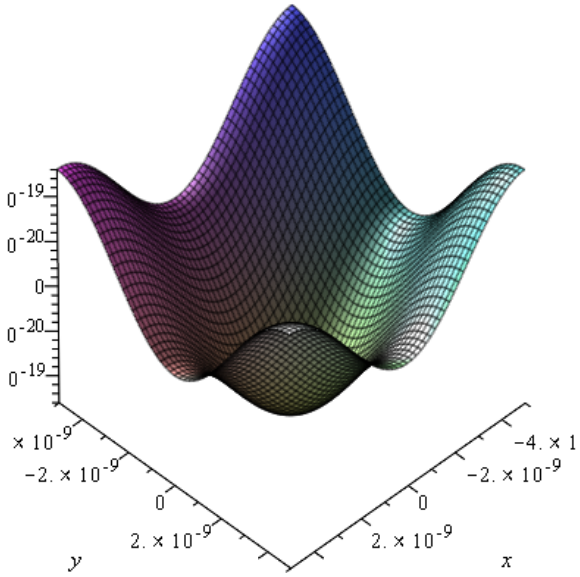

(b) Airy stress function - $\frac{\sqrt{\mu}}{a} = 0$, $\frac{\omega}{\omega_l} = 1.1$

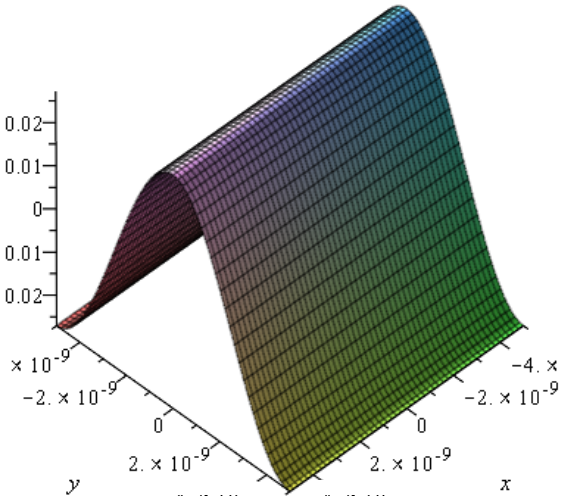

(c) N_{xx} - $\frac{\sqrt{\mu}}{a} = 0$, $\frac{\omega}{\omega_l} = 1.1$

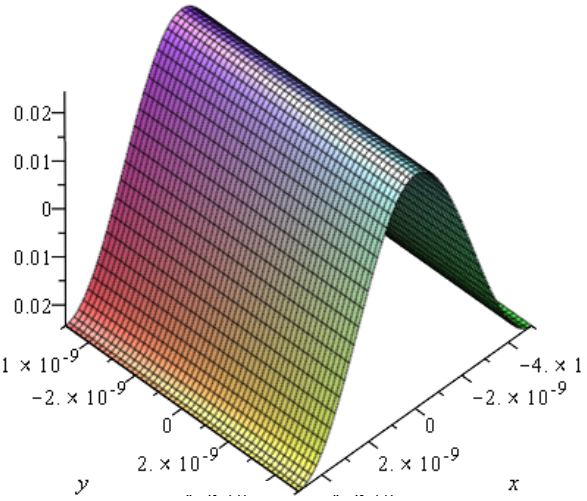

(d) N_{yy} - $\frac{\sqrt{\mu}}{a} = 0$, $\frac{\omega}{\omega_l} = 1.1$

Figure 4.3: First mode of vibration of SSSS SLGS

From Figure 4.3a the same tendency already verified in the validation of the model can be seen, where higher values of the non-local parameter result in lower natural frequencies

for a fixed amplitude of vibration, due to a less pronounced hardening spring effect. For increasingly greater values of the non-local parameter, the small-scale effect seems to become less significant resulting in a shorter distance between backbone curves, eventually leading to almost overlapping curves (in the case of $\frac{\sqrt{\mu}}{a} = 0.6$ and $\frac{\sqrt{\mu}}{a} = 0.8$). In Figure 4.3c and 4.3d the boundary conditions are satisfied and in the first case movement is allowed without restriction along the x axis while in the second case, movement along y is also unrestricted. The highest values of the in-plane forces occur in the centre of the sheet, where the amplitude of the transverse displacement is at its maximum. It should be mentioned that in-plane shear force is zero across the whole sheet since no torsion is present and only flexural modes are being studied, hence not being demonstrated.

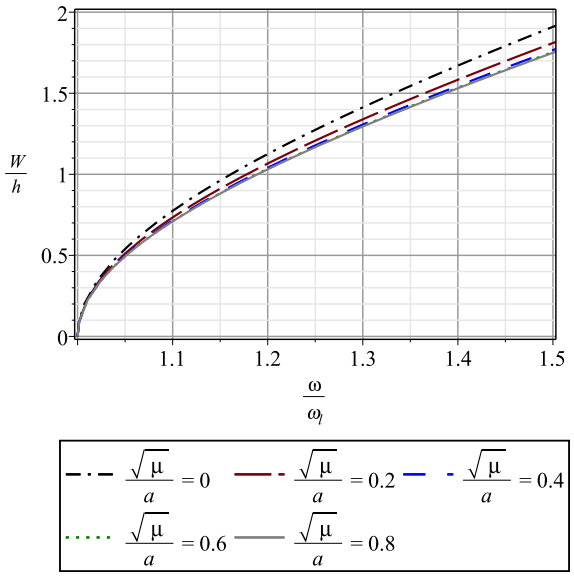

(a) Backbone curves for different $\frac{\sqrt{\mu}}{a}$

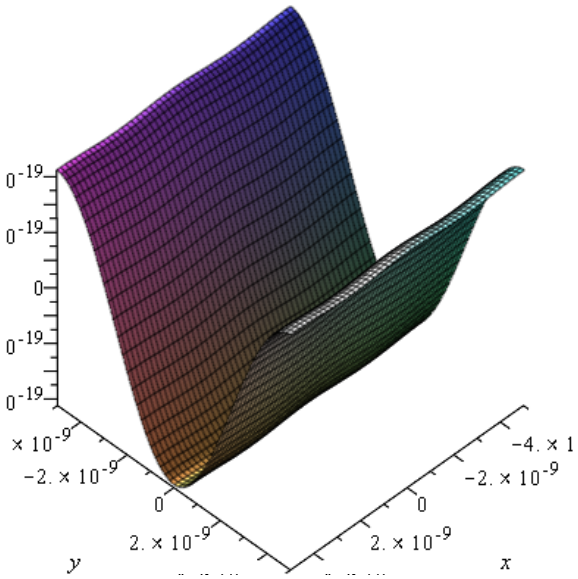

(b) Airy stress function - $\frac{\sqrt{\mu}}{a} = 0$, $\frac{\omega}{\omega_l} = 1.2$

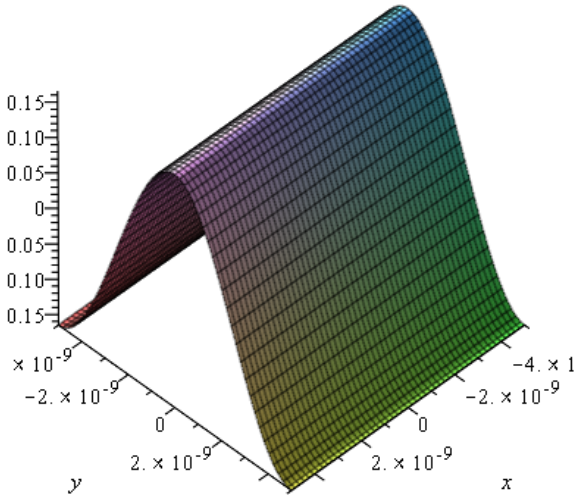

(c) N_{xx} - $\frac{\sqrt{\mu}}{a} = 0$, $\frac{\omega}{\omega_l} = 1.2$

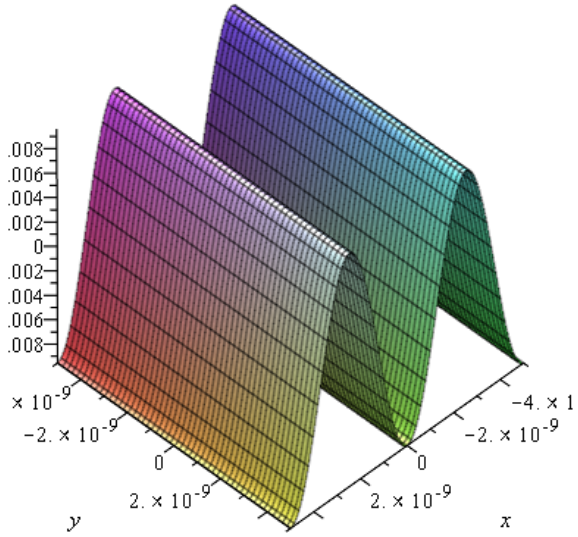

(d) N_{yy} - $\frac{\sqrt{\mu}}{a} = 0$, $\frac{\omega}{\omega_l} = 1.2$

Figure 4.4: Second mode of vibration of SSSS SLGS

The previous tendency of greater hardening spring effect for lower values of non-local parameter for simply supported plates with movable edges is the exact opposite of the behaviour of the plate under the same boundary conditions but in the second mode of vibration. In fact, it can be observed in Figure 4.4a that, similar to pinned or clamped edges in the first mode of vibration, higher values of the non-local parameter result in higher natural frequencies for a given amplitude of vibration. The Airy stress function represented in Figure 4.4b has adopted a completely different shape when compared to the first mode of vibration, but the boundary conditions are still satisfied. In Figure 4.4c the membrane force N_{xx} has the exact shape of the first mode since the shape function used in the y direction is the same as in the fundamental mode. On the other hand, N_{yy} which can be observed in Figure 4.4d, is null not only at the edges $x = -\frac{a}{2}, \frac{a}{2}$ but also when $x = 0$, since the force is inexistent at the nodal line, behaving like an additional movable support where only transverse displacement is restricted.

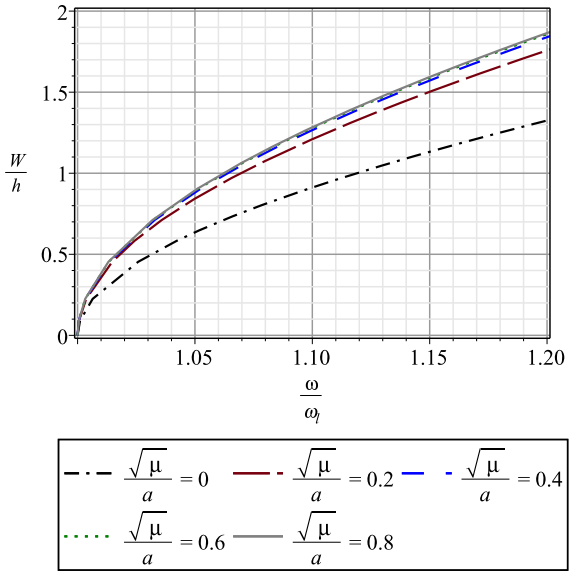

(a) Backbone curves for different $\frac{\sqrt{\mu}}{a}$

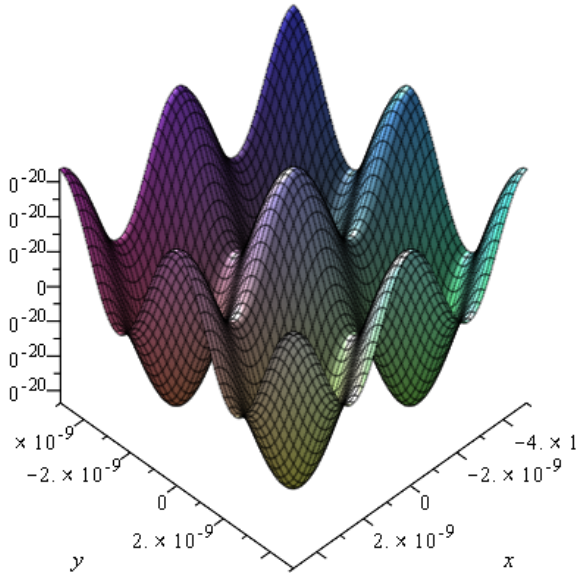

(b) Airy stress function - $\frac{\sqrt{\mu}}{a} = 0$, $\frac{\omega}{\omega_l} = 1.1$

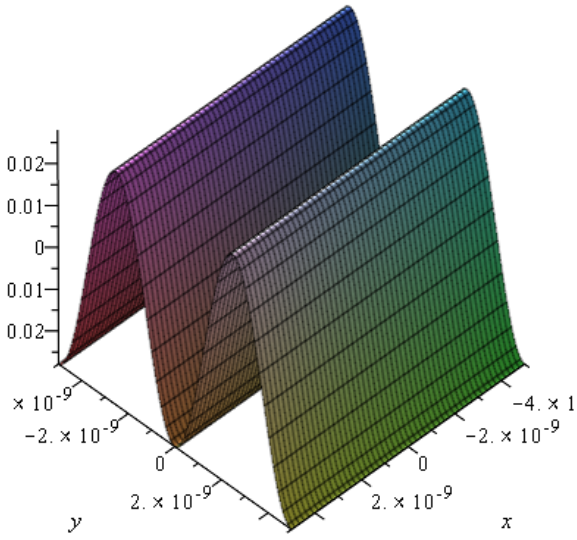

(c) N_{xx} - $\frac{\sqrt{\mu}}{a} = 0$, $\frac{\omega}{\omega_l} = 1.1$

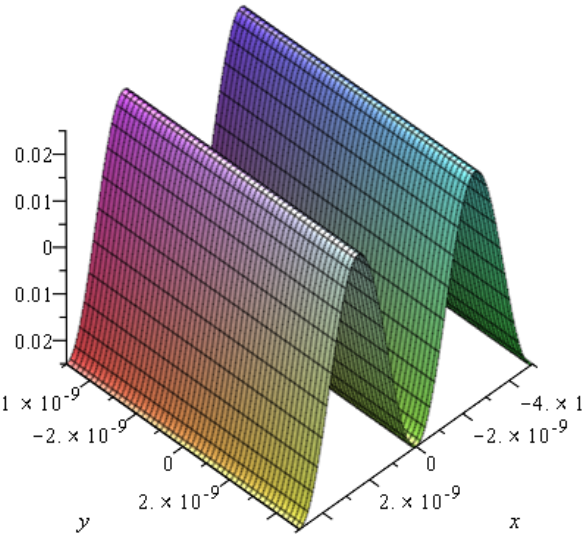

(d) N_{yy} - $\frac{\sqrt{\mu}}{a} = 0$, $\frac{\omega}{\omega_l} = 1.1$

Figure 4.5: Fourth mode of vibration of SSSS SLGS

In Figure 4.5a hardening spring effect is greater once more for the case of lower non-local parameters and consequently the fourth mode behaviour is similar to the first. This might indicate that modes of vibration that use the same functions in x and y directions present the same increased hardening effect for lower non-local parameters while modes that have a distinct number of nodal lines in x and y, requiring different sets of functions in those directions, show the opposite behaviour. The Airy stress function displayed in Figure 4.5b is also quite similar to the first mode, only with an increased number of relative maximums and minimums. In the first mode the stress function had only one absolute minimum whereas in the fourth, there are four relative ones. The second order derivatives

of the function are plotted in Figures 4.5c and 4.5d and since there is one nodal line in $x = 0$ and $y = 0$, the in-plane forces N_{yy} and N_{xx} are zero along those lines respectively.

4.3.4 Conclusions

In this chapter two different non-local non-linear models based on Airy stress function were formulated. In the first model a single function was considered for the transverse displacement while in the second, the p-version finite element method was employed.

The first model was validated considering a simply-supported plate with movable edges, with varying non-local parameter. The solutions with one and three harmonics were compared and the results obtained were in very good agreement with the published literature. It was concluded that for higher values of the non-local parameter, the contribution of higher harmonics becomes less influential in the total amplitude of vibration. The influence of the non-local parameter on the different individual harmonics considered in the periodic solution of the transverse displacement was studied and it was concluded that an increase in the parameter resulted in a less pronounced hardening-spring effect for the first mode of vibration. In fact, it was verified that for the case of a simply supported plate with movable edges, hardening-spring effect is greater for lower values of the non-local parameter, as opposed to the behaviour typically encountered in plates with constrained edges (either pinned or fully clamped).

The modes of vibration of a square SLGS were posteriorly investigated. In the second mode of vibration hardening-spring effect was greater for higher values of the non-local parameter and in the fourth mode, similar to the first, the tendency of increased hardening for lower small-scale effect is verified. One possible conclusion is that modes of vibration of simply supported plates with movable edges that employ identical functions in x and y directions and consequently share the same number of nodal lines in those axis, show increased hardening for lower values of the non-local parameter. On the other hand, modes with a different number of nodal lines in x and y exhibit greater hardening for higher values of the parameter.

The second model, where an attempt to conciliate the Airy stress function formulation and the p-version finite element method, was not applied in practice and no results were obtained due to time limitations.

Chapter 5

Conclusions and Future Work

5.1 Summary

In this dissertation two equivalent continuum models were devised to study the linear and non-linear undamped free vibrations of single-layer graphene sheets. Both models considered Eringen's non-local elasticity, so as to include small-scale effects, applied to Kirchhoff's plate theory with the inclusion of Von Kármán's geometric non-linearity. In the first model the p-version finite element method was used and the equations of motion were derived in the time domain by the application of the Galerkin method. The harmonic balance method was subsequently employed to convert the system of equations to a frequency domain algebraic problem. The resulting non-linear equations were solved numerically by an arc-length continuation method. The second model was not formulated according to a finite element approach and only one function for the transverse displacement was used. Airy stress function was also considered which was determined by solving a compatibility equation. Finally, a combination of both models was proposed but, due to time limitations, no results were obtained and only the mathematical formulation is presented.

The models were first verified and compared with other results from the published literature and then the dynamics of different SLGSs with distinct chirality, non-local parameter and boundary conditions were investigated.

In the case of the first proposed model, considering first the linear analysis, convergence was verified and both local and non-local results were in good agreement with solutions presented in the literature. The influence of the small-scale effect and size of the sheet on the linear natural frequencies was studied and, as expected, an increase in the non-local parameter or in the size of the sheet resulted in a reduction of the frequencies. In addition, larger sheets were, evidently, found to be less affected by the small-scale effects. It was verified that higher linear natural frequencies and higher mode shapes were the most affected by variation in the non-local parameter due to the smaller "effective" length of the sheet. Fully clamped sheets were also found to be more affected by the small-scale effect as a result of zero slope near the edges of the sheet and consequently shorter "effective" length. The mode shapes were analysed using different values for the non-local parameter and considering both fully clamped and pinned sheets. In the first case the shape stabilized from a certain value of the parameter and remained unaltered for higher values whilst in the latter, variation in the non-local parameter had no consequence on

the linear mode shapes.

The linear natural frequencies and the linear mode shapes of a SLGS were compared using an isotropic and orthotropic model, considering different boundary conditions and varying non-local parameter. It was concluded that for all cases the isotropic model was valid and gave very accurate results, as long as an adequate Young's modulus is used.

The non-linear vibration problem was subsequently addressed and the backbone curves for both fully clamped and pinned plates were validated first considering a local model ($\mu = 0$). The addition of the non-local effect to the already verified local non-linear model resulted in a considerable discrepancy between the solution obtained and others proposed in the literature. In fact, it was verified that for higher values of the non-local parameter this disparity further increased, which was attributed to the approximation conducted in the mathematical formulation to decouple non-linear terms comprised of forces and displacement products. This approximation was a necessity and was the only viable option that could be found so as to allow the application of the constitutive relations from non-local elasticity theory to these non-linear terms. Nonetheless, despite the erroneous results obtained, the tendency of greater hardening-spring effect for higher values of non-local parameter was observed for both pinned and fully clamped plates. In addition, it was verified that pinned plates have higher hardening ratios than fully clamped ones.

Regarding the inaccurate results obtained with the first model for the non-local non-linear case, a second single function model based on Airy stress potential was formulated. The backbone curves of a simply supported sheet with movable edges were validated considering different values of the non-local parameter and the solutions with one and three harmonics were compared. It was verified that for higher values of the non-local parameter, the contribution of higher harmonics became less influential in the total amplitude of vibration. Moreover, it was observed that an increase in the non-local parameter resulted in a less pronounced hardening-spring effect on each individual harmonic of the periodic solution for the first mode of vibration. This behaviour was the opposite to the one observed in pinned and fully clamped sheets (both with edges constrained). In the second mode of vibration this tendency changes and for higher values of the small-scale effect greater hardening is observed. For the fourth mode of vibration, lower values of the non-local parameter resulted, once more, in a more pronounced hardening-spring effect. This might indicate that modes with similar functions in x and y directions show the same increased hardening for lower non-local parameter, whereas modes with distinct functions in those directions, and therefore with a different number of nodal lines in x and y, present the opposite behaviour.

5.2 Future Work

Graphene sheets are still a very recent scientific endeavour and for the future application of this extraordinary material further research must be done.

Within the context of this dissertation, the study of the linear and non-linear vibrations of these sheets must be continued. The attempt of conciliating the p-version finite element method with an Airy stress function based formulation is a possible future work, which would allow the investigation of interesting phenomena such as mode interaction and internal resonance in single-layer graphene sheets.

Another topic to be investigated is the occurrence of bifurcations in the solutions of

the non-linear equations of motion of a SLGS. Secondary branches which diverge from the main branch of solutions is characteristic of non-linear systems, where a small change in the parameters of the system results in a completely different dynamic response.

The analysis of forced vibration is also another possible topic to be investigated. The consideration of a DC electrostatic force (which is treated like a free vibration problem with additional stiffness terms) or even an AC actuation are both interesting projects.

Lastly, the consideration of Van der Waals forces in the model to study the dynamics of multiple-layered graphene sheets is another interesting possibility.

Bibliography

[1] Edward P. Randviir, Dale A C Brownson, and Craig E. Banks. A decade of graphene research: Production, applications and outlook. *Materials Today*, 17(9):426–432, 2014.

[2] Quan Wang and Behrouz Arash. A review on applications of carbon nanotubes and graphenes as nano-resonator sensors. *Computational Materials Science*, 82:350–360, 2014.

[3] B. Behjat and M. R. Khoshravan. Geometrically nonlinear static and free vibration analysis of functionally graded piezoelectric plates. *Composite Structures*, 94(3):874–882, 2012.

[4] Z. Radivojevic, P. Beecher, C. Bower, S. Haque, P. Andrew, T. Hasan, F. Bonaccorso, a. C. Ferrari, and B. Henson. Electrotactile touch surface by using transparent graphene. *Proceedings of the 2012 Virtual Reality International Conference on - VRIC '12*, page 1, 2012.

[5] Hui Wang and Yun Hang Hu. Graphene as a counter electrode material for dye-sensitized solar cells. *Energy & Environmental Science*, 5(8):8182, 2012.

[6] David Cohen-Tanugi and Jeffrey C. Grossman. Water desalination across nanoporous graphene. *Nano Letters*, 12(7):3602–3608, 2012.

[7] Yi Han, Zhen Xu, and Chao Gao. Ultrathin graphene nanofiltration membrane for water purification. *Advanced Functional Materials*, 23(29):3693–3700, 2013.

[8] E. Jomehzadeh and A. R. Saidi. A study on large amplitude vibration of multilayered graphene sheets. *Computational Materials Science*, 50(3):1043–1051, 2011.

[9] W Han and M Petyt. Geometrically Nonlinear Vibrations Analysis of Thin , Rectangular Plates Using the Hierarchical Finite Element Method - I: The Fundamental Mode of Isotropic Plates. 63(2):295–308, 1997.

[10] W Han. *The Analysis Of Isotropic And Laminated Rectangular Plates Including Geometrical Non-Linearity Using The P-Version Finite Element Method*. PhD thesis, University of Southampton, 1993.

[11] R. Ansari, S. Sahmani, and B. Arash. Nonlocal plate model for free vibrations of single-layered graphene sheets. *Physics Letters, Section A: General, Atomic and Solid State Physics*, 375(1):53–62, 2010.

[12] M Sadeghi and R Naghdabadi. Nonlinear vibrational analysis of single-layer graphene sheets. *Nanotechnology*, 21(10):105705, 2010.

[13] Yang Zhang, L.W. Zhang, K.M. Liew, and J.L. Yu. Nonlocal continuum model for large deformation analysis of SLGSs using the kp-Ritz element-free method. *International Journal of Non-Linear Mechanics*, 79:1–9, 2016.

[14] Sandeep Singh and B.P. Patel. Nonlinear dynamic response of single layer graphene sheets using multiscale modelling. *European Journal of Mechanics - A/Solids*, 59:165–177, 2016.

[15] H. B. Li, Y. D. Li, X. Wang, and X. Huang. Nonlinear vibration characteristics of graphene/piezoelectric sandwich films under electric loading based on nonlocal elastic theory. *Journal of Sound and Vibration*, 358:285–300, 2015.

[16] K.S. Novoselov, A.K. Geim, S.V. Morozov, D Jiang, Y Zhang, S.V. Dubonos, I.V. Grigorieva, and A. A Firsov. Electric field effect in atomically thin carbon films. *Science*, 306:666–669, 2004.

[17] Alexander A. Balandin, Suchismita Ghosh, Wenzhong Bao, Irene Calizo, Desalegne Teweldebrhan, Feng Miao, and Chun Ning Lau. Superior thermal conductivity of single-layer graphene. *Nano Letters*, 8(3):902–907, 2008.

[18] Yanwu Zhu, Shanthi Murali, Weiwei Cai, Xuesong Li, Ji Won Suk, Jeffrey R. Potts, and Rodney S. Ruoff. Graphene and graphene oxide: Synthesis, properties, and applications. *Advanced Materials*, 22(35):3906–3924, 2010.

[19] A. Sakhaee-Pour. Elastic properties of single-layered graphene sheet. *Solid State Communications*, 149(1-2):91–95, 2009.

[20] P O Lehtinen, A S Foster, A Ayuela, A Krasheninnikov, K Nordlund, and R M Nieminen. Magnetic properties and diffusion of adatoms on a graphene sheet. *Physical Review Letters*, 91(1):017202, 2003.

[21] Cristina Gómez-Navarro, R. Thomas Weitz, Alexander M. Bittner, Matteo Scolari, Alf Mews, Marko Burghard, and Klaus Kern. Electronic transport properties of individual chemically reduced graphene oxide sheets. *Nano Letters*, 7(11):3499–3503, 2007.

[22] Fabrizio Scarpa, Sondipon Adhikari, and A Srikantha Phani. Effective elastic mechanical properties of single layer graphene sheets. *Nanotechnology*, 20(6):Art. No. 065709, 2009.

[23] Xin Zhao, Cary M. Hayner, Mayfair C. Kung, and Harold H. Kung. In-plane vacancy-enabled high-power Si-graphene composite electrode for lithium-ion batteries. *Advanced Energy Materials*, 1(6):1079–1084, 2011.

[24] Dhiraj Prasai, Juan Carlos Tuberquia, Robert R. Harl, G. Kane Jennings, and Kirill I. Bolotin. Graphene: Corrosion-inhibiting coating. *ACS Nano*, 6(2):1102–1108, 2012.

[25] Woo Jin Hyun, O. Ok Park, and Byung Doo Chin. Foldable graphene electronic circuits based on paper substrates. *Advanced Materials*, 25(34):4729–4734, 2013.

[26] William S. Hummers and Richard E. Offeman. Preparation of Graphitic Oxide. *Journal of the American Chemical Society*, 80(6):1339–1339, 1958.

[27] K S Novoselov, V I Fal'ko, L Colombo, P R Gellert, M G Schwab, and K Kim. A roadmap for graphene. *Nature*, 490(7419):192–200, 2012.

[28] S Garaj, W Hubbard, a Reina, J Kong, D Branton, and J a Golovchenko. Graphene as a subnanometre trans-electrode membrane. *Nature*, 467(7312):190–193, 2010.

[29] Sukang Bae, Hyeongkeun Kim, Youngbin Lee, Xiangfan Xu, Jae-Sung Park, Yi Zheng, Jayakumar Balakrishnan, Tian Lei, Hye Ri Kim, Young Il Song, Young-Jin Kim, Kwang S. Kim, Barbaros Özyilmaz, Jong-Hyun Ahn, Byung Hee Hong, and Sumio Iijima. Roll-to-roll production of 30-inch graphene films for transparent electrodes. *Nature Nanotechnology*, 5(8):574–578, 2010.

[30] Umar Khan, Arlene O'Neill, Mustafa Lotya, Sukanta De, and Jonathan N. Coleman. High-concentration solvent exfoliation of graphene. *Small*, 6(7):864–871, 2010.

[31] Mustafa Lotya, Yenny Hernandez, Paul J. King, Ronan J. Smith, Valeria Nicolosi, Lisa S. Karlsson, Fiona M. Blighe, Sukanta De, Wang Zhiming, I. T. McGovern, Georg S. Duesberg, and Jonathan N. Coleman. Liquid phase production of graphene by exfoliation of graphite in surfactant/water solutions. *Journal of the American Chemical Society*, 131(10):3611–3620, 2009.

[32] Victor Yu Aristov, Grzegorz Urbanik, Kurt Kummer, Denis V. Vyalikh, Olga V. Molodtsova, Alexei B. Preobrajenski, Alexei A. Zakharov, Christian Hess, Torben Hänke, Bernd Büchner, Ivana Vobornik, Jun Fujii, Giancarlo Panaccione, Yuri A. Ossipyan, and Martin Knupfer. Graphene synthesis on cubic SiC/Si wafers. Perspectives for mass production of graphene-based electronic devices. *Nano Letters*, 10(3):992–995, 2010.

[33] Caterina Soldano, Ather Mahmood, and Erik Dujardin. Production, properties and potential of graphene. *Carbon*, 48(8):2127–2150, 2010.

[34] a M Affoune, B L V Prasad, H Sato, T Enoki, Y Kaburagi, and Y Hishiyama. Experimental evidence of a single nano-graphene. *Chemical Physics Letters*, 348(October):17–20, 2001.

[35] Pin Lu, P.Q. Zhang, H.P. Lee, C.M. Wang, and J.N. Reddy. Non-local elastic plate theories. *Proceedings of the Royal Society A: Mathematical, Physical and Engineering Sciences*, 463(2088):3225–3240, 2007.

[36] J. N. Reddy. Nonlocal nonlinear formulations for bending of classical and shear deformation theories of beams and plates. *International Journal of Engineering Science*, 48(11):1507–1518, 2010.

[37] Jarosaw Meller. Molecular Dynamics. *Encyclopedia of Life Sciences*, pages 1–8, 2001.

[38] Mp Allen. Introduction to molecular dynamics simulation. *Computational Soft Matter: From Synthetic Polymers to ...*, 23(2):1–28, 2004.

[39] A. Sakhaee-Pour, M. T. Ahmadian, and A. Vafai. Applications of single-layered graphene sheets as mass sensors and atomistic dust detectors. *Solid State Communications*, 145(4):168–172, 2008.

[40] K. Behfar and R. Naghdabadi. Nanoscale vibrational analysis of a multi-layered graphene sheet embedded in an elastic medium. *Composites Science and Technology*, 65(7-8):1159–1164, 2005.

[41] A Sakhaee-Pour, M T Ahmadian, and R Naghdabadi. Vibrational analysis of single-layered graphene sheets. *Nanotechnology*, 19(8):85702, 2008.

[42] Wanda Szemplińska Stupnicka. *The Behavior of Nonlinear Vibrating Systems, Volume II: Advanced Concepts and Applications to Multi-Degree-of-Freedom Systems*. Kluwer Academic Publishers, Warsaw, Poland, 1990.

[43] A. Farajpour, M. R. Hairi Yazdi, A. Rastgoo, M. Loghmani, and M. Mohammadi. Nonlocal nonlinear plate model for large amplitude vibration of magneto-electro-elastic nanoplates. *Composite Structures*, 140:323–336, 2016.

[44] A. Cemal Eringen. On differential equations of nonlocal elasticity and solutions of screw dislocation and surface waves. *Journal of Applied Physics*, 54(9):4703–4710, 1983.

[45] John Peddieson, George R. Buchanan, and Richard P. McNitt. Application of nonlocal continuum models to nanotechnology. *International Journal of Engineering Science*, 41(3-5):305–312, 2003.

[46] J.N. Reddy. *Theory and Analysis of Elastic Plates and Shells*. Taylor & Francis, Philadelphia, PA, second edition, 2007.

[47] Pedro Ribeiro. On the influence of membrane inertia and shear deformation on the geometrically non-linear vibrations of open, cylindrical, laminated clamped shells. *Composites Science and Technology*, 69(2):176–185, 2009.

[48] M. E. Golmakani and J. Rezatalab. Nonlinear bending analysis of orthotropic nanoscale plates in an elastic matrix based on nonlocal continuum mechanics. *Composite Structures*, 111(1):85–97, 2014.

[49] I. Babuska, B.A. Szabo, and I.N. Katz. The p-Version of the Finite Element Method. *Journal on Numerical Analysis*, 18(3):515–545, 1981.

[50] P. Ribeiro and M. Petyt. Nonlinear vibration of plates by the hierarchical finite element and continuation methods. *International Journal of Mechanical Sciences*, 41(4-5):437–459, 1999.

[51] N.S. Bardell. Free vibration analysis of a flat plate using the hierarchical finite element method. *Journal of Sound and Vibration*, 151(2):263–289, 1991.

[52] Wanmin Han and M. Petyt. Linear Vibration Analysis of Laminated Rectangular Plates Using The Hierarchical Finite Element Method - I. Free Vibration Analysis. *Journal of Sound And Vibration*, 1995.

[53] Mário Oliveira. Vibrações de Nanoplacas, Faculdade de Engenharia da Universidade do Porto, 2014.

[54] P. Ribeiro. *Geometrical Nonlinear Vibration of Beams and Plates by The Hierarchical Finite Element Method*. PhD thesis, University of Southampton, 1998.

[55] R. Lewandowski. Non-Linear Free Vibrations of Beams by The Finite Element and Continuation Methods. *Journal of Sound and Vibration*, 1992.

[56] Arthur W. Leissa. *Vibrations of Plates*. Scientific and Technical Information Division, Office of Technology Utilization - National Aeronautics and Space Administration, 1969.

[57] Saeid Sarrami-Foroushani and Mojtaba Azhari. Nonlocal vibration and buckling analysis of single and multi-layered graphene sheets using finite strip method including van der Waals effects. *Physica E: Low-Dimensional Systems and Nanostructures*, 57:83–95, 2014.

[58] Ramin Aghababaei and J. N. Reddy. Nonlocal third-order shear deformation plate theory with application to bending and vibration of plates. *Journal of Sound and Vibration*, 326(1-2):277–289, 2009.

[59] AR. Setoodeh, P. Malekzadeh, and AR. Vosoughi. Nonlinear free vibration of orthotropic graphene sheets using nonlocal Mindlin plate theory. *Proceedings of the Institution of Mechanical Engineers, Part C: Journal of Mechanical Engineering Science*, 226(7):1896–1906, 2011.

[60] M.S Sarma, A. Venkateshwar Rao, S.R.R. Pillai, and B.Nageswara Rao. Large Amplitude Vibrations of Laminated Hybrid Composite Plates. *Journal of Sound and Vibration*, 1992.

[61] R. Benamar. *Nonlinear dynamic behaviour of fully clamped beams and isotropic rectangular and laminated plates*. PhD thesis, University of Southampton, UK, 1990.

[62] S.R Asemi, M. Mohammadi, and A. Farajpour. A study on the nonlinear stability of orthotropic single- layered graphene sheet based on nonlocal elasticity theory. *Latin American Journal of Solids and Structures*, (2014):1541–1564, 2014.

[63] Le Shen, Hui-Shen Shen, and Chen-Li Zhang. Nonlocal plate model for nonlinear vibration of single layer graphene sheets in thermal environments. *Computational Materials Science*, 48(3):680–685, 2010.